

NOAO DATA HANDBOOK

VERSION 2.2, MAY 2015



User Support

For help with accessing or understanding NOAO data products or data services, email the Help Desk:

Email: sdmhelp@noao.edu

This *Handbook*, along with other documentation on NOAO data, is available online at:

<http://ast.noao.edu/data/docs>

Revision History

Version	Date	Editor(s)
1.0	2007 December	Richard A. Shaw
1.1	2009 May	Richard A. Shaw
1.2	2011 July	Richard A. Shaw, Rob Swaters
2.0	2015 February	Richard A. Shaw
2.1	2015 April	Richard A. Shaw
2.2	2015 May	Richard A. Shaw

Copyright © 2015, Association of Universities for Research in Astronomy, Inc. All rights reserved.

Citations to this version of the *NOAO Data Handbook* should read:

Shaw, R. A., ed. 2015, NOAO Data Handbook (Version 2.2; Tucson: National Optical Astronomy Observatory)

Send comments or corrections to:

Science Data Management Group
NOAO
950 N. Cherry Ave.
Tucson, AZ 85719
USA



NOAO is operated by the Association of Universities for Research in Astronomy under cooperative agreement with the National Science Foundation



Cover photo: Nighttime view of the dome of the Blanco 4-m telescope at Cerro Tololo Inter-American Observatory. The DECam wide-field camera is being used with this telescope to conduct the Dark Energy Survey. Photo credit: Reidar Hahn and Fermilab National Accelerator Laboratory.

Table of Contents

<i>User Support</i>	<i>ii</i>
<i>Revision History</i>	<i>ii</i>
Preface	v
<i>Scope of This Handbook</i>	v
<i>Handbook Structure</i>	v
<i>Special Notes</i>	vi
<i>Handbook Updates</i>	vii
<i>Source Material & Attribution</i>	vii
Introduction to NOAO Data	1-1
1.1 <i>NOAO Data Holdings</i>	1-1
1.1.1 Data Sources	1-2
1.1.2 Processing Levels	1-3
1.1.3 Types of Data Products	1-4
1.1.4 Data File Nomenclature	1-6
1.2 <i>NOAO Data Formats</i>	1-7
1.2.1 Imaging Data	1-8
1.2.2 Spectroscopic Data	1-9
1.2.3 Concomitant Data	1-9
1.3 <i>Accessing NOAO Data</i>	1-9
1.3.1 Survey Data Archive	1-9
1.3.2 Science Archive	1-11
1.3.3 Proprietary Data Access	1-15
1.4 <i>Data Use Policy</i>	1-16
1.4.1 Proprietary Period	1-16
1.4.2 Nonproprietary Data	1-16
1.4.3 Proper Citation for NOAO Data	1-17
1.5 <i>References & Further Information</i>	1-17
Mosaic Cameras	2-1
2.1 <i>Instrument Overview</i>	2-1
2.1.1 Instrument Capabilities & Design	2-1
2.1.2 Operations	2-6
2.2 <i>Data Products</i>	2-7
2.2.1 Image Formats	2-7
2.2.2 Header Keywords	2-11
2.2.3 Environmental Data	2-14
2.3 <i>Calibration</i>	2-14
2.3.1 Single-Frame Processing	2-14
2.3.2 Image Stacks	2-20
2.3.3 Calibration Reference Files	2-21

2.4 Sources of Error	2-25
2.4.1 Astrometry	2-25
2.4.2 Photometry	2-26
2.4.3 Anomalies	2-27
2.5 References & Further Information.....	2-28
NEWFIRM Camera.....	3-1
3.1 Instrument Overview	3-1
3.1.1 Instrument Capabilities & Design.....	3-1
3.1.2 Operations.....	3-5
3.2 Data Products	3-8
3.2.1 Image Formats	3-9
3.2.2 Header Keywords.....	3-12
3.2.3 Environmental Data.....	3-15
3.3 Calibration	3-15
3.3.1 Processing Steps	3-15
3.3.2 Calibration Reference Files.....	3-20
3.4 Sources of Error	3-22
3.4.1 Astrometry	3-22
3.4.2 Photometry.....	3-23
3.4.3 Anomalies.....	3-23
3.5 References & Further Information.....	3-25
Dark Energy Camera.....	4-1
4.1 Instrument Overview	4-1
4.1.1 Instrument Capabilities & Design.....	4-2
4.1.2 Operations.....	4-6
4.2 Data Products	4-7
4.2.1 Image Formats	4-7
4.2.2 Header Keywords.....	4-11
4.2.3 Environmental Data.....	4-13
4.3 Calibration	4-13
4.3.1 Single-Frame Processing.....	4-14
4.3.2 Image Co-addition.....	4-22
4.3.3 Calibration Reference Files.....	4-24
4.4 DECam Sources of Error	4-27
4.4.1 Astrometry	4-27
4.4.2 Photometry.....	4-28
4.4.3 Anomalies.....	4-28
4.5 References & Further Information.....	4-33
C/KOSMOS.....	5-1
5.1 Instrument Overview	5-1
5.1.1 Optical Design.....	5-2
5.1.2 Imaging and Field Acquisition	5-5
5.1.3 Spectroscopy	5-6

5.1.4 Operations.....	5-7
5.2 <i>Data Products</i>	5-9
5.2.1 Raw Data.....	5-9
5.2.2 KMS Files.....	5-10
5.2.3 Header Keywords.....	5-10
5.3 <i>Data Reduction</i>	5-11
5.4 <i>References & Further Information</i>	5-13
Glossary	G-1

Preface

Version 2.0, February 2015

SCOPE OF THIS HANDBOOK

The purpose of this *NOAO Data Handbook* is to describe the instruments and archived data products in enough detail that an Archive user who is not familiar with them (or who may be new to the optical/infrared wavelength regime) can make informed use of these data products and services for scientific analysis. This *Handbook* is also intended for Principal Investigator teams who obtain data at NOAO or partner facilities and who wish to understand how their data are reduced and calibrated by the applicable pipelines. One of the key aims of this *Handbook* is to provide one-stop shopping for vital background material for each instrument, with references to more detailed material where it exists. Another key aim is to be the most up-to-date reference material and to be central to establishing the pedigree of datasets in the NOAO Science Archive (NSA). However, this *Handbook* is *not* intended to replace instrument manuals, online cookbooks, descriptions of *filters*, instrument design documents, or detailed technical descriptions of the archive or pipelines. It is also not a user guide for data analysis—the suite of available tools for data analysis is already quite rich, and growing. It will, however, draw upon all of these resources in order to provide a self-contained and complete manual for scientific use of the data from all instruments that are archived in the NSA. The complete list of the NSA holdings by instrument is given in Chapter 1.

The first edition of this *Handbook* coincided with the initial deployment of the End-to-End (E2E) data processing system at NOAO. E2E is the system that manages the flow of information and data from the database of approved observations, through data acquisition, transport from the telescope to an NOAO Archive Center, pipeline processing, and retrieval by an end-user. Because E2E was created *after* many instruments were deployed, rather than before, it will be some time before the Archive is populated with all intended data products from all instruments. Thus, this *Handbook* is necessarily incomplete.

HANDBOOK STRUCTURE

This *Handbook* is relatively modular in its construction, and is organized conceptually into two parts: an introductory chapter that describes general properties of NOAO data and the means to identify and access data for retrieval from the NSA, and chapters containing reference material for each instrument or class of instruments. These latter chapters are intended to give users a concise overview of each instrument and a good understanding of the metadata and data products that are produced. Instrument chapters are organized identically at the section level and consist of the following topics:

- **Instrument Overview.** Each instrument is described in enough detail to acquaint the user with the basic design and configuration, capabilities, typical operation, and the associated vocabulary.
- **Data Products.** Each of the data products that are produced for an instrument (including file formats) and essential metadata (e.g., header keywords) are described in depth to enable their effective use.

- **Calibration.** A detailed description of the processing that occurs to produce each calibrated data product is presented, along with the mechanisms by which the calibration reference information (e.g., master bias frames, flat-fields, etc.) is created and applied.
- **Sources of Error.** This section describes the accuracies that can be expected of the data products (e.g., astrometric and photometric uncertainties), instrument peculiarities, anomalous conditions that may have occurred at one time or another, known data foibles, and any other limitations to the scientific use of the data products.
- **References and Further Information.** Lists of contributing authors, cited references, and pointers to background information are provided at the end of each chapter. Novel uses of the data or useful processing and analysis techniques found in the literature may also be cited.

In addition to the material listed above, this *Handbook* contains a glossary of often used terms and acronyms.

SPECIAL NOTES

Selected fonts are used to indicate special terminology, or to indicate user interaction with tools:

- ***Bold italic*** indicates technical terms of interest the first time they appear in a chapter; these terms are defined in the Glossary;
- **Bold** indicates names of software tools or packages;
- **Fixed-width type** indicates text that is intended for input to a software application or web tool; and
- **Underlined Arial bold in teal** indicates text that appears on a button in an application.

Special notes appear throughout this *Handbook* to convey information of special interest or urgency, particularly for the casual reader. They are the following:



Informative notes are denoted like this, and generally contain tips and pointers that deserve special attention.



Cautionary notes are indicated like this, and indicate potential limitations of the data, the instrument, or the processing software that may affect the use or interpretation of the data products.



Warnings of serious consequences are indicated like this, and caution users of problems with the data that could lead to erroneous scientific interpretations, or problems with the software that could lead to errors that may not be apparent to users.

HANDBOOK UPDATES

New data products will be offered in the NOAO Science Archive in the future as new instruments are built and deployed at NOAO and partner facilities, as new processing pipelines are constructed to produce higher levels of data reduction for existing instruments, and as teams of scientists in the community create specialized products as a result of their research endeavors. Improvements may also be made to the existing processing pipelines, and/or to the characterizations of instrument performance upon which the pipelines depend. When new or improved products are offered, chapters of this *Handbook* will be created or updated as necessary. This *Handbook* has been designed so that each chapter can be independently versioned; updates will be announced on the NOAO web pages and in the *NOAO Newsletter*. Users can download¹ the *Handbook* as needed.

SOURCE MATERIAL & ATTRIBUTION

The source material for this *Handbook* was drawn from a large number of documents, including instrument manuals, instrument and software design documents, published papers, web pages, data file headers, and informal conversations with many experts within and outside of NOAO. Often, figures, tables, and even text are taken directly from these sources. In order to keep the style and presentation of this *Handbook* relatively clean, the attribution to the source material is cited the first time it is used in the main body of each chapter. The last section of each chapter is devoted to a listing of references, contributing authors, and background references to details that fall outside the scope of this document.

¹ From <http://ast.noao.edu/data/docs>.

Chapter 1

Introduction to NOAO Data

Version 2.2, May 2015

	In This Chapter...
	NOAO Data Holdings.....1-1
	NOAO Data Formats.....1-7
	Accessing NOAO Data.....1-9
	Data Use Policy.....1-16
	References & Further Information.....1-17

NOAO instruments routinely produce large quantities of digital data from a variety of science and survey programs directed by principal investigators (PIs). Data from some of these instruments are reduced and calibrated with automated pipelines, and both raw and reduced data products are published through the *NOAO Science Archive*. This chapter describes the scope of the data holdings in the Archive and the means to access them.

1.1 NOAO Data Holdings

NOAO collects a large quantity and variety of scientific data products, including images, spectrograms, etc., from dozens of instruments on several telescopes that are deployed on three mountain tops on two continents. The primary repository for these data is the *NOAO Science Archive*. The data holdings can be categorized in a number of ways, including the source of the data, the type of data product, and the level(s) of processing required to produce them. Each of these views will be described in the following subsections. Since calibration pipelines exist for only a few instruments, much of the current Archive holdings consist only of raw data products.

NOAO also hosts a second science data archive: the *NOAO Survey Archive* contains reduced, science-ready data products that were generated by NOAO Survey PI teams; it can be accessed through its custom web interface (see Section 1.3.1 for details). This legacy archive will receive few content updates in the future.

The main *NOAO Science Archive* (hereafter, Archive), which contains all raw data and calibrated data products for select instruments as produced by NOAO pipelines, is accessed through a portal: <http://portal-nvo.noao.edu>. It also hosts PI-processed data products for high-value, large surveys including the *Dark Energy Survey*. The remainder of this chapter will describe the data holdings and access methods for the Archive.



Users of NOAO data products should be aware that, with few exceptions, the data were obtained from observing programs that were designed and carried out by PI teams, who obtained the data for the purpose of achieving their particular science objectives, and who obtained supporting calibration observations at their discretion. In addition, the quality of the data and the calibrations are strongly affected by the weather and other conditions that prevailed during the observing run.

1.1.1 Data Sources

The scope of the Archive data holdings includes data streams from more than 30 instruments. Data from most instruments that are offered on NOAO facilities (with the exception of visitor instruments) are captured and stored in the Archive. In addition, most data from partner institutions (i.e., observatories operated by consortia of institutions of which NOAO is a partner) are also captured, though in some cases only data obtained through the NOAO time allocation process may be stored in the Archive. The Archive holdings consist of data from the instruments and telescopes listed in Table 1-1, which also lists the instrument in-service dates and the highest level of scientific data processing that is currently offered (see next subsection).



At present only raw data from semester 2004B (beginning in August 2004) and forward have been archived; calibrated products are also available for instruments with processing pipelines. Earlier raw data are stored on tape; early data from some high-use instruments may at some point be ingested into the Archive.

Table 1-1: Archive Data Holdings by Instrument

Instrument ²	Type	In-Service Dates	Highest-Level Product ³
NOAO/Cerro Tololo			
COSMOS	Multi-object spectrograph	Since 2014-Jul	1
DECam	Wide-field optical imager	Since 2012-Dec	3
Hydra	Optical fiber spectrograph	1999-Jul to 2012-Sep	1
ISPI	IR imager	Since 2003-Jan	1
Mosaic-2 Camera	Optical imager	1999-Aug to 2011-Dec	3
NEWFIRM ⁴	Wide-field IR imager	2010-May to 2011-Oct	3
R-C Spectrograph	Optical spectrograph	1998-Feb to 2011-Feb	1
NOAO/Kitt Peak			
2.1-m direct	Optical imager	1998-Feb to 2014-Jul	1
4-m Echelle	Optical spectrograph	1997-Nov to 2015-Jan	1

² Instruments in active service appear in **bold face**.

³ See Table 1-2 on page 1-4 for a description of the data product levels.

⁴ Shared with KPNO 4-m.

Instrument²	Type	In-Service Dates	Highest-Level Product³
FLAMINGOS ⁵	IR imaging spectrograph	2000-Dec to 2014-Jan	1
2.1-m GoldCam	Optical spectrograph	1997-Aug to 2011-Nov	1
KOSMOS	Optical multi-slit spectrograph	Since 2013-Oct.	1
MARS	IR spectrograph	2002-Jun to 2011-Oct	1
Mosaic-1 Camera	Optical imager	1999-Mar to 2010-Jun	3
Mosaic-1.1 Camera	Optical imager	Since 2010-Oct	3
NEWFIRM	IR imager	Since 2007-Jun	3
Phoenix	Hi-res IR spectrometer	Since 1997-Sep	1
R-C Spectrograph	Optical spectrograph	Since 1997-Sep	1
SQIID	IR imager	2000-Sep to 2011-Feb	1
SMARTS/Cerro Tololo			
1.5-m CHIRON	Optical fiber spectrograph	Since 2012 Mar	1
1.5-m Cass Spectrograph	Optical spectrograph	1998-Mar to 2007-Jul	1
1.3-m ANDICAM	Optical/IR imager	Since 2003-Feb	1
1.0-m Y4KCam	Optical imager	2004-May to 2012-Aug	1
0.9-m Direct	Optical imager	Since 1998-Feb	1
SOAR/Cerro Pachón			
Goodman Spectrograph	Optical imaging spectrograph	Since 2008-Aug	1
OSIRIS	IR imaging spectrograph	Since 2006-Sep	1
SAM	Optical imager	Since 2013-Sep	1
SOI	Optical imager	Since 2006-Sep	1
Spartan	IR imager	Since 2010-Apr	1
WIYN/Kitt Peak			
Bench Spectrographs⁶	Optical fiber spectrographs	Since 1997-Aug	1
Mini-Mosaic	Optical imager	2000-Aug to 2013-Apr	1
WHIRC	IR imager	Since 2007-Nov	1
0.9-m HDI	Optical imager	Since 2013-Oct	1
0.9-m Mosaic-1	Optical wide-field imager	1999-Feb to 2013-May	1
0.9-m Direct	Optical imager	1998-Feb to 2013-Oct	1

In order to be included in the Archive, the instrument data stream must flow through the NOAO Data Transport Service, include sufficient metadata for an instrument to be recognized, and be facility-class. Thus, data from many (>50) instruments are *not* included in the Archive, including visitor and engineering-grade instruments, and instruments that were not in service at the start of Archive operations. Data from WIYN/pODI are archived separately at: <http://portal.odi.iu.edu/>.

1.1.2 Processing Levels

The basic data files that are generated by the instruments in the observing environment are referred to as *raw* data products. Data from certain instruments have been processed to remove the instrumental signature and to provide some type of calibration. Such advanced, higher-level science data products, along

⁵ Offered on both the 4-m and 2.1-m telescopes at KPNO.

⁶ WIYN has offered a variety of fiber-fed spectrographs, including HYDRA, SparsePak, etc., all of which are included here.

with concomitant data, are also available from the archive; detailed descriptions of these data products may be found in subsequent chapters, which are specific to each instrument. The degree to which data have been processed is expressed in terms of *levels*, as described in Table 1-2.

Table 1-2: Levels of Data Processing

Level	Description	Example Products
1	Raw data, as it is formatted by the data collection software at the telescope	Raw Mosaic camera frames, including overscan; may include approximate WCS predicted from the telescope pointing.
2	Single-frame reduced data	These single-frame images come in two flavors: instrument signature removed, WCS and photometric calibrations applied (<i>InstCal</i>); and calibrated images that have been re-projected to a common grid (<i>Resampled</i>).
3	Combinations of two or more frames	<i>Stacked</i> and/or tiled images of a region of sky derived from multiple, spatially overlapping exposures with the same filter. Artifacts and gaps between detectors in a focal-plane array are masked.
4	Measurements from one or more processed data frames (level 2 or 3)	Source catalogs, including position, magnitudes, colors; identifications of moving objects; time-series of object brightnesses. There are currently no level-4 data products offered in the Archive.

Not all data products can be usefully described in terms of *processing level*, including exposures obtained to support calibration and ancillary data that are described in the next subsection.

1.1.3 Types of Data Products

The Archive contains a variety of data products that are relevant for a scientist end-user. The following categories of products are part of the vocabulary used throughout this *Handbook* to describe NOAO data. Generally, each type of data product (apart from metadata) is stored in its own file.



At present there are only limited ways of associating reduced science data files with related files such as the original raw data and data quality masks, although the new file nomenclature convention (see Section 1.1.4) will make this easier. The value of the header keyword `DTNSANAM` will be identical for raw science data files and products derived directly from them. For Stacked images and other products with more than one parent, `DTNSANAM` will correspond to the first raw file that was used in creating the stack. Spatial coincidences of the instrument FoV may be useful, but bear in mind that the WCS is updated from raw to reduced data products.

Science Data

Frames of data obtained with an instrument of an astrophysical source are generally referred to as *science* data. Such data include images and spectrograms, and consist primarily of contiguous blocks of pixel values from one or more detector arrays in the instrument. The science data are packaged with headers of metadata (see below) within a file; these metadata describe essential details of the science data. Science data products may also include high-level products, such as catalogs or time-series, that may or may not contain pixel values.

Science data in raw form are produced from the instruments listed in Table 1-1 on page 1-2. Science data in processed form are generated either by dedicated processing pipelines or they are provided by PI teams to the Survey Archive as advanced science products. In the first case, the data products are described in this *Handbook*. In the second case, PI teams provide the documentation necessary to understand the data products; links to this documentation are provided on the NOAO Survey Archive website.⁷

Metadata

Metadata, or data that describe data products, are collected or created at various points in the planning, acquisition, and processing of science data. Most of the metadata that are available to a user are stored in the headers of science data files as keyword–value pairs. Metadata fall into a variety of categories, but perhaps the most practical categories for the end-user are the following (see Shaw 2007):

Telescope/Environment. These metadata include telescope name and configuration information, celestial coordinates of the telescope pointing, airmass/ zenith distance, tracking information, ambient temperature and wind speed, use of an atmospheric dispersion corrector, etc.

Instrument/Detector. These metadata are required for generating Level-2 products from Level-1 raw data and include the instrument configuration, detector/amplifier designations, gain settings, operating temperatures, photo-active regions of the image, *filter*/disperser or other optical elements, and pixel scale.

Science/Calibration. These metadata include the World Coordinate System (**WCS**) mapping, field of view, resolution or delivered image quality, start of the exposure and its duration, effective bandpass and sensitivity of the system, brightness units and dynamic range, background level, and transformation to a standard photometric system.

Pedigree/Provenance/Quality Assurance. These metadata include the observer name and proposal identifier, version identifier of the control software, version of the data processing/calibration software, the processing steps performed, calibration reference files used, etc.



Critical metadata in raw science data files may be missing or incorrect. No mechanism exists to validate and correct corrupted metadata, apart from the proposal identifier (`PROPID`) and the date of the observation (the `date` portion of `DATE-OBS`). However, certain of the metadata in the headers of calibrated data, notably the WCS information and the filter name, are corrected during the course of pipeline processing. Metadata added by the pipelines during processing are not in question.

Calibration Data

Calibration data in raw form are often very similar to (or indistinguishable from) science data products. These include exposures obtained for bias (zero duration), dark (finite duration with shutter closed), flat-field (including flats taken of the twilight sky), and standard star calibration. The *Master Calibration* reference files are generated by instrument scientists or by the processing pipeline from exposures obtained during the same observing run as the science data. The methods by which master calibration files are gen-

⁷ See the NSA Survey Archive website at <http://archive.noao.edu/nsa/>.

erated and how they are applied during processing is specific to each instrument, and they are discussed in detail in subsequent chapters.

Concomitant Data

Concomitant data quantify the detailed quality of the science data, generally at the pixel level, and are generated during the course of pipeline processing. These data are intimately related to the scientific interpretation of the data products. Examples of concomitant data include data quality masks (**DQMs**) which codify one or more pathologies that affect (usually) small areas of the image, exposure masks that quantify the exposure level per pixel in an image stack, and weight maps (i.e., inverse variance arrays) that quantify the uncertainty associated with pixel values.

Ancillary Data

Most ancillary data are generated contemporaneously with science data, but are not part of the science or engineering data streams. Some ancillary data, such as processing logs, are generated by the processing pipeline. Ancillary data are used to establish the context of an observation, or to enable a rough, qualitative assessment of science data quality or applicability. Examples of ancillary data include observation logs and environmental data such as that from seeing and atmospheric transparency monitors, images from all-sky cameras at or near the observing site, and weather satellite images.



No contemporaneous weather data are available from the Archive. However, weather data and images from all-sky cameras are available for KPNO;⁸ statistical weather data are also available for CTIO,⁹ as well as historical cloud coverage information¹⁰ dating back to 1975.

1.1.4 Data File Nomenclature

Raw science data as obtained at the telescopes are captured from the observing environments by the Data Transport System (Fitzpatrick 2010) and persisted as FITS files in the Archive mass data store with unique names. Each name consists of a prefix, which is a few-letter code indicating the origin of the file, a numeric identifier, and (for newer data) a few-letter code indicating the file contents; these are followed by a file-type suffix indicating the file format. The file naming syntax for the old and new conventions is the following:

Old: <code>ooNNNNNNN.fff[.zz]</code>
New: <code>ooo_YMMDD_HHMMSS_ccc.fff[.zz]</code>

In the above file name templates, the codes have the meanings given in Table 1-3.

⁸ KPNO weather and sky conditions: http://www-kpno.kpno.noao.edu/Info/Mtn_Weather/.

⁹ CTIO weather: <http://www.ctio.noao.edu/environ/environ.html>.

¹⁰ CTIO historical cloud coverage: http://www.ctio.noao.edu/site/phot/sky_conditions.php.

Table 1-3: Data File Name Codes

CODE	Old	New	Meaning
ooo	•	•	Origin of data
NNNN	•		Running serial number
fff	•	•	File format (usually fits)
zz	•	•	Compression type (fz or gz)
YYMMDD		•	UT date of observation start
HHMMSS		•	UT Time of observation start
ccc		•	Content type

The content type (ccc) includes codes for calibration frames or science object exposures, processing type, and product type (see Seaman et al. 2014 for details). The files are post-pended with the file type, which will also reflect the type of compression applied to the file, if applicable, e.g., .fits.fz for a tile-compressed FITS file. *Note that these file names are not related in any way to the names assigned by observers to data files at the telescope.* However, the new convention is more amenable to constructing associations between related files, and related files named in this way will be adjacent when sorted alphabetically by file name.



Participants in observing programs should note that the filenames they assigned via the data taking system are preserved in the data headers, as the value of the keyword DTACQNAME. For some instruments this name includes the file pathname. After raw data are retrieved from the Archive, it is possible to restore the file names to those assigned in the observing environment using a script, an example of which can be found in the Archive Portal contributed software tab.¹¹

1.2 NOAO Data Formats

Most data from the Archive will be provided to users in FITS format (FITS 2008), which is the well-known data interchange format for astronomy. As most users know, the FITS standard allows for many complex representations of data. The general features of FITS file structures that are used for data in the Archive are described here, but implementation details for each instrument are deferred to subsequent chapters. Most data products as published by the Archive have been compressed, which minimizes storage volume and the time required for users to download their data. Depending upon the software that is used to examine or analyze the data, users may need to uncompress their data after download.

¹¹ Available at <http://nvo.noao.edu/noaonvo/contrib.shtml>.



Data files from the Archive are stored using FITS tile compression (Pence et al. 2009). The **fpack/funpack** applications¹² are available to transform these data to and from compressed form, though many popular applications and libraries support FITS compressed data directly.

1.2.1 Imaging Data

In imaging cameras, it is common to use multiple detectors arranged in a contiguous array to cover a large fraction of the available focal plane of a telescope focal station. The detectors in these *focal plane arrays (FPAs)* are operated simultaneously, and are read out in parallel. (Some detector electronics allow for parallel read-out of portions of a single detector.) The signal from each of the detectors (or portions thereof) is generally stored in raw form as a separate image, along with the associated metadata; all of the images from a single exposure with the FPA are collected into a single FITS file for convenience. On the other hand, images from cameras with single CCDs, or composite images from, e.g., multiple, overlapping pointings that have been combined into a single image, are often stored in simple FITS images in the Primary Header-Data Unit.

A schematic representation of the structure of NOAO FITS files for storing data from FPAs is given in Figure 1-1. Generally, the pixel values for multiple components of an image are stored in image extensions, rather than in the primary header/data block at the beginning of the file. The headers of each image extension contain metadata that pertain specifically to a particular sensor (e.g., the WCS information). Global metadata that apply to all the images (e.g., filter name, exposure duration, etc.) may be stored in the primary header, in which case the keyword `INHERIT = T` will be found in the extension headers.¹³

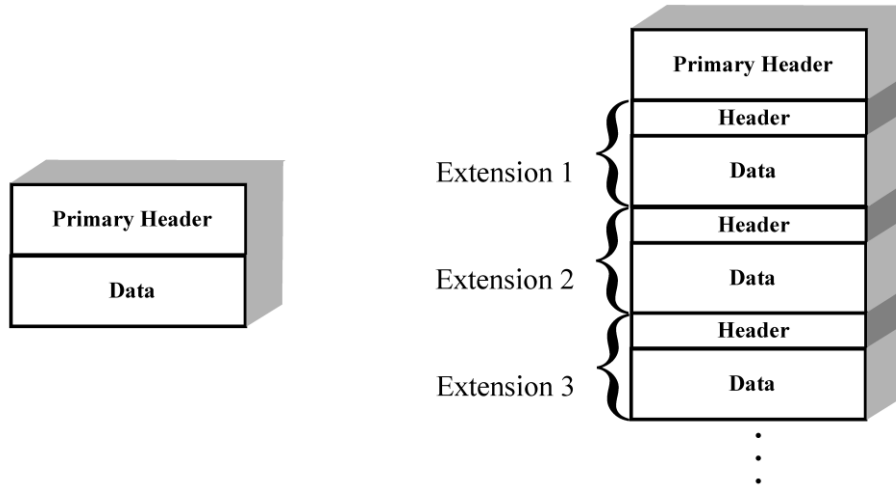


Figure 1-1: Schematic of the structure of a simple FITS file that stores a single image (*left*) and a Multi-Extension Format (MEF) file that stores one or more components of an image (*right*). Metadata that apply to all extensions are often stored in the Primary Header.

¹² FITS image compression programs are available at: <http://heasarc.gsfc.nasa.gov/fitsio/fpack/>.

¹³ In practice, the most critical metadata in the primary header often also appear in the extension headers because not all data analysis systems support the FITS `INHERIT` convention, which is described at <http://fits.gsfc.nasa.gov/registry/inherit.html>.

1.2.2 Spectroscopic Data

The storage format for raw spectrograms is conceptually similar to that for imaging cameras, i.e., pixel values from single or multiple detectors are stored in simple FITS or FITS MEF format, respectively. No Level-2 or higher (i.e., processed) data products for spectra are offered in the Archive.

1.2.3 Concomitant Data

Concomitant data are also stored in compressed form. DQMs usually contain only a small fraction of pixels with values different than zero (zero indicates no data quality problem). These data are stored as images, with as many extensions as the parent science image, similar to the structure illustrated in the right panel of Figure 1-1. Similarly, exposure maps mostly consist of large regions with a common effective exposure time; these files compress very well. Weight maps, like science data, may compress well using the Rice et al. (1993) algorithm with insignificant loss of precision.

1.3 Accessing NOAO Data

Access to and use of nonproprietary data is available to everyone, consistent with the *Conditions of Use* policy described in Section 1.4, and requires neither registration nor login. Authorized users who wish to download *proprietary* data may do so only after logging in as a registered user with the NOAO Science Archive. New registrations are available only to PIs and Co-Is of NOAO-approved observing programs.



The NOAO Science Archive Portal can only be used successfully with compatible browsers, which are Safari 7, Chrome 35, and Firefox 29, or higher versions. Use with incompatible browsers may result in missing or erroneous functionality that may not be apparent to the user!

1.3.1 Survey Data Archive

NOAO has for many years allocated time to survey programs that required many observations, and from one to three years to complete. The Principal Investigator teams, as a requirement of the Survey Program, have contributed their reduced *image*¹⁴ products to the NOAO Survey Archive for use by the astronomical community. The Survey Archive has accumulated data products from nearly 20 surveys since 2001, and more are expected to be added as ongoing surveys are completed.¹⁵ The images were obtained with a variety of instruments, including some from non-NOAO telescopes.

The Survey Archive images may be accessed from <http://archive.noao.edu/nsa/>, which enables searches of these data from a web form, shown in Figure 1-2.

¹⁴ While some survey teams have produced catalogs, the Survey Archive does not include them; see the team websites for these products.

¹⁵ See <http://archive.noao.edu/nsa/holdings.html> for a complete list.

Figure 1-2: Web interface for the NOAO Survey Archive, which provides access to PI-provided reduced data products from NOAO Survey programs. The web form enables basic searches by various parameters, including sky position, survey name, filter, and photometric depth.

The Survey Archive provides simple tools for previewing the images, defining image subsets and extracting cut-outs, and retrieving data in one of two ways:

- Retrieving individual images, by clicking a hyperlink
- Adding images to a cart, the contents of which can be downloaded in bulk via **ftp** or similar client programs



The Survey Archive contains data products that were reduced by individual, PI-led teams. The techniques that were used differ in detail among teams, and from the pipeline reductions described in subsequent chapters. Users should be aware that, while the data processing for surveys was uniform and of high quality, it was optimized for the science of the particular survey. Users should consult the specific team website and the astronomical literature for detailed descriptions of the surveys and the data processing.

The data products are often limited to simple FITS files containing science data; *the header keywords may not correspond to the metadata described in this Handbook*. A few surveys also offer more advanced products, such as data quality masks or weight images.



Data products in the Survey Archive may be merged with the NOAO Science Archive (see below) at a future date. Calibrated images as produced by the *Dark Energy Survey* are being hosted in the Science Archive.

1.3.2 Science Archive

The NOAO Science Archive contains the bulk of the NOAO data holdings; data are accessed through the Archive Portal, shown in Figure 1-3. The Portal provides the capability to conduct simple (forms-based) or advanced (SQL-based) searches for data products, categorize and filter search results, select and stage data products for download, and retrieve staged data using a variety of tools. The vast majority of the data, including all PI-provided products in the NOAO Survey Archive, are non-proprietary: anyone can search and download these data products.

Figure 1-3: Web Portal for the NOAO Science Archive, showing buttons (*lower right*) to access search pages for public or proprietary data, or PI-provided reduced data products from NOAO Survey programs. The Portal tutorial can be accessed from the “Help” pull-down menu.

Click the [General search...](#) button or select the “Search NOAO data” option in the orange banner menu to bring up the [Simple Query Form](#), shown in Figure 1-4. Click the [Search NOAO Survey Program...](#) button to search for high-level Survey data products (discussed in Section 1.3.1).

Obtaining data from the Portal is straightforward and consists of the following steps:

1. **Construct a query** for data that meet your science criteria.
2. **Refine the search** using categories or a filter.

You may click the [Retrieve](#) link under the **Access** column in the table of results to immediately download any single file. To efficiently retrieve many files at once:

3. **Select data products** of interest from the list of query matches (e.g., by ticking the selection box).
4. **Stage the selected data**.
5. **Download the data** to your machine from the staging area.



The Portal tutorials (https://portal-nvo.noao.edu/tutorials/get_my_data) provide detailed instructions on data searches and downloads.

Figure 1-4: The Simple Query interface for searching the NOAO Science Archive contents, showing several menus and dialog boxes for constraining a search with a variety of attributes, or ranges of attributes. The [Advanced Query Form](#) tab (upper left) provides an SQL interface for more precisely tailored searches.

Constructing a Query

The initial query is easy to construct by filling out the search form shown in Figure 1-4 and clicking [Search](#). The results are displayed in tabular form (click the [Results](#) tab to display them), possibly on multiple pages that may be navigated by absolute or relative page number; the results may be sorted by attribute by clicking a table column name. Depending on the query, the results may be too numerous to

manage. In this case it may help to return to the [Simple Query Form](#) and further restrict the search criteria, or construct an advanced search (see below).



The Archive contains (by end of April 2015) nearly 8 million raw exposures from all instruments and 1.1 million reduced data products. The maximum allowed size of the search results list is considerably smaller (currently 50,000 matched data products in a form query, and 250,000 in an advanced query), and **it is not possible to access the results beyond that limit**. It is therefore critical to construct a query as narrowly as possible to ensure that the list of matched results is complete. This often requires some iteration and refinement.

Categorizing and Filtering. Even after constructing a reasonably narrow query, the quantity of results may be unwieldy. It might help to *categorize* the search results by one of a set of column attributes (e.g., observation type: raw, dark, flat, object). In addition, it is possible to *filter* the results based on a match to some attribute, such as a filter name.

Advanced Searches. If simple queries cannot restrict the matched results to a manageable number, clicking the [Advanced Query Form](#) tab will allow you to construct a direct SQL query. The most recent query you made from the [Simple Query Form](#) is displayed as SQL in a dialog box to serve as a guide. Several examples are provided on this page to help you customize the SQL to suit your need.



Writing effective advanced queries requires some familiarity with the Archive database schema (i.e., the names of tables and fields within tables that contain metadata). The parts of the schema that are available to Archive users may be viewed at: http://portal-nvo.noao.edu/adql/show_schema.

Advanced searches of the Archive database are restricted, mostly for reasons of security and support limitations:

- No SQL operations are allowed that would modify, augment, or delete the database; only queries are allowed.
- The range of SQL features is intentionally limited (COUNT is not supported, for instance).
- Only two tables in the database are available for searches: **voi.siap** and **voi.skyimage**.
- Some fields must be included in the SELECT clause: **reference**, **release_date**, **start_date**, **filesize**, **dtpropid**, **md5sum**, and **noao_id**, either explicitly or by using a wildcard.
- The result of the query must be presentable as a table in the [Results](#) tab.

Users unfamiliar with SQL may benefit from the many tutorials that are available online.¹⁶

Downloading Data

Data sets can be staged for bulk download either by using the [Download](#) pull-down menu (on the [Results](#) tab) to select all (or only visible) rows, or individually selected rows. Doing this will create a set of links from the selected files identified in your Portal session to the mass data store, which is presented to

¹⁶ Documentation for querying a *Postgres* database may be found online: <http://www.postgresql.org/docs/9.1/interactive/tutorial-select.html>. Beginners to SQL may want to start with a tutorial, e.g., <http://www.postgresqltutorial.com>.

the user as a view of a staging area on the Archive as illustrated in Figure 1-5. The Portal **Download Manager** provides an easy and efficient way to retrieve the data files once they have been staged. To download it to your computer, click [Launch download manager](#). This Java application permits simultaneous parallel (multi-threaded) file downloads and offers an easy way to stop or restart file transfers. To invoke it, double-click the downloaded NOAODownloadManager.jnlp file (and enter your Archive password if the staged files contain proprietary data). *Note that the Download Manager contains only enough information to retrieve data from the most recent staging operation; to retrieve data staged subsequently, you will need to fetch a new Download Manager instance.*



The Download Manager may be prohibited from launching when invoked, depending upon your system's security settings. You may need to temporarily disable those settings or launch via some modified process. On recent OS X systems, for instance, launch the Download Manager with **Ctrl-Button1** and select "Open" from the pull-down menu, then select "Run" from the dialog box.

If you choose to use another, third-party client such as **Iftp** to retrieve your data, the login information for your staging area is given in the **retrieval information** box, including the directory for your data. Using a multi-threaded download client will speed up your data retrieval considerably, and is highly recommended.

File name	File size	Stage status
psg_150216_194826_cri.fits.fz	0.792 [MB]	Staged
psg_150216_194946_cri.fits.fz	0.827 [MB]	Staged
psg_150216_195016_cri.fits.fz	0.829 [MB]	Staged
psg_150216_195056_cri.fits.fz	0.832 [MB]	Staged
psg_150216_195116_cri.fits.fz	0.832 [MB]	Staged
psg_150216_195136_cri.fits.fz	0.838 [MB]	Staged
pag_150216_195156_cri.fits.fz	0.844 [MB]	Staged
psg_150216_195206_cri.fits.fz	0.850 [MB]	Staged
psg_150216_195216_cri.fits.fz	0.841 [MB]	Staged
psg_150216_195446_cri.fits.fz	0.818 [MB]	Staged

Figure 1-5: Data staging area for the NOAO Science Archive Portal, showing buttons (top) to manage the staging process, status and retrieval information (left), and a list of individual staged files (right). The download manager may be downloaded by clicking the green button.

Prompt retrieval of your files is advised, since the “staging” information is purged after awhile. To enable downloads beyond the staged-file limit, delete your old data from the stage area by clicking the [Clear my stage area](#) text. Users who need to retrieve large numbers of files, e.g., from programs with large numbers of short exposures from lengthy observing runs, should be aware of limitations of the Archive services for such requests.

1.3.3 Proprietary Data Access

Access to most data obtained through an NOAO observing program is restricted for a period of time to Principal Investigators (PIs) and the Co-Investigators (Co-Is) they authorize, per the *NOAO Data Use Policy* described in Section 1.4. PIs wishing to retrieve their *proprietary* data from the Archive must have an Archive account and log in with an ID and password. PIs and Co-Is of approved NOAO observing programs are *automatically registered* with the Archive prior to their (first) observing run.



Only PIs and authorized Co-Is of observing programs are permitted to retrieve data during the proprietary period, and they must log in to the Archive portal using their assigned login ID and password in order to stage or download their data. Queries for proprietary data from non-PIs will populate the results pane, but these data cannot be staged for retrieval.

- **If you have not been registered before**, view the invitation email from `archive-noreply@noao.edu` (which will automatically be sent in advance of your observing run, with the subject line “NOAO Science Archive Registration Invitation”). It will contain your pre-assigned user name and an initial password. The user name by default is the user’s surname, followed by the first initial of their first name.
- **If you are already registered**, simply log in. PIs are automatically granted access to their proprietary data when they sign in to the Archive. PIs must authorize Co-Is of each of their programs in order for Co-Is to be granted access to the associated data. If you are a PI of an observing program in future semesters, data from that program will automatically be assigned to your existing Archive user account. There is no need to re-register, but you will need to authorize your Co-Is to allow them access to the data.



Co-Is: you must have the PI of your program(s) authorize access for you to obtain data from your program(s). PIs can enable access by clicking the [PI Admin](#) link in the banner of the Search page. For details, see the tutorial: http://portal-nvo.noao.edu/tutorials/get_my_data#CoIAccess.



New Archive registrations are *not available* to users unless they are a PI or Co-I of an NOAO observing program. Registrations do not expire, so your login will remain valid; access to new proprietary data will be authorized automatically in future observing semesters should you be awarded observing time.

To log in to the NOAO Archive Portal at <http://portal-nvo.noao.edu/>, select [Log in](#) at the far right of the menu bar (see Figure 1-6), and enter your user ID and password.



Figure 1-6: Banner for the NOAO Science Archive Portal, highlighting the Log in link (*right*). Users will also be taken to the login page using the Search My Data option from the Search Type pull-down menu on the Search NOAO Data page in Figure 1-4.

Once an Investigator for a program is logged in to the Portal, queries and retrievals for proprietary data proceed in exactly the same way as for nonproprietary data.

1.4 Data Use Policy

There are a number of conditions that apply to the use of data from the NOAO Science Archive and the Survey Archive; see <http://www.noao.edu/noaoprop/help/datarights.html> for details. In general, AURA (or one of the partner observatories), possibly in addition to the PI of the program, assert ownership of the intellectual property that includes the data and derived products (including catalogs, but not including scientific papers), subject to a royalty-free license to the US federal government. AURA policy provides for free use of these data for scientific research, following a limited period during which the investigator of a program has exclusive (proprietary) rights to those science data. Use of the data and derived products also requires that users provide appropriate attribution (see below).

1.4.1 Proprietary Period

The applicable proprietary period for science data depends upon the policy of the host observatory, and may be different under some circumstances. The default period for observing programs obtained through the NOAO time allocation process is 18 months from the calendar date of the exposure, except for programs granted “survey” status, for which the proprietary period is usually less. Requests for extensions may be granted by the NOAO Director, after receipt by the Time Allocation Committee of a well justified request from the PI. See <http://www.noao.edu/noaoprop/help/standard.html#ppperiod> for details. The proprietary period for a program may be *shortened* at any time at the discretion of the PI for that program.

1.4.2 Nonproprietary Data

Nonproprietary data include the following:

- all data obtained with any program to characterize the instrument health and performance, including bias and dark frames, flat-fields (including dome- and twilight-flats), comparison arc-lamp exposures, and focus exposures;
- all contemporaneous weather data, all-sky camera images, and seeing monitor data;
- all calibration reference frames that are produced by NOAO calibration pipelines, whether generated from closed-dome calibrations or on-sky science frames;

- all metadata from all exposures as soon as they are archived, including those from science frames, unless specific authorization has been granted by the NOAO Director to withhold these metadata for the duration of the proprietary period; and
- all science data for which the proprietary period has expired.

1.4.3 Proper Citation for NOAO Data

Acknowledgements for Archive Data

Authors of papers that make use of data from the NOAO Science Archive or the Survey Archive should include one of the following credit statements in their publications:

National Optical Astronomy Observatory / Association of Universities for Research in Astronomy / National Science Foundation

The above citation applies to data collected and processed by NOAO.¹⁷ If you use high-level science products that were generated by one of the Survey Project PI teams, the following credit statement should appear in your publication:

This research draws upon data provided by [Survey PI] as distributed by the NOAO Science Archive. NOAO is operated by the Association of Universities for Research in Astronomy (AURA), Inc. under a cooperative agreement with the National Science Foundation.

The identity of the Survey PI is given on the archive holdings¹⁸ web page.

Acknowledgements for DECam Data

Authors of papers that make use of DECam data products should provide a special acknowledgement.¹⁹ If you make use of DES data products produced by the *DES Collaboration*. The first line should be:

This research used public archival data from the Dark Energy Survey (DES).

Or, if you make use of DECam data products from NOAO-awarded community programs, as provided by NOAO, the first line of the acknowledgement should be:

This research used data obtained with the Dark Energy Camera (DECam), which was constructed by the Dark Energy Survey (DES) collaboration.

In either case, to the initial line add the following:

Funding for DES projects has been provided by the U.S. Department of Energy, the U.S. National Science Foundation, the Ministry of Education and Science of Spain, the Science and Technology Facilities Council of the United Kingdom, the Higher Education Funding Council for England, the National Center for Supercomputing Applications at the University of Illinois at Urbana-Champaign, the Kavli Institute of Cosmological Physics at the University of Chicago, the Center for Cosmology and Astro-Particle Physics at the Ohio

¹⁷ If you are an investigator of a program awarded through the NOAO time allocation process and *collected* the data you are publishing, there are additional acknowledgement requirements: see http://www.noao.edu/noao/library/NOAO_Publications_Acknowledgements.html.

¹⁸ <http://archive.noao.edu/nsa/holdings.html>.

¹⁹ Download the full text of the acknowledgement with LaTeX mark-up at: <http://www.noao.edu/noao/library/DECamAcknowledgement.tex>

State University, the Mitchell Institute for Fundamental Physics and Astronomy at Texas A&M University, Financiadora de Estudos e Projetos, Fundação Carlos Chagas Filho de Amparo à Pesquisa do Estado do Rio de Janeiro, Conselho Nacional de Desenvolvimento Científico e Tecnológico and the Ministério da Ciência e Tecnologia e Inovação, the Deutsche Forschungsgemeinschaft, and the DES collaborating institutions. The collaborating institutions are: Argonne National Laboratory, the University of California Santa Cruz, the University of Cambridge, Centro de Investigaciones Enérgéticas, Medioambientales y Tecnológicas-Madrid, the University of Chicago, University College London, the DES-Brazil Consortium, the University of Edinburgh, the Eidgenössische Technische Hochschule (ETH) Zürich, Fermi National Accelerator Laboratory, the University of Illinois at Urbana-Champaign, the Institut de Ciències de l'Espai (IEEC/CSIC), the Institut de Física d'Altes Energies, Lawrence Berkeley National Laboratory, the Ludwig-Maximilians Universität München and the associated Excellence Cluster Universe, the University of Michigan, National Optical Astronomy Observatory, the University of Nottingham, the Ohio State University, the University of Pennsylvania, the University of Portsmouth, SLAC National Laboratory, Stanford University, the University of Sussex, and Texas A&M University.

1.5 References & Further Information

Contributing Authors

People who have contributed to the description of the NOAO Science Archive and the NOAO Survey Archive include Dick Shaw, Mark Dickinson, Chris Miller, Howard Lanning, and Rob Seaman.

References

- FITS 2008, *Definition of the Flexible Image Transport System*, IAU FITS Working Group (Version 3.0: Greenbelt, MD: FITS Support Office, NASA/GSFC); available at http://fits.gsfc.nasa.gov/fits_standard.html
- Fitzpatrick, M. 2010, DTS: *The NOAO Data Transport System*, [SPIE, 7737, 44](#)
- Pence, W. D., Seaman, R., & White, R. L. 2009, *Lossless Astronomical Image Compression and the Effects of Noise*, [PASP, 121, 414](#)
- Rice, R. F., Yeh, P.-S., & Miller, W. 1993, *Algorithms for High-speed Universal Noiseless Coding*, in Proc. of the 9th AIAA Computing in Aerospace Conf., 499
- Seaman, R., Stobie, E., Economou, F., Valdes, F., & Herrera, D. 2014, *File Naming Convention for the NOAO Science Archive*, (Tucson: NOAO)
- Shaw, R. A. 2007, *Essential Imaging Metadata, DPP System Technical Report STR2007–01* (Tucson: NOAO)
- Smith, R. C., Dickinson, M., Lowry, S., Miller, C. J., Trueblood, M., & Valdes, F. 2007, *The NOAO End-to-End Data Management System: An Overview*, in ASP Conf. Ser. 376, ADASS XVI, ed. R. A. Shaw, F. Hill, & D. Bell (San Francisco: ASP), 615

For Further Reading

Additional documentation on the NOAO Archive Portal, including examples and tutorials, is available at <http://portal-nvo.noao.edu/tutorials/query>.

Chapter 2

Mosaic Cameras

Version 2.0, February 2015

In This Chapter...

Instrument Overview	2-1
Data Products	2-7
Calibration ...	2-14
Sources of Error ...	2-25
References & Further Information ...	2-28

The Mosaic cameras have been in operation at NOAO since 1999, and a good deal of technical literature exists on the instrument design, operation, and performance. The material presented here is drawn primarily from the *KPNO Mosaic-1.1 Imager User Manual* (Schweiker, Howell, & Sawyer 2011), and its precursor, the *NOAO CCD Mosaic Imager User Manual* (Schweiker & Jannuzi 2004). Interested users should consult these authoritative documents for details of the instrument configuration and operation. Additional resources are cited throughout this chapter and are listed along with other background material in the last section.

2.1 *Instrument Overview*

The Mosaic cameras have been among the most heavily used instruments offered by NOAO, as measured both by number of nights awarded to principal investigator (PI) programs, and by the volume of data in the NOAO Science Archive. There are actually three Mosaic cameras. **Mosaic-1** was used on both the Mayall 4-m and the WIYN 0.9-m telescopes on Kitt Peak, before it was upgraded to **Mosaic-1.1** in the fall of 2010 for exclusive use on the Mayall. **Mosaic-2** was used on the Blanco 4-m telescope at Cerro Tololo prior to its retirement in 2012. This chapter will cover all usages of these cameras; differences in the instrument design, usage, or other technical details that affect the data will be called out.

2.1.1 *Instrument Capabilities & Design*

The Mosaic cameras are optical/near-IR imagers with a wide, roughly square field of view (**FoV**) and a large focal plane array (**FPA**) containing a total of 8096×8096 pixels. A schematic of the instrument is

shown in Figure 2-1. Both KPNO and CTIO have a large number of *filters*²⁰ that are designed to be used with these cameras, up to 14 of which can be held in the filter track at one time. The filter sets include standard broad *passbands*, such as Harris *UBV* and Cousins *R*, *SDSS g r i z*, narrowband filters near $\text{H}\alpha$, $[\text{O III}] \lambda 5007$, and various others for nebular emission lines. Other filters, including filters provided by PIs for their observing programs, have been used occasionally. Consult the instrument manuals for details.

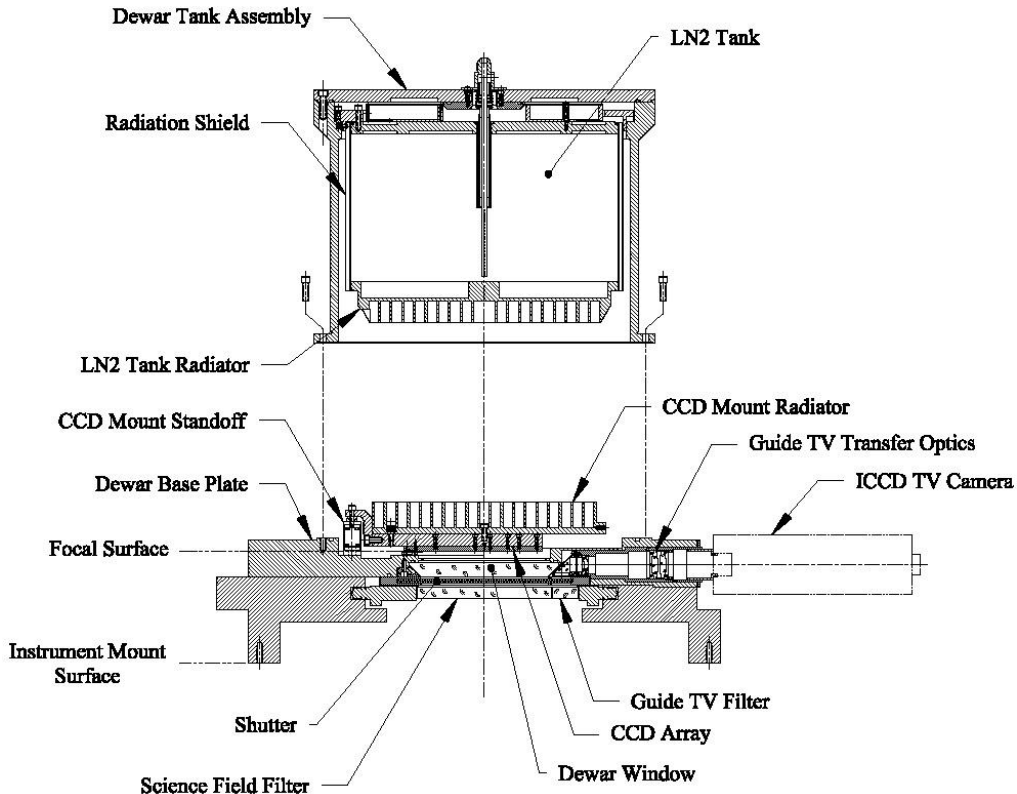


Figure 2-1: Cross-section view of the Mosaic Dewar, showing the arrangement of the CCD array and the filter. Light enters from below in this diagram and passes through the corrector optics (not shown) prior to passing through the Science Field Filter.

The details of the observing configurations for the Mosaic cameras are given in Table 2-1. The cameras are mounted at the Prime focal station of the 4-m telescopes, and at the Cassegrain focus of the 0.9-m telescope, with converging beams as indicated in the table. The detectors sample the delivered point-spread function (*PSF*) very well; image quality is seeing-limited at all wavelengths. The image quality at the 4-m telescopes is good, with little focus gradient or PSF variation across the FoV. The pixel scale changes slightly from the center to the edge of the field due to pincushion distortion. The image quality at the 0.9-m telescope is not as good: there is a small focus gradient across the FoV, resulting in degraded images near the corners of the field. Also, the corners of the field are slightly vigneted (~5–10%) by the internal telescope baffle. The image scale at the 0.9-m is relatively constant across the FoV.

²⁰Filter properties can be viewed at <http://www.noao.edu/kpno/mosaic/filters/filters.html>.

Table 2-1: Mosaic Camera Characteristics

	Mosaic 1 & 2	Mosaic 1.1	WIYN 0.9-m
Field of view	36' × 36'	36' × 36'	59' × 59'
Telescope focal ratio	f3	f3	f7.9
ADC ²¹ usage	Recommended	Recommended	N/A
Pixel scale at center/edge of FoV (arcsec/unbinned pixel)	0.261 / 0.245	0.261 / 0.245	0.425 / 0420
CCD Gaps			
in rows:	50 pix / 13.1"	80 pix / 20.9"	50 pix / 21.3"
in columns:	35 pix / 14.9"	80 pix / 20.9"	35 pix / 14.9"

An atmospheric dispersion corrector (**ADC**) is available on the 4-m telescopes for the Mosaic cameras (see Jacoby, et al. 1998 for details), and its use is recommended. The effect of atmospheric dispersion is greatest for very wide filters, and especially in the blue (stretching a stellar image by 0.9 arcsec in the *U* passband at a zenith distance of 60°, or 2 airmasses). Because of the wide FoV, differential atmospheric refraction within the field is noticeable even when using the ADC. In practice, though, the image quality is also limited by other factors such as telescope focus, differences in temperature between ambient and the primary mirror, and other factors (see Dey & Valdes 2014).



Note that the ADC is used at the discretion of the observer, though the Archive database suggests it was used >80% of the time when it would have significantly affected image quality. Users should check the `ADCSTAT` header keyword to determine whether the ADC was set to adjust continuously during the observation (`track`), set to be correct at the midpoint of the observation (`preset`), or disabled (`null`). Since no ADC was available at the WIYN 0.9-m telescope, broadband images obtained there suffered significant image degradation.

The shutter for the Mosaic cameras consists of a pair of opposing sliding blades, which serves to regulate the exposure time. The motion of the shutter blades is along columns (E–W), and the time-of-flight is approximately 23 ms. The accuracy of the shutter timing is good, but not perfect: a commanded 1 s exposure illuminates the FPA for 0.97 s at the top of the array, and 0.98 s at the bottom. A shutter shading correction is in principle possible, but most Mosaic science data usually are obtained with exposures greatly exceeding 1 s so that the correction would be negligible most of the time.

Focal Plane

The focal plane of the Mosaic cameras is populated with an array of eight **CCD** detectors, arranged in a 4×2 mosaic, as shown in Figure 2-2. Each of the thinned CCD sensors was operated²² with two **amplifiers** to read the arrays using both amplifiers in parallel. All the detectors have very few cosmetic defects.

²¹ Atmospheric Dispersion Corrector.

²² The Mosaic-1 camera did not have working dual amplifiers on all CCDs, and so was operated with one amplifier per CCD.

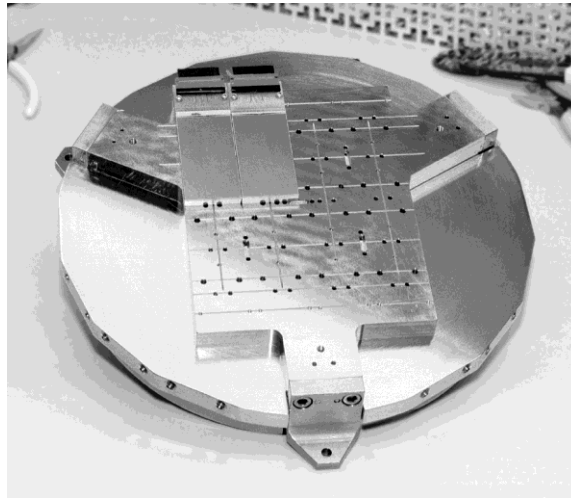


Figure 2-2: Mounting for the Mosaic-1 detectors, showing two of the eight 2048×4096 pixel CCD arrays in position.

The detector properties, or ranges of properties, are given in Table 2-2. The linearity is good, but the dynamic range for Mosaic-1 and Mosaic-2 was modest by modern standards and varied from detector to detector. The charge transfer efficiency (CTE) is good or excellent and is not believed to have degraded in time. The pixels may have been binned at read-out by integral factors. Observers using the Mosaic-1 and Mosaic-2 cameras have selected this option with some regularity to reduce the read-out time (e.g., for observations of variable phenomena or moving targets that require a rapid cadence), or to reduce the read noise per binned pixel (compared to post-read down-sampling). The penalty, of course, is the possibility of under-sampled images and reduced spatial resolution, depending upon the seeing at the time of the observations.

Table 2-2: CCD Sensor Characteristics

Parameter	Mosaic 1 & 2	Mosaic 1.1
Sensor Type	SITe thinned CCD, 1-layer AR coating	e2v thinned, deep-depletion CCD, 2-layer AR coating
A-to-D dynamic range	16-bit	18-bit
Max. linear count	70,000 e^-	~210,000 e^-
CTE	>0.999995	>0.99998
Array Dimensions		
Axis 1:	2048 pix	2048 pix
Axis 2:	4096 pix	4096 pix
Pixel Size	15 μm	15 μm
Binning factors ²³	1, 2, 3, 4	1, 2
Gain	1.8 to 3.3 e^-/ADU	1.2 or 0.47 e^-/ADU
Read noise	5.0 to 9.0 e^-	5.9 or 3.2 e^-
Dark Current	5 $e^- / pix / hr$	4.4 $e^- / pix / hr$
Exposure overheads ²⁴		
binned 1 × 1	154 s	22 s
binned 2 × 2	66 s	11 s

²³ Configurable by observer, independently for each image axis.

²⁴ Times dominated by detector read-out, assuming a single amplifier.

The detectors reach peak quantum efficiency (QE) above 85% (see Figure 2-3), but have useful sensitivity from the atmospheric cut-off near 3200 Å to ~1 μm. The quantum efficiency (QE) varies somewhat from detector to detector in the older cameras, both on average and as a function of wavelength. Therefore, the transformation from instrumental magnitudes to standard systems depends upon both the passband and the detector. This problem is greatly reduced with Mosaic-1.1, except in the *U*-band. See “Photometry” on page 2-26.

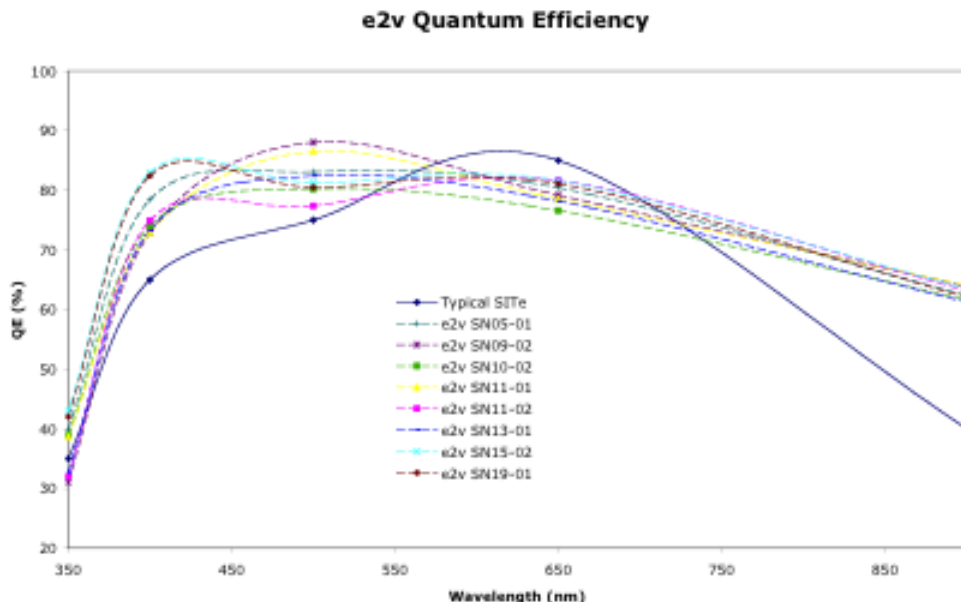


Figure 2-3: Quantum efficiency for the e2v detectors in Mosaic-1.1, along with the typical QE curve for the older Mosaic cameras (see legend).

Figure 2-4 shows the arrangement of the FPA on the sky using the same nomenclature as is found in the science data extension headers. Note that the orientation is rotated in the Southern Hemisphere relative to the Northern Hemisphere. The raw image array coordinates are re-mapped from the detector coordinates, such that the origin is always in the lower-left corner when oriented as in the figure. For reduced data, the images are reoriented so that north is up and east is to the left.

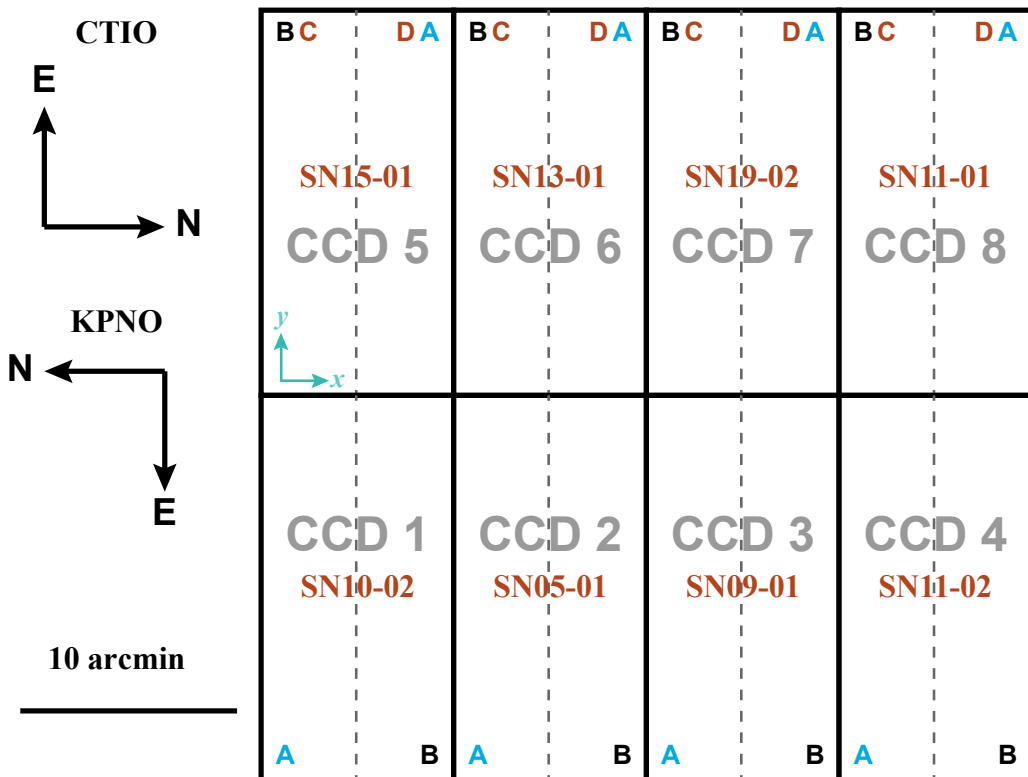


Figure 2-4: Orientations on the sky and spatial footprint of the FPA for the Mosaic cameras, with CCD detector designations indicated for Mosaic-1 and Mosaic-2 (grey) and for Mosaic-1.1 (brown). Two amplifiers on each chip are normally used for parallel read-out (except for Mosaic-1) over areas separated by dashed lines. Amplifier designations are indicated near the origin of the sub-arrays for Mosaic-1 (black), Mosaic-2 (blue and black), and Mosaic-1.1 (same as Mosaic-2, except for brown in the upper row). Image coordinate axes also are indicated for one array (teal arrows); the coordinate origin is in the lower-left corner of each detector array or sub-array.

2.1.2 Operations

Most data obtained with the Mosaic cameras have a binning of 1×1 or 2×2 pixels. Many observers obtained multiple exposures of their fields using the same filter in order to reject cosmic rays; often this was combined with a sequence of small spatial *dithers* in order to observe in the gaps between the CCDs in the FPA and to enable the construction of continuous regions of sky free of gaps and detector artifacts. A few observing programs construct sequences of (slightly) overlapping images to *map* larger regions of sky from the component tiles. Finally, most (but not all) observing programs obtain calibration frames, such as bias (zero) frames and dome flats, in order to facilitate calibration. See “Calibration” on page 2-14 for a detailed discussion of how the calibration frames are used in the data reduction process.

2.2 Data Products

This section describes the content and format of the various data products that are produced for the Mosaic cameras. Most of the products are generated during the course of calibration processing, the details of which are discussed in the next subsection. The data products can be distinguished by the combination of the PROCTYPE, PRODTYPE, and OBSTYPE **keywords** in the FITS primary header; the possible values are summarized in Table 2-3. The *processing level* (see Table 1-2, “Levels of Data Processing,” on page 1-4) of the generated product is listed under *Proc. Level*.

Table 2-3: Data Product Content Type

PROCTYPE	PRODTYPE	OBSTYPE	Proc. Level	Description
Raw	image	object zero dark dome flat	1	Raw data as obtained at the telescope, with additional metadata included in the header. Note: OBSTYPE value unreliable in raw data.
InstCal	image	object	2	Calibrated, single-frame reduced image with instrument signature removed, WCS and rough photometric calibrations applied
	dqmask	object	2	Data quality mask for InstCal
Resampled	image	object	2	Calibrated, reprojected image
	dqmask	object	2	Data quality mask for Resampled image
Stack	image	object	3	Stack of 2 or more overlapping images
	dqmask	object	3	Data quality mask for Stacked image
	expmap	object	3	Exposure map for Stacked image
MasterCal	image	zero	2	Bias Residual structure image
MasterCal	image	dome flat	2	Dome Flat-field image
MasterCal	image	sky flat	2	Sky Delta-flatfield image
MasterCal	image	pupil	2	Pupil Ghost template image: generated only for Mosaic-1 data obtained at KPNO
MasterCal	image	fringe	2	Fringe pattern template image

2.2.1 Image Formats

The image data from the Mosaic cameras is stored either in FITS multi-extension files (**MEFs**) or, for some reduced data products, in simple FITS files with no extensions. Although most images are stored in extensions, the detailed arrangement of the image portions among the extensions differs depending upon whether the data are raw (unprocessed) or reduced, and upon the operational practice for each Mosaic camera.

The internal structure and data type for the various data products is summarized in Table 2-4 below, including the number and type of FITS extension(s). When retrieved from the Archive, the data files have

all been compressed with FITS tile-compression. This applies to images with both integer and floating-point native representations; floating-point compression is applied using the Rice compression technique, which should not significantly degrade the dynamic range of the data.

Table 2-4: Product Organization and Data Types

PROCTYPE	PRODTYPE	Ext Type	N. Ext	Data Type
Raw	image	IMAGE	16/8	16-bit ²⁵ int
InstCal	image	IMAGE	8	32-bit float
	dqmask	IMAGE	8	32-bit int
Resampled	image	[primary]	0	32-bit float
	dqmask	IMAGE	1	32-bit int
Stack	image	[primary]	0	32-bit float
	dqmask	IMAGE	1	32-bit int
	expmmap	IMAGE	1	32-bit int
MasterCal	image	IMAGE	16/8	32-bit float

Raw Data

Raw pixel values from the Mosaic cameras are integers, and include virtual overscan along each row at the beginning (pre-scan, for Mosaic-1 and Mosaic-2) and at the end (over-scan, for all cameras) of the CCD read-outs, which is stored with the raw image pixels as shown in Figure 2-5. Note that the coordinate origin for all images is in the lower-left corner of the read-out section (for the convenience of image display), rather than at the location of the read-out amplifier. Each detector in the Mosaic cameras has two read-out amplifiers to enable parallel read-out of both halves of the arrays. But in practice, the Mosaic-1 camera uses only one amplifier. The output from each amplifier (including the virtual overscan regions) is stored in a separate image extension in the FITS MEF file (see Chapter 1); thus, there are as many image extensions in the raw science file as the total number of amplifiers used to read out all detectors in the focal plane. The size and location of the photo-active regions and the overscan are given in Table 2-5 below. Only a portion of the overscan region is used by the processing pipeline: see “Bias Correction,” on page 2-17.

²⁵ Raw images from Mosaic-1.1 are 32-bit integers.

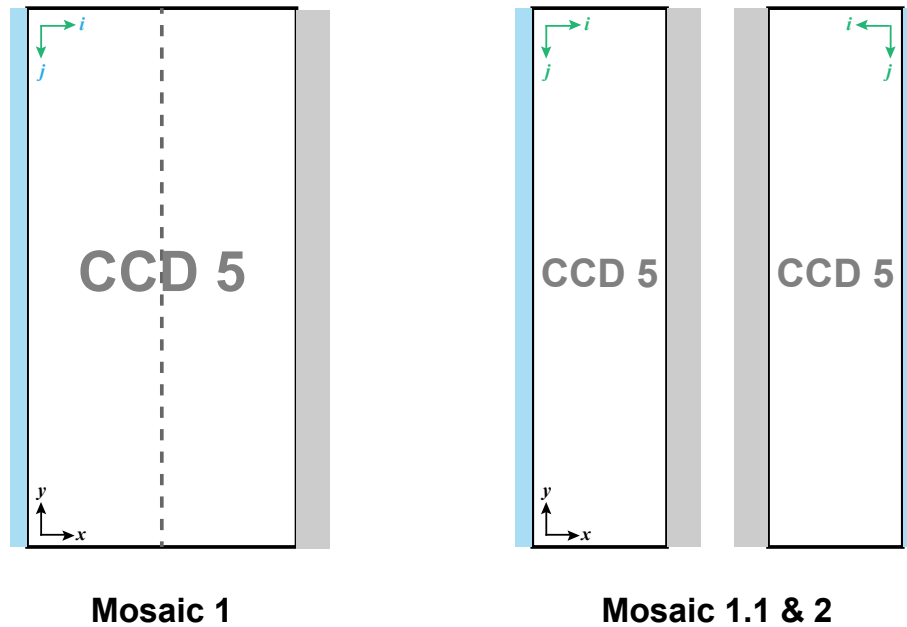


Figure 2-5: Schematic of the image arrays just after read-out for detector 5 of the Mosaic cameras (*left*, Mosaic-1; *right*, Mosaic-1.1 and Mosaic-2). Virtual overscan regions are indicated as shaded boxes (*blue*: pre-scan for Mosaic-1 and Mosaic-2; *grey*: over-scan), but are expanded horizontally for clarity. Amplifier locations are near the origin of the green amplifier coordinate axes, prior to transformation to FPA coordinates. The black coordinate axes are near the origin of the CCD pixel array.

Table 2-5: Raw Data and Overscan Regions

Raster Dimensions	Detectors	Image Extension	Amp	Photo-Active Data Section	Bias Section (Columns)
Mosaic-1					
2136 × 4096	1–4	1–4	B	[65:2112, 1:4096]	[1:50]
	5–8	5–8	B	[25:2072, 1:4096]	[2087:2136]
Mosaic-1.1					
1074 × 4096	1–4	1–4	A	[1:1024, 1:4096]	[1025:1074]
		9–12	B	[1:1024, 1:4096]	[1025:1074]
1074 × 4096	5–8	5–8	C	[1025:2048, 1:4096]	[1025:1074]
		13–16	D	[1025:2048, 1:4096]	[1025:1074]
Mosaic-2					
1112 × 4096	1–4	1–4	A	[25:1048, 1:4096]	[1063:1112]
			B	[65:1088, 1:4096]	[1:50]
5–8	5–8	A	[65:1088, 1:4096]	[1:50]	
		B	[25:1048, 1:4096]	[1063:1112]	

Calibrated Data

The Archive contains data products that are produced with the Mosaic calibration pipeline. The specific calibrated science data products are listed in Table 2-3 on page 2-7 and are described in more detail below. Each image has an associated *data quality mask (DQM)*, which is described at the end of this subsection.

InstCal. These images have been processed to remove instrumental signature, and have been astrometrically and photometrically calibrated (see “Calibration” on page 2-14), although there are some cases where the calibration can fail (see “Sources of Error” on page 2-25). The data are organized almost identically to that for the raw science data, except for the following:

- The overscan regions have been trimmed from the image arrays.
- Image portions for a given detector that were read by different amplifiers have been joined. Thus, the files contain 8 image extensions, one for each detector.
- The resulting images in each extension are all 2048×4096 pixels.

Resampled. These images are the result of geometrically rectifying InstCal images, where each array has been re-projected to a common *tangent-point* on the sky, with pixels aligned to a common grid with uniform scale. The pixels have been reoriented so that, when displayed, images will appear with north “up” (i.e., declination increases along Axis 2) and east “left” (i.e., Right Ascension decreases along Axis 1). The images are stored in the primary header-data unit within the file. The tangent-point is selected from a grid with roughly 1° steps in RA, and exactly 1° in Dec. The aim is to maximize the probability that exposures from different nights and processing runs may be combined without requiring further interpolation. Within a single night, all overlapping exposures, such as from dither sequences or serendipitous overlapping pointings, are assigned a common tangent point even if some elements of a dither would have been assigned to different grid points when considered independently. The Resampled images are approximately 8526×8642 pixels; the actual size depends on the degree of differential atmospheric refraction and the *WCS* tangent point selected for a particular image.

Stacked. If two or more observations of a given target are obtained on the same night using the same filter and have a sufficient degree (~10%) of spatial overlap, these images are combined using an average with outlier rejection to remove detector blemishes, gaps between the detectors, and artifacts such as image persistence and cosmic rays. The result is a union of the spatial footprints of the stack, which is stored in a simple FITS image (i.e., not in image extensions), with the same pixel scale as the Resampled images. In general, these images will be larger—sometimes very much larger—than the Resampled images because the area of the sky that is mapped can be significantly larger than the instrument FoV.



The exposure duration for Stacked images, as recorded in the EXPTIME keyword, refers to the sum of all exposure durations of all images used to create the stack. The exposure depth and noise properties of a stack of dithered images are a discontinuous and possibly complicated function of position in the image. Use the exposure map to track the detailed exposure depth at the pixel level

Master Calibration. Reference files are created from many calibration exposures, often from exposures obtained during the same observing run, and include residual bias structure, flat-fields, etc. These files are used in pipeline processing to remove particular instrumental signatures from the science data. (See “Calibration Reference Files” on page 2-21.)

Concomitant Data. All reduced images are accompanied by data quality masks (DQM); Stacked images also are accompanied by exposure maps. The DQMs and exposure maps are images, with as many extensions as in the corresponding science image. The pixel values in the DQMs are nonzero when affected by detector pathologies and image artifacts such as bleed trails, saturation, and cosmic rays; the values are zero otherwise. Table 2-6 lists mask values that are applicable to *non-stacked* images.

Table 2-6: Data Quality Mask Values

Value	Meaning
0	No problem
1, 6	Bad/compromised pixel identified in static DQM; generally indicates known detector blemishes
2	[Not used]
3	[Not used]
4	Saturated (plus padding)
5	Bleed trail (plus padding); indicates possibly compromised pixels
7, 8	Transient artifacts (includes cosmic rays)

Most *Stacked* images are created from dithered frames, so that most of the pathologies affecting single frames will not be applicable. DQMs for Stacked images have the following values: “1” for areas of the re-projected image with no data, “2” for areas with no data *after rejection*, and zero otherwise.

The exposure maps are images whose values are the cumulative exposure duration at each pixel, which can be a complicated function of position. The value of the EXPTIME keyword in a Stacked image is the sum of the exposure durations for all images that contributed to the stack.

2.2.2 Header Keywords

A wide variety of metadata are recorded in the headers of the science frames. Users should review these headers (and the extension headers) to familiarize themselves with the content. The more critical metadata are described in this subsection. Table 2-7 lists metadata by the keyword name, the Mosaic camera(s) to which the keyword applies, the header unit in which it will be found (Primary or Extension), the point in the data processing where it is introduced (or where the value is updated), and the meaning of the keyword (or group of keywords, if they are related). Some of the keywords are indexed by image axis, meaning they come in pairs, as indicated by the suffixes *i* and *j*.

Table 2-7: Important Processed Image Keywords

Keyword Name	1&2	1.1	HDU	Origin	Meaning
Telescope					
ADC	•	•	P	R	Identification of the Atmospheric Dispersion Corrector (ADC)
ADCSTAT	•	•	P	R	ADC tracking status
AIRMASS	•	•	P	R	Atmospheric path-length for target at observation start
PARALL		•		R	Parallactic angle (deg)
TELESCOP	•	•	P	R	Telescope used to obtain these data
TELDEC	•	•	P	R	Declination for the telescope position on the sky (deg)
TELRA	•	•	P	R	Right ascension for the telescope position on the sky (hr)
Instrument/Detector Configuration					
CCDSUM	•	•	E	R	CCD binning factors along Axis1 and Axis2
DETECTOR	•		E	L2	Detector designation
FILTER	•	•	P	R	Filter name/designation
GAIN	•	•	E	R, U	Detector effective gain (e^-/ADU)
INSTRUME	•	•	P	L2	Instrument name
OGAIN	•		E	L2	Original detector gain setting for the exposure (e^-/ADU); same as GAIN for raw images
SATURATE		•	E	R	Approximate saturation level (ADU)
Dither Sequence²⁶					
NOCDDOF		•	P	R	Dither offset in Dec (arcsec)
NOCDHS		•	P	R	DHS script name
NOCDITER		•	P	R	Dither iteration count
NOCDPOS		•	P	R	Dither position
NOCDROF		•	P	R	Dither RA offset (arcsec)
NOCNO		•	P	R	Observation number in this sequence
NOCNUM		•	P	R	Observation number request
NOCPAT		•	P	R	Map pattern
NOCDREP		•	P	R	Dither repetition count
NOCTOT		•	P	R	Total exposures in dither set
Time					
DATE-OBS	•	•	P	R	Date and time of observation start
EXPTIME	•	•	P	R	Exposure duration(s)
MJD-OBS	•	•	P	R	Time of observation start in MJD
TIME-OBS	•	•	P	R	Time of observation start
TIMESYS	•	•	P	R	The principal time system for all time-related keywords. Always UTC.
World Coordinates					
CD <i>i,j</i>	•	•	E	R, U	Transformation matrix from pixel to intermediate world coordinates; CD <i>i,j</i> is the pixel scale for axis <i>i</i>
CRPIX <i>i</i>	•	•	E	R, U	Location of the reference point along axis <i>i</i> (pix)

²⁶ These keywords are not used by the processing pipeline.

Keyword Name	1&2	1.1	HDU	Origin	Meaning
CRVAL <i>i</i>	•	•	E	R, U	Value of the world coordinate at the reference point for axis <i>i</i> (deg)
CTYPE <i>i</i>	•	•	E	R	Name of the coordinate represented in axis <i>i</i>
DEC	•	•	P	R, U	Declination for the center of the detector FoV (deg)
EQUINOX	•	•	E	R	Equinox in years for the celestial coordinate system in which the positions are expressed
NAXIS <i>i</i>	•	•	E	R	Number of pixels along axis <i>i</i>
PIXSCAL <i>i</i>	•		E	R	Pixel scale along axis <i>i</i> (arcsec/pix)
RA	•	•	P	R, U	Right ascension for the center of the detector FoV (hr)
RADESYS <i>i</i>	•		E	R, U	Name of the reference system in which the world coordinates labeled by <i>i</i> are expressed
RADECSYS		•	P	R, U	Name of the reference system in which the world coordinates (in the extensions) are expressed
WAT <i>i_nnn</i>	•	•	E	R, U	IRAF-specific description of the nonlinear portion of the transformation from detector to world coordinates for axis <i>i</i> . This character string contains coefficients for a polynomial; the length of the string is such that it must continue for <i>nnn</i> FITS header records.
Calibration					
BLDPROC	•	•	E	L2	Bleed trail processing parameters (bleed threshold & grow radius)
BUNIT	•	•	E	L2, L3	Brightness units, normally “electron/s” for calibrated images
MAGZERO	•	•	E	L2	Magnitude corresponding to one count/s in the image
OBSTYPE	•	•	P	R, U	Type of target observed (see Table 2-3 on page 2-7)
PHOTBW	•	•	P	L2	RMS width of bandpass (Å)
PHOTCLAM	•	•	P	L2	Central wavelength of bandpass (Å)
PHOTDPTH	•	•	P	L2	Photometric depth of the exposure (see “Photometric ” on page 2-19)
PHOTFWHM	•	•	P	L2	FWHM of bandpass (Å), i.e., width measured at 50% of peak transmission
PIPELINE	•	•	P	L2, U	Pipeline name
PLVER	•	•	P	L2, U	Pipeline version identifier
PROCTYPE	•	•	P	L2, U	Product type (see Table 2-3 on page 2-7)
PRODTYPE	•	•	P	L2, U	Product data description (image mask expmap)
SATPROC	•	•	E	L2	Saturation processing parameters (saturation threshold & grow radius)
SEEING	•	•	P	L2	Average FWHM of bright point sources within image (arcsec)
SKYADU		•	P	L2	Sky background (ADU)
SKYBG	•		P	L2	Brightness level of background averaged over all CCDs (ADU)
SKYBG1	•		E	L2	Brightness level of background in single CCD (ADU)
SKYMAG		•	P	L2	Sky flux (mag/arcsec ²)
SKYNOISE	•	•	P	L2	RMS noise in the background level (ADU)

2.2.3 Environmental Data

At present no environmental data are accessible from the Archive, although data from all-sky cameras and seeing monitors are often available. A terse summary of sky conditions at CTIO²⁷ and at KPNO²⁸ are available online.

2.3 Calibration

The current generation of pipeline processing produces Level-2 products, i.e., images where the instrumental signature has been removed and geometric and photometric calibrations have been applied; and Level-3 products, where spatially overlapping images in the same filter (and that have been obtained within the same observing run) have been stacked. The pipeline uses both calibration exposures, such as bias frames and dome flats, as well as portions of science exposures (i.e., areas free of defects, artifacts, and astrophysical objects) to construct the calibration reference files that are used as input to the processing. For simplicity, the subsections below will first describe the processing of single-frame science images once the calibration reference files are available, followed by the combination of overlapping science exposures; the processes for constructing the calibration reference files will then be described with the overall flow as context. The actual sequence of processing in the pipeline software differs somewhat in detail, in part to optimize the performance of the parallel processing environment.



The calibration pipeline for Mosaic reductions is tuned to maximize the use of exposures within the observing run in which they were obtained. As such, the quality of the data depends to a large degree on the quality of the calibration exposures that were obtained by the observer. However, if the quality of the master calibrations is poor (as judged by the pipeline operator), the pipeline will attempt to use calibration data from the nearest prior or subsequent observing runs.



This pipeline *does not* process Mosaic data that were obtained with the WIYN 0.9-m telescope. This pipeline *only* processes data obtained with a CCD binning of 1×1 (using either 4-m telescope).

2.3.1 Single-Frame Processing

The flow of single science exposures through the pipeline is shown in Figure 2-6. Each step of the processing, indicated by the boxes in the center of the figure, is described in detail in the following subsections. As explained below, certain steps are not performed for data where the correction in question is not needed. Inputs to the processing include the raw science frames, calibration reference files (see

²⁷ http://www.ctio.noao.edu/site/phot/sky_conditions.php.

²⁸ http://www-kpno.kpno.noao.edu/Info/Mtn_Weather/.

“Calibration Reference Files” on page 2-21), and photometric and astrometric catalogs. Outputs include the various reduced science images, plus their associated mask files (see “Image Formats” on page 2-7). Intermediate products that are produced during the course of pipeline processing, but are not archived, are not shown. The processing is segregated by observing block and filter, and further by spatially overlapping observing sequences when deriving Stacked images.

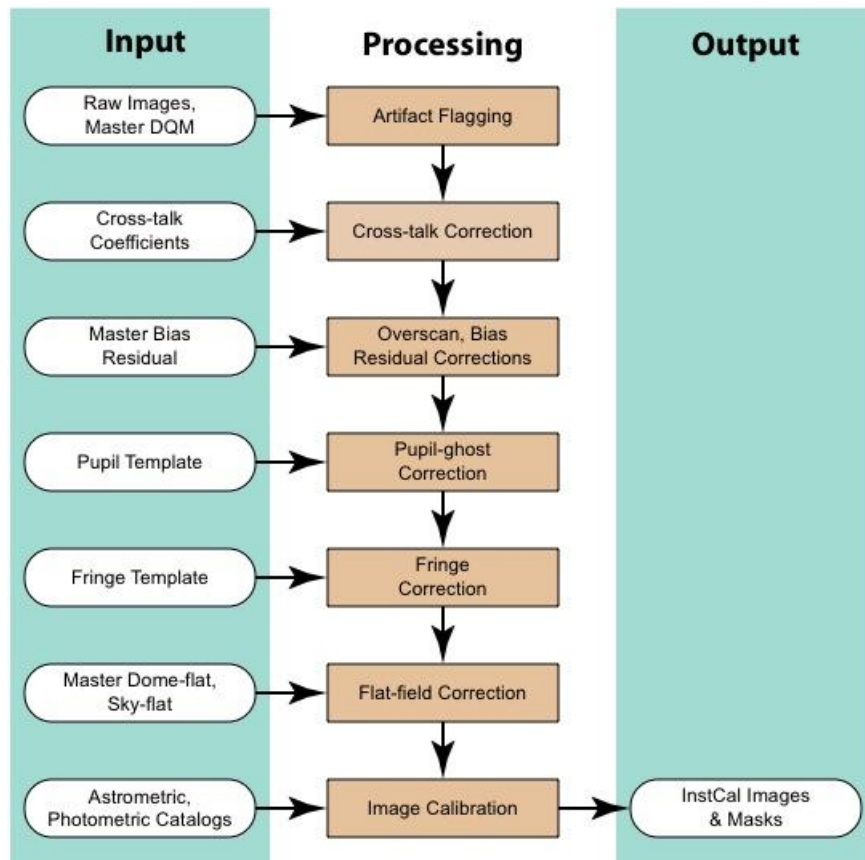


Figure 2-6: Flow of Mosaic data taken with a common filter through pipeline processing and calibration to produce Level-2 data products. External catalogs, and data products defined in Table 2-3 on page 2-7, are shown as inputs or outputs of the processing.

Artifact Flagging

Various image artifacts, including detector defects marked in the Master DQM reference file, are flagged in the DQM for each science image. In addition, pixels with values above the saturation threshold²⁹ (given by the SATURATE keyword) for the parent CCD are flagged near the beginning of the processing. Further artifact flagging occurs later in the processing, including *transients* (e.g., moving objects and cosmic rays) which are detected during the final image stack. Note that the regions flagged using the saturation and bleed trail thresholds are grown by up to a few adjacent pixels to minimize the risk of compromised data near artifacts. The final data quality mask for each InstCal image indicates all detected artifacts noted

²⁹ The pipeline does not distinguish between saturation of the full-well vs. the A-to-D converter.

above; these values are propagated to the Resampled Images, which generally increases the number of affected pixels to include areas adjacent to the pixels in the original geometry. All flagged pixels are excluded from contributing to the Stacked image; if this process results in areas with no data, such pixels are so flagged (see “Concomitant Data” on page 2-11 for details).



All pixels in calibrated science frames (**InstCal**, **Resampled**, and **Stacked**) that are flagged in the DQM with a value other than zero will be interpolated over. The 1-dimensional linear interpolation is performed along the shortest dimension of the region over which to interpolate. This process is intended to avoid introducing “ringing” artifacts during the down-stream resampling of the images, as well as to mitigate scaling problems when using image display software. The affected pixels retain their flags in the DQM, however.

Cross-Talk Correction

A small but significant amount of *cross-talk* occurs between the video channels of the CCDs in the FPA. The effect is to introduce a small fraction of the signal from one channel of a CCD into the signal chain of the other, or between adjacent CCDs, such that “ghosts” of bright objects appear in the paired CCD. This is a significant additive effect of ~0.1% (0.2% for Mosaic 1.1) for amplifiers from the same CCD and about an order of magnitude less between adjacent CCDs. The effect is most noticeable where sources are at or near saturation. The proportionality coefficients differ from one video channel to another, but are relatively stable over time.

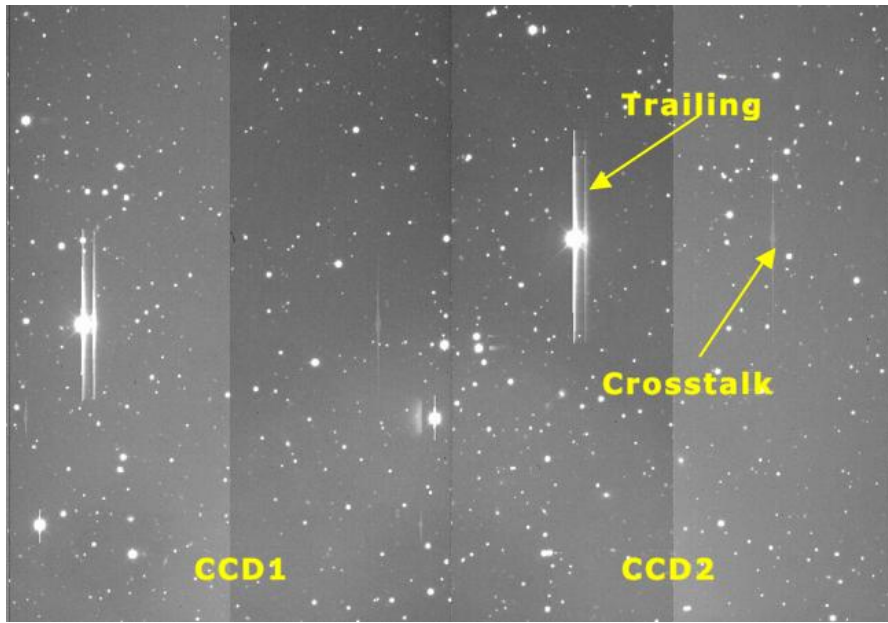


Figure 2-7: A portion of a raw Mosaic-1.1 image showing the effects of cross-talk from saturated regions (bright stars and bleed trails), as well as the trailing electronic ghost anomaly. The trailing electronic ghost is only present in Mosaic-1.1 data.

Mosaic-1.1 also exhibits a “trailing electronic ghost” anomaly where full-well saturated pixels produce a ghost image that trails the star (and bleed trail) in the readout direction (i.e., away from the read-out amplifier). The anomaly is currently not understood, nor has it been characterized in detail. The processing pipeline applies pre-calibrated proportionality coefficients and subtracts the simple cross-talk signature from the images ***but it does not correct for the trailing electronic ghost*** from Mosaic-1.1 science images. Users will likely want to mask such regions prior to making photometric measurements.

Bias Correction

This correction is applied to remove the (additive) electronic bias that is present in the signal chain. The bias is, for the most part, composed of a constant pedestal, but it has structure that is related to the electronic stability of the bias during read-out of the detector. The processing pipeline removes the bias contribution in a two-step process. In the first step, most of the post-scan region (see Table 2-5 on page 2-9) is averaged along the serial direction, and this average value for each image line is subtracted. The virtual overscan regions (i.e., the pre-scan and the post-scan; see Figure 2-5 on page 2-9) are then removed from the image. In the second step, the Master Bias Residual image is subtracted from each science image to remove higher-order structure.

[Dark Correction]

The dark current, i.e., the signal introduced by thermal electrons in the detector with the instrument shutter closed, is extremely low for the Mosaic CCDs, so ***no dark correction is applied in the processing pipeline***. Were a dark correction implemented, it would occur after bias correction and would be applied by subtracting a dark-rate master frame from the science frames, after scaling by the exposure time.

[Linearity Correction]

The CCD sensors for all Mosaic cameras are relatively linear in their response through their entire dynamic range (for Mosaic 1.1, the deviation from linearity is <0.5%), so ***no linearity correction is applied in the processing pipeline***. Were a linearity correction implemented, it would occur after dark correction and would be applied using either a functional fit to the linearity curve or by using a look-up table.

Pupil Ghost Correction

The pupil ghost is evident in data from Mosaic-1.1, and from Mosaic-1 when used at the 4-m telescope. The artifact is caused by light that reflects off the filter, off the back surface of the corrector, and returns through the filters to the detector. The effect is evident in raw data as an image of the telescope pupil near the intersection of the central four detectors (see Figure 2-4 on page 2-6). The amplitude of the effect is greatest where the coating of the corrector is least effective: in the extremes of red and blue, particularly the *U*-, *I*-, and *z*-bands, and in narrowband filters of similar wavelength. The pupil ghost template is scaled to the intensity of the pattern in each science frame and subtracted.



The pupil ghost correction is only applied to data obtained with the Mosaic-1 and Mosaic-1.1 cameras on the 4-m telescope on Kitt Peak, and only for exposures taken through broadband or narrowband filters with central wavelengths near *U*, *B*, and *I*. No pupil ghost is evident in Mosaic-1 data when used at the WIYN 0.9-m telescope, or in Mosaic-2 data on the CTIO 4-m telescope.

Fringe Pattern Correction

A fringe pattern is evident in data from both Mosaic cameras at red wavelengths. The pattern occurs because of interference between the incident, nearly monochromatic light from night sky emission lines (from both air glow and reflected city lights) and light that is reflected internally between layers of the CCD substrate. The details of the fringe pattern depend mostly upon the spatial variation in thickness of the top layer in the substrate, but also depend upon a number of other factors including the wavelengths of the incident emission lines, the composition of the substrate, the temperature of the CCD, and the focal ratio of the incident beam. (See Walsh, Pirzkal & Pasquali 2002 for a useful discussion of this phenomenon in the ACS camera on the *Hubble Space Telescope*.) The amplitude of the fringe pattern background varies with time and telescope pointing. Since the amplitude of the fringes can be large compared to the mean sky background, it is important to remove it where possible. An example of fringing over a portion of an image can be seen in Figure 2-8. To remove the effect, the fringe template is scaled to the science image and subtracted.

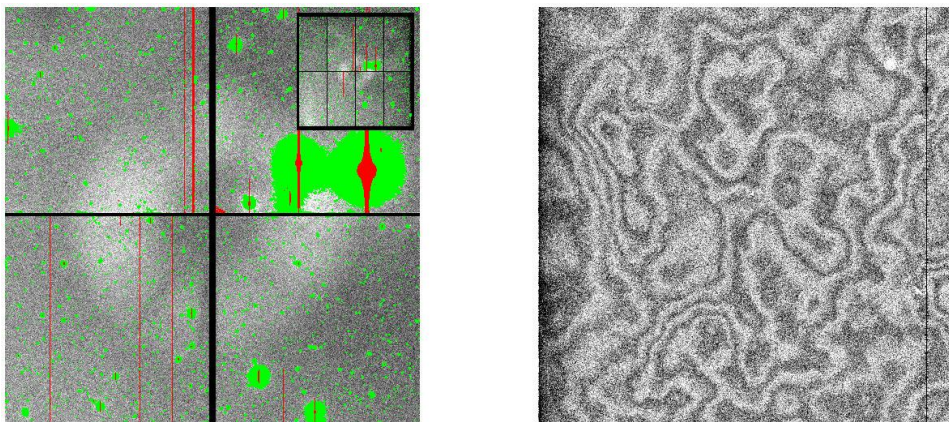


Figure 2-8: Example of the pupil ghost pattern (*left*, with bright targets and artifacts masked) near the intersection of the central four detectors in the Mosaic FPA. A fringe pattern (*right*, a 512×512 region) is evident in images obtained with red filters.



The fringe correction is only applied to exposures taken through narrowband filters, or through broadband filters with central wavelengths greater than 6290 Å.

Flat-field Correction

The flat-field correction removes the variations in the pixel-to-pixel response of the detector. The correction is derived for each filter from dome-flat exposures. Ideally the flat-field should be derived for each filter from blank sky (i.e., the sum over all science images of the background regions), in order to match the illumination of the pixels in science images as well as the color of the background. However, if there is insufficient illumination of the background pixels, it may not be possible to construct a sky flat of sufficient quality (see “Sky Delta-Flat” on page 2-24). In any case, the flat-field correction is performed by dividing each science frame by the Master Flat-field images for the corresponding filter: first by the Master Dome Flat, and then by the Master Sky Flat (if available).

Following the flat-field correction, the pixels are effectively scaled to the average gain factor in the FPA, and then normalized to unit exposure time. The brightness units, as expressed in the value of the `BUNIT` keyword, are electrons s^{-1} (or roughly, detected photons s^{-1}) for calibrated images.

World Coordinate System Calibration

The WCS calibration for science images is described by a two-dimensional polynomial (the function type and coefficients are found in the header) of a tangent-plane projection of stellar coordinates to the image pixel grid. The lower-order terms relate to the location of the reference pixel on the sky, the plate scale, and the rotation of the image, while the higher-order terms relate to nonlinear effects of the optical system (such as image distortion) and differential atmospheric refraction. The form and order of the function varies with the filter and with the airmass of the observation. The initial values for all but the zero-point terms are taken from prior, full WCS solutions of calibration images where the astrometry of the stars in the field is known with high accuracy; the initial value for the telescope pointing is taken from the `TELRA` and `TELDEC` header keywords, which are supplied by the telescope control system.

A full WCS solution is determined for each CCD by associating centroids of stars in the science images with objects in an astrometric catalog. Since the number of suitable stars in any given image (and their distribution within the image) can vary considerably, depending upon such details as the stellar density at the exposure depth, ambient seeing, and clouds, the input list to the WCS solution includes roughly 100 additional pseudo-stars, which are merely computed points from the trial WCS solution. Thus, if the number of genuine stars in the image is small compared to the pseudo-stars, the high-order terms in the WCS solution will be dominated by the trial solution. If instead the number of genuine stars is large, they will dominate the WCS solution. In all cases, only the genuine stars contribute to determining the zero-point. The WCS solution, while robust, may fail if the telescope pointing is in error by several arcminutes or more (which is rare). See “Sources of Error” on page 2-25 for details.

Photometric Characterization

An estimate is made of the magnitude zero-point of each science image by comparing the instrumental magnitude of each field star to their published magnitudes in nearby passbands in a reference catalog, applying color transformations as necessary. Currently, the reference photometric catalog is USNO-B1.0 (see Monet, et al. 2003). Note that the result of the photometric calibration is to populate the science header with keywords—the pixel values remain unchanged and have units of detected photons s^{-1} .

One quantity of use, the photometric depth of the exposure, is defined as:

$$-\frac{2.5}{2.3026} \log\left(\frac{3.988 \cdot Q \cdot \sigma}{\sqrt{A}}\right) + m_{zero}$$

In physical terms, the photometric depth is the faintest point-source that can result in a 5σ detection above the sky background, in units of magnitudes. In the equation above, Q is the FWHM of point-sources (expressed as the value of the header keyword SEEING in the image header) in units of arcseconds, σ is the noise in the background in electrons, A is the area of a pixel in arcsec², and m_{zero} is the magnitude zero-point. This quantity is stored in the header of the calibrated images as the value of the PHOTDPTH keyword. At present the photometric calibration is not adequate to support science and is intended solely as a rough estimate of exposure depth to support archive queries. See “Sources of Error” on page 2-25 for details.



Note the importance of the exposure time and the mean sky values that were determined during pipeline processing. These values, plus the detector gain, are stored in FITS header keywords and must be used to reconstruct the original source counts and background (in units of detected photons) when computing the statistical errors on measurements such as source magnitudes.

2.3.2 Image Stacks

The second phase of processing takes multiple, spatially overlapping **InstCal** images obtained with the same filter and combines them into a Stacked image. The processing flow is shown in Figure 2-9.

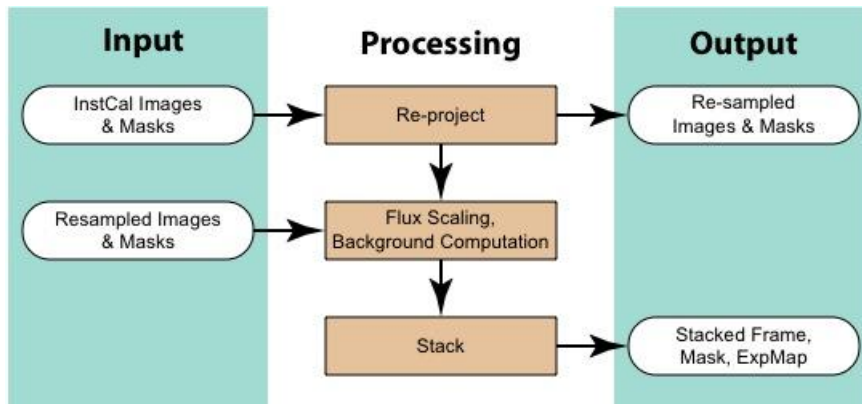


Figure 2-9: Process flow for creating Level-2 and Level-3 Mosaic data products: re-projected images and stacks of overlapping images.

Image Re-projection

A single, re-projected Mosaic image is constructed by resampling, using a *sinc* interpolation, the component science image sections. This form of the science data product is easier to use for image stacking and inter-comparisons, without the need to handle the distortion mapping. The astrometric system is a tangent-plane projection with a uniform sampling of 0.25 arcsec pixel⁻¹, oriented with north “up” (i.e., Declination increases along Axis 2) and east “to the left” (i.e., Right Ascension decreases along Axis 1). The **tangent-**

point is selected from a grid on the sky with roughly 1° steps in RA and exactly 1° in Dec. This selection makes it possible to stack images that are part of a sequence without further resampling.

Image Stacking

The spatial footprint of images obtained during a single observing run using the same filter are compared, and those that have at least a 10% areal overlap are combined into an image stack, which is an image containing the union of the spatial extent of all the constituent images. By construction, the pixel grids of the constituent images are aligned (see “Image Re-projection” above), so the first approximation to the output stack is the median of all non-masked pixels in the stack, after adjusting for the average sky background in each input image. This approximation is used to identify outliers (transients and artifacts such as cosmic rays and hot pixels) in the constituent images that are marked in the mask files. Ultimately, the stack is constructed from the mean of the constituent images, after masking bad pixels, scaling by the exposure times, offsetting for the backgrounds, and weighting the input inversely by the seeing for each constituent image. The background level in the stack is the mean of the input image backgrounds, scaled by the exposure times.

2.3.3 Calibration Reference Files

The calibration reference files that are used in the pipeline processing are constructed for each observing run where a sufficient number of appropriate exposures exist; otherwise, the necessary Master Calibration files are drawn from a library of observing runs close in epoch. For all but the bias structure file, the exposures that are used for calibration are affected by multiple instrumental signatures. It is important to distinguish between the additive backgrounds and the multiplicative sensitivity variations to avoid biasing the photometric accuracy of the processed science frames. Thus, the path to creating the reference files is an iterative one and involves isolating the various effects, storing a characterization of the effect in a reference image, and using those characterizations to construct down-stream reference files.

The background includes two artificial sources: a pupil ghost and a fringe pattern. The nature of these effects and that of the flat-field was explained above; key properties of these effects *on science images* are summarized in Table 2-8. Each effect differs somewhat in its spatial scale, amplitude, color dependence, and stability; these differences are in fact what make it possible to distinguish their respective contributions. Note that the background effects may not be apparent at all in some science images.

Table 2-8: Background Characteristics

Effect	Contribution	Spatial Scale (pix)	Amplitude	Color Dependence	Notes
Pupil Ghost	Additive	2300	10%	High ³⁰ @blue & red	Spatially stable per filter; amplitude depends on field brightness.
Fringe Pattern	Additive	10 to 100	1–10% of sky	Strong	Spatially stable per filter; amplitude variable in minutes to hours.
Flat-Field	Multiplicative	2	~1–2% ³¹	Moderate	Stable spatially & temporally, apart from shadows of dust particles.

³⁰ Effect is much smaller for Mosaic-2, where the corrector has a superior AR coating.

³¹ Localized variations of >10% are common near detector blemishes or dust particles.

With the exception of the bias and dome-flat images, all calibration reference files are generated from the bias- and cross-talk-corrected science frames themselves. Masks are then generated for each science frame that marks the locations of artifacts (e.g., bad columns, bleed trails, and cosmic rays) and astrophysical objects in the field. The masked science frames for each filter are then combined to yield master sky frames in order to characterize the background effects, as explained below.

Bias Structure

The Master Residual Bias Structure file is constructed very simply by applying the bias overscan correction to each of several zero-second exposures, trimming the overscan regions, and averaging the result (with rejection of outliers). Once constructed, both steps in the bias correction can be applied to all images.

Dome Flat-field

Dome flats, or exposures of an illuminated screen affixed to the interior of the telescope enclosure, are used to form the first approximation to the true flat-field. The process for constructing the Master Dome-flat is illustrated in Figure 2-10. After the bias correction is applied, the images for each filter are averaged (with rejection of outliers and masking of bad columns). The next step³² is to apply a template mask (from a library) with the same shape and spatial extent as the pupil ghost, so that a ratio may be determined between the portions of the dome flat-field image that are affected by the pupil ghost and those that are not. The ratio is applied to the pupil mask to generate a ghost template image that is *divided*³³ out of the averaged dome flat-field image for each filter. This leaves the dome-flat template images, sans pupil ghost.

For some observing runs or some filters (narrowband or very blue filters) there are few if any dome-flat exposures, but there may be exposures of the twilight sky. In this case, these sky-flats are processed in much the same way as described above and are used to correct the Master Dome-flats.

³² For Mosaic-1.1 data, and Mosaic-1 data obtained at the 4-m telescope only.

³³ An additive effect in a science image amounts to a *multiplicative* effect in a flat-field calibration image.

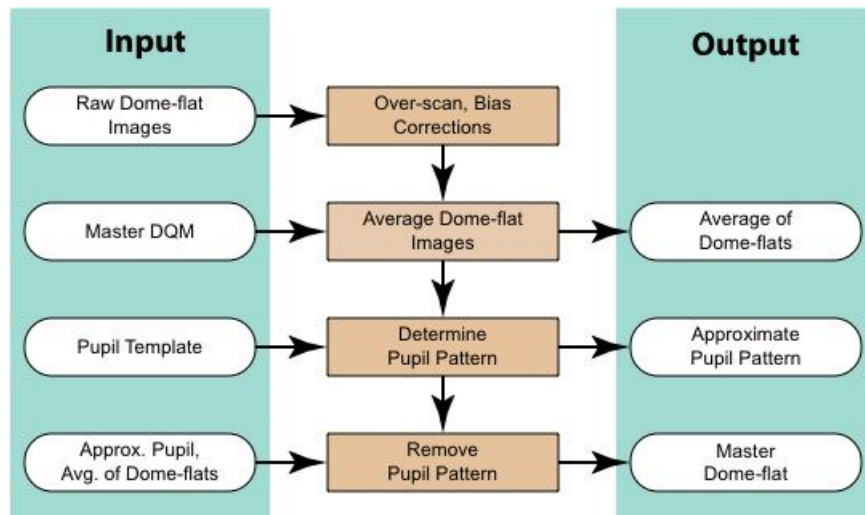


Figure 2-10: Process for constructing the Master Dome Flat-field for each filter. Input dome-flat images are uncalibrated. Pupil pattern characterization and removal applies to Mosaic-1 data obtained at the 4-m telescope only.

Pupil Ghost

An accurate pupil ghost pattern is created³⁴ for each affected filter from the science images themselves, as illustrated in Figure 2-11. The science images are first corrected for cross-talk and bias, before applying the dome flat. The non-masked portions of the images are averaged to produce a sky frame. The same pupil template mask mentioned above is used to create a much improved pupil template for each filter. The pupil pattern is fairly stable over time.

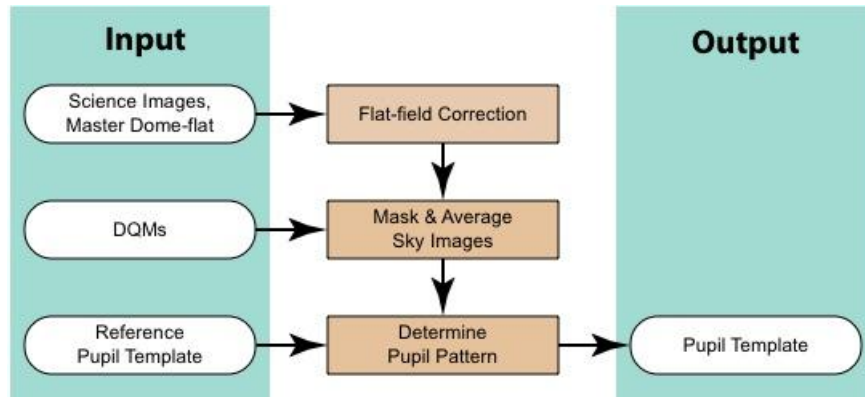


Figure 2-11: Process for characterizing the pupil ghost pattern for each filter. Input Mosaic science frames have had cross-talk and bias corrections applied.

³⁴ For Mosaic-1 and Mosaic-1.1 data only.

Fringe Pattern

Having characterized the additive pupil ghost pattern, the science images are processed once again to scale and remove this pattern from each individual science image and to correct the results by the dome flat. As illustrated in Figure 2-12, the frames are masked and combined, leaving a sky frame for each filter with the fringe pattern signature. This pattern can be characterized by smoothing the sky frame with a smooth, two-dimensional function with a width comparable to the fringe period, leaving a fringe template for each filter. Although in practice some or all of the fringe pattern within the pupil ghost template region is corrected by the Master Pupil Ghost, this is not of concern because both terms are additive.

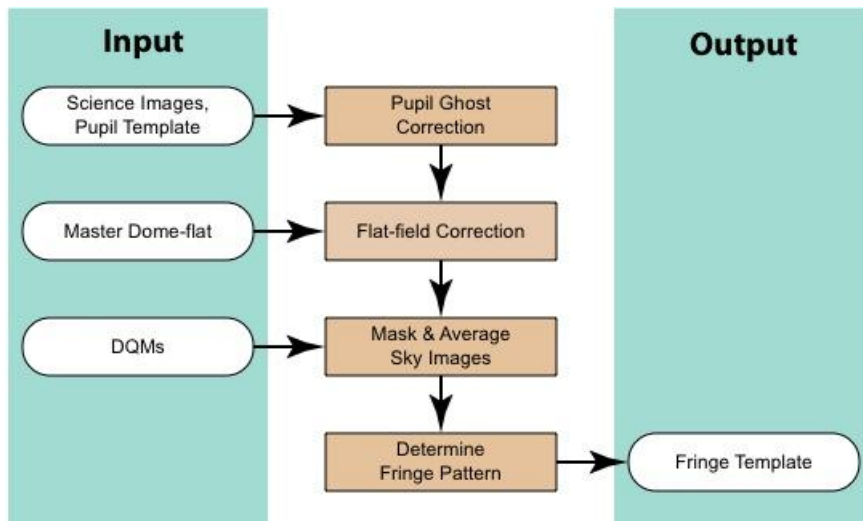


Figure 2-12: Process for characterizing the fringe pattern for each filter. Input Mosaic science frames have had cross-talk and bias corrections applied.

Sky Delta-Flat

Once the pupil ghost and fringe pattern templates have been determined, an improvement to the flat-field can be generated from the accumulated night-sky background for each filter, provided there are enough counts. A flat-field generated in this way will more closely match the illumination pattern of the science frames (i.e., large-scale, artificial gradients can be minimized), and in the color of the incident light (where the effect is greatest for objects that are at or below the sky brightness). The processing of science data to determine the sky flat-field is shown in Figure 2-13. After correcting for cross-talk and bias, the pupil ghost and the fringe pattern are each scaled and subtracted from the science images, and the dome flat is applied. The sources are masked, and the resulting images are averaged to form a sky delta-flat template. The effect of applying this correction at full resolution is to use the sky as the flat-field, rather than the dome flats.

To be of sufficient quality, the sky flat-field must be composed of at least five (masked) input images, and have a signal-to-noise ratio of at least 50. If there are insufficient counts in the pixel-to-pixel sky delta-flat template, the sky delta-flat is smoothed by a function with a width of 255 pixels. In this case, the Master Dome-flat corrects for pixel-to-pixel variations in sensitivity and normalizes the gain, but the Master Sky Delta-flat corrects the dome-flat for low-order illumination effects.

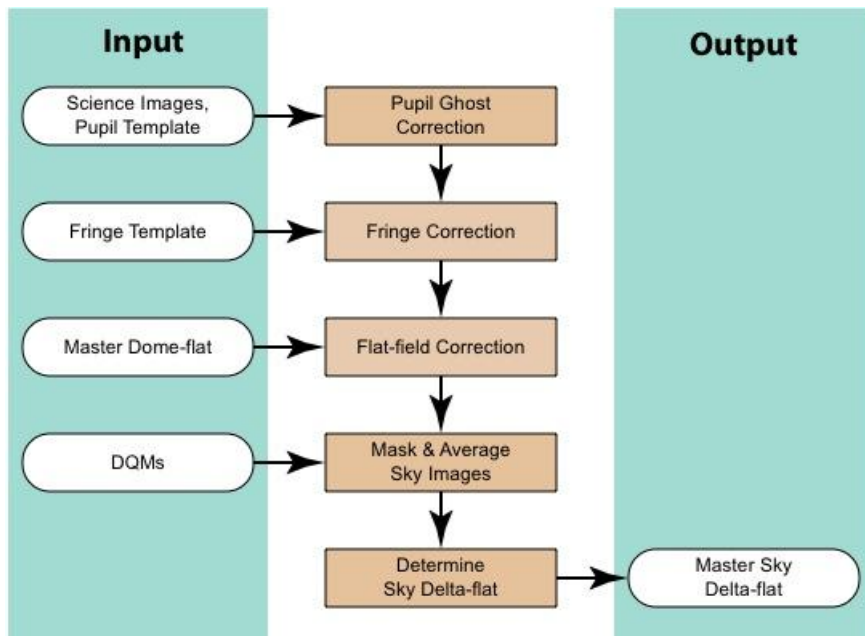


Figure 2-13: Process for creating the Master Sky-flat for each filter. Input Mosaic science frames have had cross-talk and bias corrections applied.

2.4 Sources of Error

This section describes the accuracy that can be expected for the major data products, the major sources of error, instrument foibles, and other noteworthy problems and issues with data from the Mosaic cameras.

2.4.1 Astrometry

The astrometric accuracy for the image coordinate system is fundamentally limited by the accuracy of the astrometric catalog used to determine the WCS solution, which for the present is limited to USNO-B1.0. This catalog has the advantages of full-sky coverage and a faint limiting magnitude that provides a good overlap in the brightness range covered by most Mosaic exposures. Typical accuracies obtained for the WCS solution (250 mas measured in RMS deviations from the fit) are comparable to the accuracy at the faint end of the catalog. The geometric stability of the Mosaic cameras is good, although rotations of the field of $\sim 1^\circ$ are common after the camera has been reinstalled for an observing run.

There are two known circumstances where the pipeline WCS solution may fail entirely. The first is if the trial WCS is missing entirely from the raw data header, which is rare. The second case is if the telescope pointing as recorded in the RA and DEC (or TELRA and TELDEC) keywords is too far from the actual pointing, in which case the WCS solution will not converge.

2.4.2 Photometry

The photometric stability of the Mosaic cameras is relatively good, and with care and good flat-fielding, it is possible to achieve photometric accuracies of 1%. However, **at present the photometric calibration provided by the pipeline processing is not adequate to support science** and is intended solely to provide a rough estimate of exposure depth to support archive queries. While the systematic uncertainty may be large, within a sequence of observations covering the same region of the sky, the relative uncertainties are significantly smaller and provide a useful diagnostic on the photometric stability of the sky.



The magnitudes for the USNO-B1.0 catalog were for the most part derived from photographic source material and have high uncertainties. In addition, the association of filters used with the Mosaic cameras to USNO-B passbands, and then the color transformation from USNO-B to the SDSS filter set, introduces substantial (but uncharacterized) additional uncertainties. The resulting magnitude zero-point and photometric depth given in the headers of Mosaic science data are uncertain by an unknown amount that may approach 0.5 mag.

The photometric performance for any given image depends mostly on a number of external factors, including the sky conditions and reflectivity of the telescope optics (both of which are time dependent). Representative photometric zero-points and color terms for some standard, broadband filters are given in Table 2-9 for the Mosaic-2 camera. The equations used to fit the standard star photometry are of the form:

$$u = \mathbf{U} + A_0 + A_1X + A_2(\mathbf{U} - \mathbf{B})$$

$$b = \mathbf{B} + B_0 + B_1X + B_2(\mathbf{B} - \mathbf{V})$$

$$v = \mathbf{V} + C_0 + C_1X + C_2(\mathbf{B} - \mathbf{V})$$

$$r = \mathbf{R} + D_0 + D_1X + D_2(\mathbf{V} - \mathbf{R})$$

$$i = \mathbf{I} + E_0 + E_1X + E_2(\mathbf{V} - \mathbf{I})$$

where **bold** letters are the standard Harris magnitudes, lower-case letters are instrumental magnitudes ($25 - 2.5\log(\text{ADU} \cdot \text{s}^{-1})$), X is the airmass, and the first and last subscripted coefficients are given in the table.

Table 2-9: Representative Photometric Coefficients for Mosaic-2 Camera

Filt.	CCD 1	CCD 2	CCD 3	CCD 4	CCD 5	CCD 6	CCD 7	CCD 8
Zero-Point								
<i>U</i>	2.217±0.007	2.220±0.005	2.231±0.005	2.254±0.008	2.234±0.010	2.215±0.005	2.216±0.005	2.227±0.009
<i>B</i>	-0.107±0.008	-0.120±0.008	-0.115±0.008	-0.111±0.009	-0.111±0.008	-0.101±0.008	-0.106±0.008	-0.104±0.008
<i>V</i>	-0.448±0.008	-0.472±0.004	-0.472±0.004	-0.476±0.011	-0.475±0.004	-0.471±0.006	-0.472±0.005	-0.475±0.007
<i>R</i>	-0.636±0.004	-0.633±0.004	-0.648±0.004	-0.632±0.004	-0.628±0.004	-0.616±0.004	-0.629±0.005	-0.624±0.006
<i>I</i>	-0.089±0.010	-0.118±0.008	-0.076±0.010	-0.094±0.008	-0.094±0.004	-0.123±0.007	-0.113±0.011	-0.088±0.010

Filt.	CCD 1	CCD 2	CCD 3	CCD 4	CCD 5	CCD 6	CCD 7	CCD 8
Color Term								
<i>U</i>	0.027±0.019	0.028±0.015	0.021±0.015	0.018±0.019	-0.025±0.024	0.019±0.016	0.015±0.016	-0.002±0.021
<i>B</i>	-0.069±0.010	-0.062±0.010	-0.058±0.010	-0.055±0.011	-0.056±0.010	-0.079±0.011	-0.081±0.010	-0.068±0.010
<i>V</i>	0.038±0.009	0.044±0.005	0.042±0.005	0.060±0.012	0.063±0.005	0.041±0.007	0.039±0.006	0.056±0.008
<i>R</i>	-0.025±0.008	-0.037±0.008	-0.022±0.008	-0.032±0.008	-0.028±0.008	-0.045±0.008	-0.035±0.010	-0.029±0.011
<i>I</i>	0.009±0.009	-0.002±0.007	-0.008±0.009	0.006±0.007	0.003±0.004	-0.002±0.006	0.003±0.011	0.011±0.010

2.4.3 Anomalies

Metadata

Critical metadata in raw (Level-1) science data files may sometimes be missing or have incorrect values. However, certain of the metadata in the headers of calibrated data, notably the WCS information and the filter name, are corrected during the course of pipeline processing (unless the calibration fails). Metadata *added* by the pipeline during processing are reliable in Level-2 and Level-3 data products.

Absolute time metadata in Mosaic-2 image headers, such as that recorded in the DATE-OBS keyword prior to May 2003, may be inaccurate by between a few seconds and a few minutes. Afterward, the time was derived from NTP, which is accurate to a few tenths of a second.

Detector Performance

In September 2003, the CCD 3 in the **Mosaic-2** camera failed and was replaced in April 2004. Between these dates, the image extensions for this detector are still present in the data files, but contain no meaningful data.

The CCD array controllers for **Mosaic-1** are known to suffer data drop-outs on occasion. The most recent documented cases occurred intermittently during January–May 2009 with array 2. This anomaly manifests itself in the data as a constant value everywhere in the affected array.

Detector Temperature Stability

The temperature control loop for the CCDs in the **Mosaic-2** camera was not closed prior to late 2003. That is, the temperature of the focal plane was free to vary according to its instantaneous thermal load and coupling quality with the LN2 tank. The temperature varied by several degrees Celsius within a night and by as many as 10–12 °C over the course of an observing block.

The consequence was to induce QE variations at the red end of the passband. In particular, data taken with the SDSS z' filter was affected, as for any other filter where the red cutoff is set by the drop off of the CCD QE rather than the filter itself. The variation in QE of a silicon detector can show up to 1% variation per degree temperature change in the far red.

Bias Stability

It is possible to improve upon the bias correction by fitting the averaged overscan vector with a polynomial (of order ~100). This approach would have the effect of smoothing the correction to reduce the effect of noise in the overscan region. Unfortunately, the bias level is known on occasion to change suddenly (or jump) during read-out. This makes the line-by-line approach to the overscan correction more robust.

Negative Saturated Pixels

For Mosaic-1 and Mosaic-2, saturated pixels (where the accumulated charge exceeds the full-well, e.g., in the cores of over-exposed stars) will have negative values when the binning factor (given in the `CCDSUM` keyword) is 2×2 or higher.

Electronic Ghost

There is an electronic ghost in Mosaic-1.1 images associated with full-well saturated stars and bleed-trails. See Figure 2-8 on page 2-18. This effect is currently not understood or characterized, and is not removed by the pipeline. Users will likely want to mask regions affected by this ghost prior to making photometric measurements.

2.5 References & Further Information

Contributing Authors

A large number of people have contributed to the technical knowledge of the Mosaic cameras. Extensive material has been contributed by George Jacoby (lead author of the first version of the Mosaic Instrument Manual), by Heidi Schweiker and Buell Jannuzi (lead authors of Version 3 of the Instrument Manual), and by Steve Howell and Dave Sawyer (who contributed to Version 4 of the instrument manual). Other substantial contributors were: Taft Armandroff, Todd Boroson, Jim De Veny, Steve Heathcote, Tod Lauer, Bob Marshall, Phil Massey, Gary Muller, Knut Olsen, Rich Reed, Frank Valdes, David Vaughn, and Dick Shaw. Documentation on the reduction of Mosaic data is also fairly extensive, much of which was authored (see below) by Frank Valdes (in IRAF documentation); Frank Valdes, Rob Swaters, and Tracy Huard (in pipeline documentation); and Heidi Schweiker, Buell Jannuzi, and Frank Valdes (in the form of the NDWFS data reduction notes).

References

- Dey, A, & Valdes, F., 2014, *The Delivered Image Quality with the MOSAIC Cameras at the Kitt Peak 4-m Mayall and the Cerro Tololo 4-m Telescopes*, [PASP, 126, 296](#)
- Jacoby, G. H., Laing, M., Vaughn, D., Reed, R, & Armandroff, T., 1998, *A New Wide-Field Corrector for the Kitt Peak Mayall 4-m Telescope*, [SPIE 3355, 721](#)
- Monet, et al. 2003, [AJ, 125, 984](#)

Schweiker, H., & Jannuzzi, B. T. 2004, *NOAO CCD Mosaic Imager User Manual* (Version 3.0: Tucson: NOAO), available online at: http://www.noao.edu/kpno/mosaic/manual/man_sep04.pdf

Schweiker, H., Howell, S., & Sawyer, D. 2011, *KPNO Mosaic-1.1 Imager User Manual* (Version 4.3: Tucson: NOAO), available online: <http://www.noao.edu/kpno/mosaic/manual/>

Walsh, J. R., Pirzkal, N., & Pasquali, A. 2002, *Modelling the Fringing of the ACS CCD Detectors*, in 2002 *HST Calibration Workshop*, ed. S. Arribas, A. Koekemoer, & B. Whitmore (Baltimore: STScI), 90

For Further Reading

A document repository³⁵ for the Mosaic-1 camera is available online, which includes papers on the design of the Mosaic cameras:

Massey, P., Armandroff, T., De Veny, J., Claver, C., Harmer, C., Jacoby, G., Schoening, W., & Silva, D. 2002, *Direct Imaging Manual for Kitt Peak* (Tucson: NOAO)

Muller, G. P., Reed, R., Armandroff, T., Boroson, T., & Jacoby, G. 1998, *What is Better than an 8 K × 8 K Mosaic?*, [SPIE, 3355, 577](#)

Wolfe, T., Reed, R., Blouke, M., Borson, T., Armandroff, T., & Jacoby, G. H. 1998, *CCD Detector Upgrade for NOAO's 8192 by 8192 MOSAIC*, [SPIE 3355, 487](#)

A general discussion of data reduction techniques for CCD mosaics was published by Frank Valdes, who also implemented these techniques in IRAF, including most of the applications that are used in the current Mosaic pipeline. Additional papers on the Mosaic pipeline appeared in the proceedings of the ADASS XVI conference.

Swaters, R. A., & Valdes, F. G. 2007, *The NOAO High-Performance Pipeline System: Mosaic Camera Pipeline*, in ASP Conf. Ser. 376, ed. R. A. Shaw, F. Hill, & D. J. Bell (San Francisco: ASP), 269

Valdes, F. G. 2002, *The Reduction of CCD Mosaic Data*, in *Automated Data Analysis in Astronomy*, ed. H. P. Singh, R. A. Gupta, & C. A. L. Bailer-Jones (New Delhi: Narosa Pub. House), 309; available online at <http://iraf.noao.edu/projects/ccdmosaic/reductions/adaa/valdes2.pdf>

Valdes, F. G., & Swaters, R. A. 2007, *The NOAO High-Performance Pipeline System: Mosaic Camera Pipeline Algorithms*, in ASP Conf. Ser. 376, ed. R. A. Shaw, F. Hill, & D. J. Bell (San Francisco: ASP), 273

Various PI teams have used the Mosaic cameras to conduct major surveys. Two teams, one lead by Buell Jannuzzi (formerly NOAO) and the other by Phil Massey (Lowell Observatory), have published extensive notes³⁶ on their data reduction procedures. The following journal papers describe the calibration techniques and science results from these surveys.

³⁵ Mosaic-1 document repository: <http://www.noao.edu/kpno/mosaic/mosaic.html>.

³⁶ Available at <http://www.lowell.edu/users/massey/lgsurvey/splog2.html>.

Jannuzzi, B., Claver, J., & Valdes, F. 2003, *The NOAO Deep Wide-Field Survey Mosaic Data Reduction Notes* (Tucson: NOAO), available online at:
<http://www.noao.edu/noao/noaodeep/ReductionOpt/frames.html/>

Massey, P., Olsen, K. A. G., Hodge, P. W., Strong, S. B., Jacoby, G. H., Schlingman, W., & Smith, R. C. 2006, [AJ, 131, 2478](#)

Massey, P., Olsen, K. A. G., Hodge, P. W., Jacoby, G. H., McNeill, R. T., Smith, R. C., & Strong, S. B. 2007, [AJ, 133, 2393](#)

Chapter 3

NEWFIRM Camera

Version 2.0, January 2015

In This Chapter...

Instrument Overview	3-1
Data Products.....	3-8
Calibration....	3-15
Sources of Error ...	3-22
References & Further Information ...	3-25

The NEWFIRM camera was placed in routine operation at KPNO in late 2007 and was operated in a campaign at CTIO from spring 2010 through late fall 2011. The material presented here is drawn primarily from Probst (2008) and Probst et al. (2008), and from the *NEWFIRM Quick Reduce Pipeline and Data Analysis Tools* notes by Dickinson et al. (2008). Interested users should consult these documents for details of the instrument description and pipeline operation. Additional resources³⁷ are cited throughout this chapter and are listed along with other background material in the last section.

3.1 *Instrument Overview*

The NOAO Extremely Wide-Field Infrared Mosaic (NEWFIRM) camera has rapidly become one of the most heavily used instruments offered by NOAO because of its excellent infrared (IR) sensitivity and very large field of view. NEWFIRM has been used at both the Mayall 4-m telescope on Kitt Peak and the Blanco 4-m telescope on Cerro Tololo, in alternating campaigns. This chapter describes both usages of the camera.

3.1.1 Instrument Capabilities & Design

The NEWFIRM camera is a near-IR imager with a wide field of view (*FoV*) and a large focal-plane array (*FPA*) containing four InSb detectors with a total of 4096×4096 pixels. A schematic of the instrument is shown in Figure 3-1. The detectors have quantum efficiency (QE) near 90% over the wavelength range 0.8–4.5 μm, with the exception of one detector (SN019), where a thicker anti-reflection coating degrades the QE by ~10% shortward of ~2.5 μm. There are two *filter* wheels, each with seven slots, that can hold a subset of the available filters for NEWFIRM. The filter sets³⁸ include standard broad passbands, such as

³⁷ See the NEWFIRM instrument website at <http://www.noao.edu/ets/newfirm/>.

³⁸ The filter properties can be viewed in the online Users Manual at <http://www.noao.edu/ets/newfirm/>.

JHKs, mediumband filters, and a few narrowband filters including [Fe II] 1.64 μm , H₂ 2.12 μm and Br γ 2.17 μm . Because the detector has high QE well beyond the passbands of the current filter set, blocking filters are sometimes used to minimize red leak.

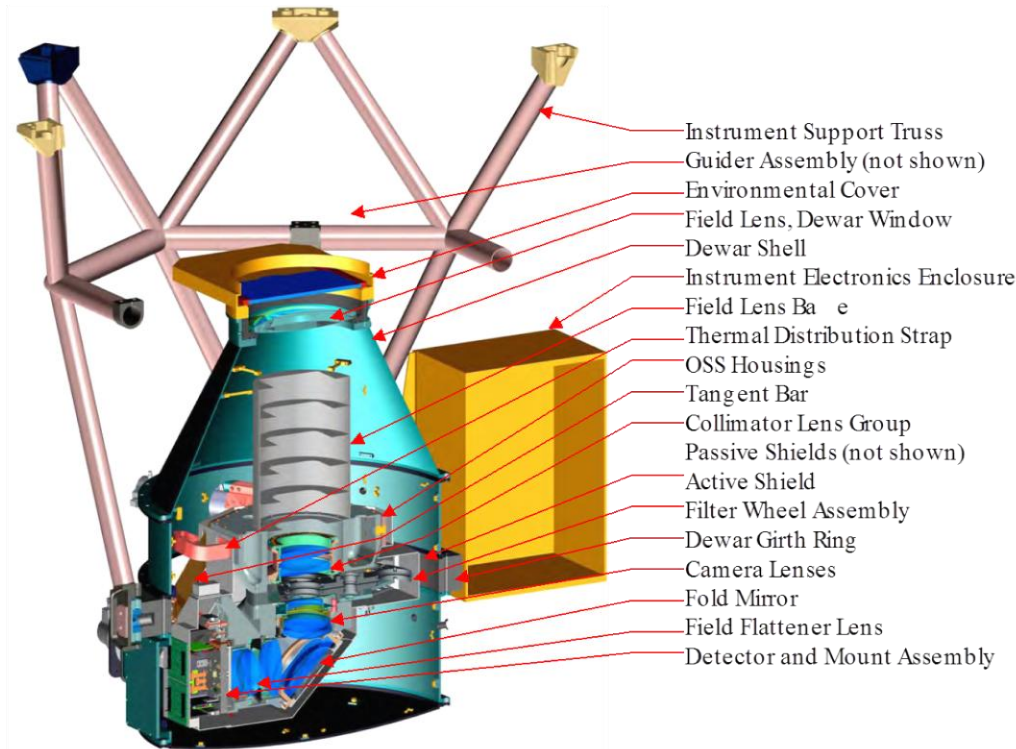


Figure 3-1: Cross-section view of the NEWFIRM camera. Light enters from above in this diagram, and passes through various optical elements (see labels).

The details of the observing configurations for NEWFIRM are given in Table 3-1. The camera is mounted at the Cassegrain focal station of the 4-m telescopes, with a converging beam as indicated in the table. The pixel scale samples the point-spread function (**PSF**) well, which is seeing-limited at all wavelengths. The image quality at the 4-m telescopes is good, with little (<10%) focus gradient or PSF variation across the FoV. The pixel scale changes slowly from the center to the edge of the FoV due to pincushion distortion. There is very little vignetting.

Table 3-1: NEWFIRM Camera Characteristics

Field of view	28' \times 28'
Pixel scale of FPA	0.40 arcsec/pixel
Inter-array gaps	35 arcsec, or 88 pixels
Delivered image quality	0.8 arcsec in excellent seeing conditions
Telescope focal ratio	f3.1

It is important to note that there is no mechanical shutter for the NEWFIRM camera; rather, the exposure duration is regulated by the difference between the initial and final nondestructive reads of the array. This

has important implications for the linearity and measured counts, particularly at high count rates: see “Array Operation” on page 3-5 for details.

Focal Plane

The focal plane of the NEWFIRM camera is populated with an array of four Orion InSb detectors, arranged in a 2×2 mosaic, as shown in Figure 3-2. Each of the detectors has 64 *amplifiers* to provide high-speed, parallel readout of the entire array as fast as 1.4 s. Representative detector properties are given in Table 3-2; most values do not differ significantly from array to array. Compared to present-day CCD detectors for the optical band, the sensitivity and dynamic range of this generation of large-format IR detectors are excellent, but the array cosmetics, noise, and linearity are inferior. The response of the NEWFIRM Orion detectors is linear to within about 6% for exposures less than 80% of the full-well. The QE varies somewhat from detector to detector, both on average and as a function of wavelength, in part due to differences in the anti-reflection coatings (see Merrill 2008 for details). Therefore, the transformation from instrumental magnitudes to standard systems depends upon the detector. See “Photometric Calibration” on page 3-19 and “Photometry” on page 3-23.

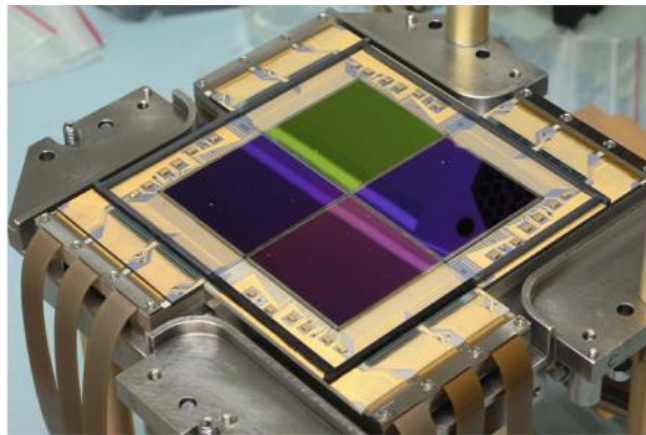


Figure 3-2: Mounting for the NEWFIRM focal plane array, showing the four 2048×2048 pixel Orion InSb detectors.

Table 3-2: Orion InSb Array Characteristics

Array Dimensions	2048×2048
Pixel Size	$24 \mu\text{m}$ square
Gain	$8 \text{ e}^-/\text{ADU}$
Read noise, RMS	35 e^- (1 Fowler sample)
Dark current	$0.17 \text{ e}^-/\text{s}$
Well capacity	$\sim 100,000 \text{ e}^-$
Nonlinearity	$\sim 6\%$ at 10,000 ADU
Read Time (Dig. Avg. = 4, Fowler samples = 1)	1.4 s

The flat-field image shown in Figure 3-3 shows the most significant cosmetic defects in the photo-active areas of the arrays. The spatial extent of these defects (along with the inter-chip gap) determines the minimum separation of the spatial dithers that are required during observing to minimize their effect on the final Stacked images. A brief description of the defect types, numbered as in the figure, follows.

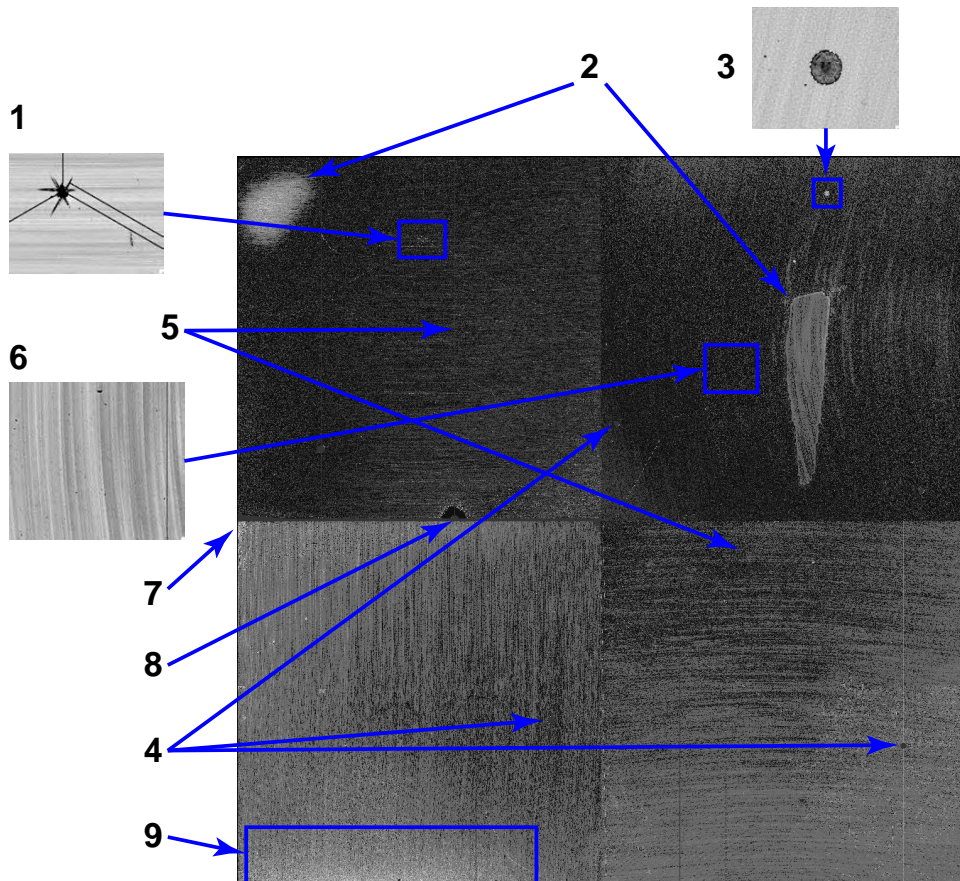


Figure 3-3: H-band flat-field image showing all four arrays abutted. Examples of various cosmetic defects in the NEWFIRM sensors are enumerated: see text for descriptions.

1. Diagonal cracks in the InSb substrate, where there is zero sensitivity.
2. Broad regions of slightly reduced sensitivity and higher dark current.
3. Small regions of reduced sensitivity due to contaminants on the arrays.
4. Photo-Emissive Defects (PED), which result from shorts in the bonded readout electronics, and which have been passivated at the expense of a number of roughly circular areas as large as ~50 pixels in diameter with zero sensitivity.
5. Inoperable rows or columns, which are often but not always associated with a PED.
6. Residual patterns (with few-percent amplitude) of substrate crystal formation (i.e., “growth rings”), which are easily removed with the flat-field correction.
7. Regions at the detector edges or corners that have debonded from the readout electronics, resulting in zero sensitivity.
8. Damaged region on detector, with surrounding area of high dark current and nonlinear response that is masked in pipeline processing.
9. Extended regions of elevated dark count and pixel nonlinearity.

Figure 3-4 shows the arrangement of the NEWFIRM focal plane array on the sky, using the same nomenclature as is found in the FITS file extension headers.³⁹ Note that the raw image array coordinates are remapped from the detector coordinates, such that the image origin is always in the lower-left corner when oriented as in the figure.

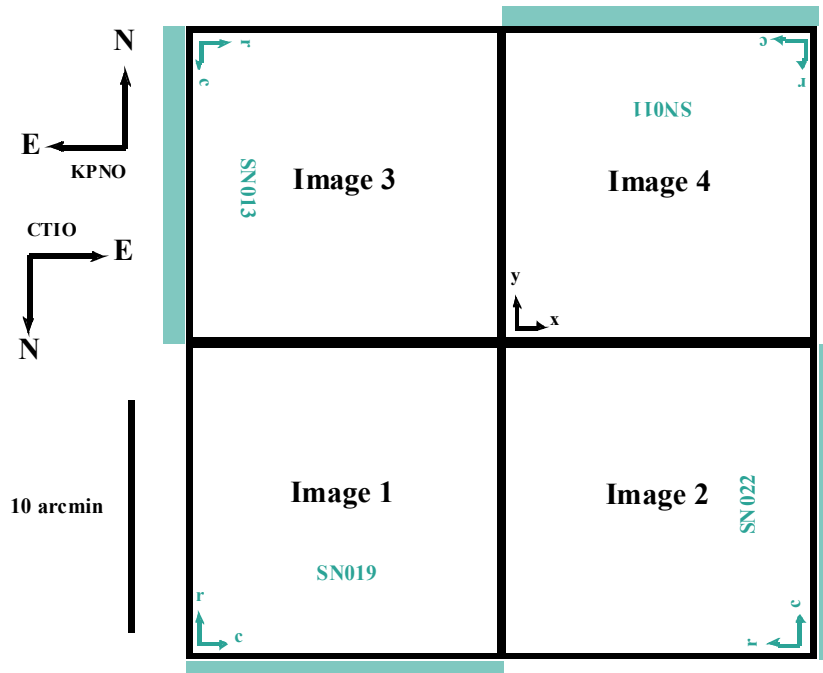


Figure 3-4: Orientations on the sky and spatial footprint of the focal plane array for the NEWFIRM camera, with FITS image extension and IR detector designations indicated. Coordinate (x,y) axes originate in the lower-left corner for all images (black arrows). The detector coordinate (row,column) origin is indicated for each array (teal arrows). Location of the 64 output amplifiers for each array is also indicated (teal bars). Gap between adjacent sensors is 35 arcsec.

3.1.2 Operations

An understanding of NEWFIRM data products requires a basic knowledge of how data are obtained during an observing run, which in turn requires knowing both how the arrays are operated and the strategies used to optimize the spatial coverage of the intended region of interest on the sky.

Array Operation

There are a few key points to bear in mind when trying to understand data from NEWFIRM. First, the exposure duration is not regulated with a mechanical shutter, as is done with CCD cameras, but is instead controlled by rapid, precisely timed, nondestructive reads of the detector array. The strategy for operating the NEWFIRM detectors is called *correlated double-sampling* (CDS), where the pixel values in the output image are in reality a *difference* between a final and an initial read of each pixel. The integration time

³⁹ The detectors and the orientation of the image arrays were changed during the course of instrument commissioning; this diagram reflects the final configuration for data obtained after semester 2007B.

is constant across the array, but the interval over which a given pixel integrates depends on its position on the array. This differencing also masks the fact that the pixels are accumulating counts during the finite time required to reset the array and read it out; this “hidden” flux affects the linearity correction at high count rates. The total elapsed time from the array reset to the last read of the last detector pixel depends upon four parameters that are set by the observer, as shown in Table 3-3.

Table 3-3: NEWFIRM Array Readout Parameters

Parameter	Default Value	Description
Exposure Time	—	Duration of exposure, which is the elapsed time between the first sampling of the initial readout of the array and the first sampling of the final readout of the array.
Digital Averages	4	Number of back-to-back samples of each pixel during the course of a single array read; samples are averaged to determine the raw pixel value.
Fowler Samples	1	Number of times the entire array is read just after reset, and again at the end of the integration. Resulting raw image is the difference between the sum of the last readouts and the sum of the initial readouts. Using N > 1 is appropriate when the S/N ratio is dominated by read noise, rather than the background.
Co-adds	1	Number of integrations taken in sequence and summed (on-board) into a single output image.

Each combination of these readout parameters changes the readout timing (see Table 3-4 below), the effects of which can be quite significant: at high count rates, the main effect is in the linearity correction as illustrated in Figure 3-5; at low count rates, the amplitude and structure of the dark “pedestal” is affected by the readout timing. This change in readout timing is the reason that dark frames must match the science frames with respect to the integration time and the array operation parameters in the above table; otherwise, the dark frames will not accurately represent the accumulated dark current during a science exposure.



Note that raw data frames obtained with **N Fowler Samples** will, in effect, contain the **sum** of the N readouts, rather than the average. Raw data frames obtained with **M Co-Adds** will also be recorded as the **sum** of M images, although this is perhaps the expected behavior. Images calibrated by the NEWFIRM pipeline are normalized to unit exposure time.

Table 3-4: Array Readout Times

No. Digital Averages	Number of Fowler Samples		
	1	4	8
1	0.565	1.52	2.753
2	0.894	2.270	4.103
4	1.195	3.014	5.439
8	1.785	4.092	8.101
16	2.965	7.448	13.425

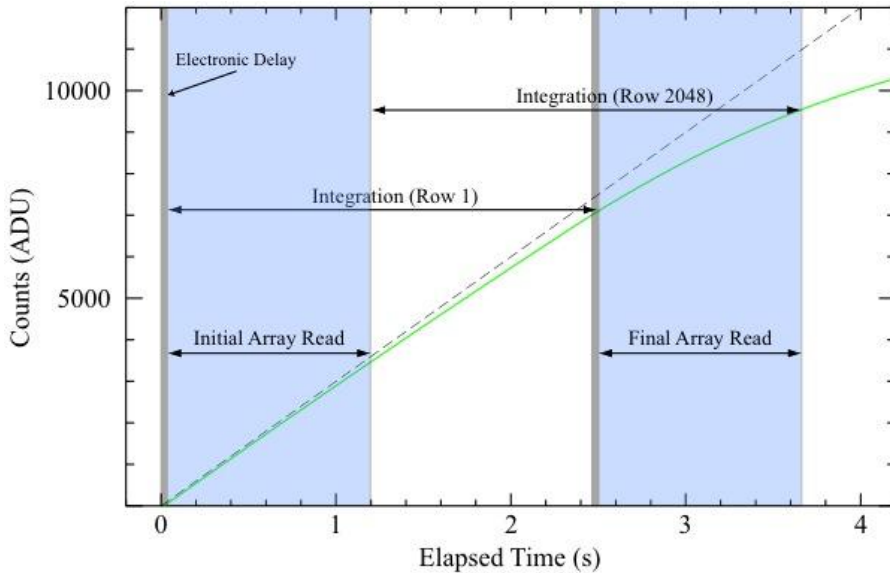


Figure 3-5: Schematic of the detector response (green curve) to a very high incident flux of 3000 ADU s^{-1} (dashed line) as a function of time. After the array is reset, the counts begin accumulating from zero. In *correlated double-sampling*, after a brief delay the array begins reading out, which takes 1.16 s when DigAvg = 4 and one Fowler sample (blue shaded regions); following a programmed delay to achieve the integration time of 2.5 s, the detector is read again. Although the integration time is constant across the array, the interval over which a given pixel integrates depends on its position in the array.

Observing Sequences

Nearly all NEWFIRM observers obtain multiple exposures of their science fields per filter; usually in a sequence of small spatial dithers about a reference position in order to obtain data in the gaps between the detectors in the FPA and to ameliorate the effects of detector artifacts (see Figure 3-3 on page 3-4). Many observing programs also obtain sequences of (slightly) overlapping images, which enables the mapping of large regions of sky from the component images. These sequences are enabled at the telescope with a set of standard scripts, the parameters of which specify the observing pattern on the sky and the relative offsets between pointings within the pattern; these sequence parameters are written to the FITS headers of the science images.

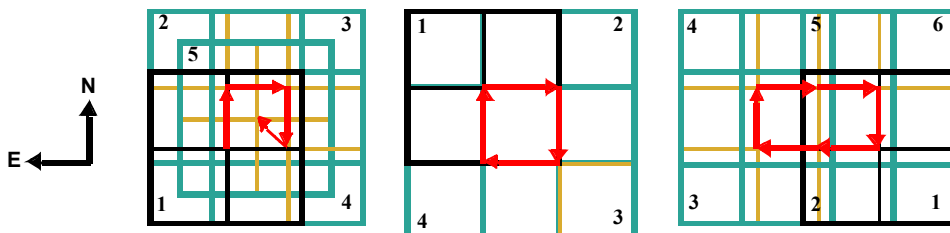


Figure 3-6: Schematic of three types of offset observing sequence patterns: a five-point "X" (5PX, left), four quadrants (4Q, center), and a 3x2 rectangle (RA \times Dec, right) of six positions. Translation of the center of the FoV from the initial exposure in the sequence (*black footprint*) is indicated (red arrows).

A few of the pre-scripted observing patterns are shown in Figure 3-6, where the footprint of the NEWFIRM FPA is shown as a series of overlapping “window panes.” While the magnitude of most offsets is set by individual observers via a script, the “5PX” and “Random” patterns are most often used with small offsets to *Dither*, the “4Q” pattern positions a source of modest angular extent in the center of each detector, and the “RA × Dec” pattern is used either with small offsets to dither or with large offsets to *Map* an extended region of sky. It is also possible to obtain separate “sky” (or background reference) frames at a very large offset from an angularly very extended target (see the NEWFIRM operations manual for details). Note that these patterns can be combined: e.g., a *Dither* sequence may be executed at each position in the *Map* sequence to mosaic a large area of sky free of data gaps. The calibration pipeline will create a dithered stack of the entire map provided that the offset between map centers is no greater than 20 arcmin.

Finally, most observing programs obtain calibration frames, such as dark frames and dome flats, using scripted sequences in order to facilitate automated pipeline processing, because the pipeline is able to recognize calibration frames from the sequence identifier. See “Calibration” on page 3-15 for a detailed discussion of how the calibration exposures are used in the data reduction process.

3.2 Data Products

This section describes the content and format of the various data products that are produced for the NEWFIRM camera. Most of the products are generated during the course of calibration processing, the details of which are discussed in the next section. The data products can be distinguished by the combination of the PROCTYPE, PRODTYPE, and OBSTYPE keywords in the primary header; the possible values are summarized in Table 3-5. The processing level (see Table 1-2, “Levels of Data Processing,” on page 1-4) at which the product is generated is listed in column 5 (Proc. Level).

Table 3-5: NEWFIRM Data Product Types and Contents

PROCTYPE	PRODTYPE	OBSTYPE	Proc. Level	Description
Raw	image	Object dark dome flat	1	Raw data as obtained at the telescope, with some additional metadata included in the header
InstCal	image	object	2	Calibrated, sky-subtracted, single-frame image
InstCal	dqmask	object	2	Data quality mask for InstCal
Resampled	image	object	2	Calibrated, sky-subtracted, re-projected image
Resampled	dqmask	object	2	Data quality mask for Resampled image
Stack	image	object	3	Stack of multiple, overlapping, calibrated frames with sky subtracted
Stack	dqmask	object	3	Data quality mask for calibrated Stacked image
Stack	expmap	object	3	Exposure map for calibrated, Stacked image
MasterCal	image	dark	2	Master Dark calibration image
MasterCal	image	dome flat	2	Master Dome Flat-field calibration image

3.2.1 Image Formats

The science image data from the NEWFIRM camera is stored either in FITS multi-extension files (MEFs), the general structure of which was described in Chapter 1, or in simple FITS files with no extensions. The detailed arrangement of the image portions among the extensions differs, depending upon whether the data are raw (unprocessed) or reduced. The internal structure and data type for the various data products is summarized in Table 3-6 below, including the number and type of FITS extension(s).

Table 3-6: Product Organization and Data Types

PROCTYPE	PRODTYPE	Ext Type	N. Ext	Data Type
Raw	image	IMAGE	4	32-bit int
InstCal	image	IMAGE	4	32-bit float
	dqmask	IMAGE	4	32-bit int
Resampled	image	[primary]	0	32-bit float
	dqmask	IMAGE	1	32-bit int
Stack	image	[primary]	0	32-bit float
	dqmask	IMAGE	1	32-bit int
	expmap	IMAGE	1	32-bit int
MasterCal	image	IMAGE	4	32-bit float

Raw Data

Raw data from the NEWFIRM camera are organized by detector, with the output from each sensor stored in a separate image extension in the FITS MEF file (see Chapter 1). Thus, there are as many image extensions in the raw science file as the number of sensors in the focal plane. The coordinate origin for all images is in the lower-left corner of the readout section, rather than at the location of the first readout amplifier (see Figure 3-4 on page 3-5). This approach means that individual array images, displayed as image extensions, all have the same orientation on the sky.

The Orion detectors contain reference pixels that enable tracking of the electronic stability during readout. There are actually three varieties of reference pixels on each detector, as illustrated in Figure 3-7 and Figure 3-8. The first detector column consists of pixels that electronically simulate the effect of unilluminated pixels, and the last column consists of pixels that simulate saturated pixels. There is, in addition, one reference pixel for each of the 64 parallel readout amplifiers. That reference pixel is read once for each row during the course of the readout. The 64 amplifier reference pixels are stored at the end of each image row, as illustrated in Figure 3-7. At present, the reference pixels are not used in pipeline processing.

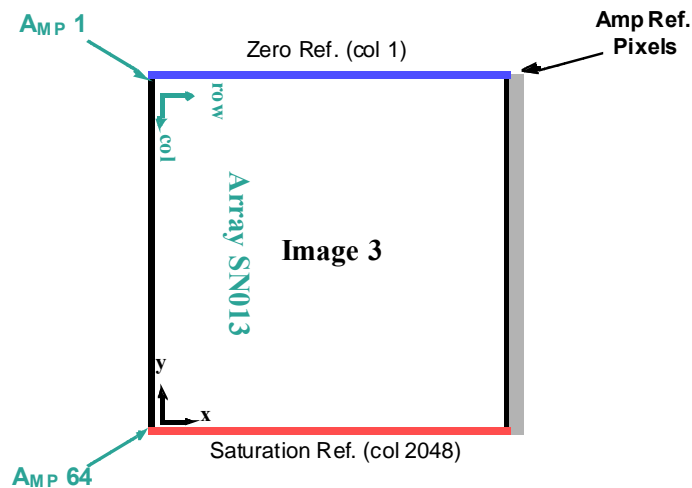


Figure 3-7: Schematic of the image arrays just after readout for detector SN013 of the NEWFIRM camera. Note that the image coordinates are rotated relative to the detector array. Location of the first and last of the 64 output amplifiers are indicated, as are the zero (blue, upper) and saturated (red, lower) detector reference columns. The photo-active region of the detector is indicated in white, while the amplifier reference pixel values (grey, right) are stored in the highest columns of the image.

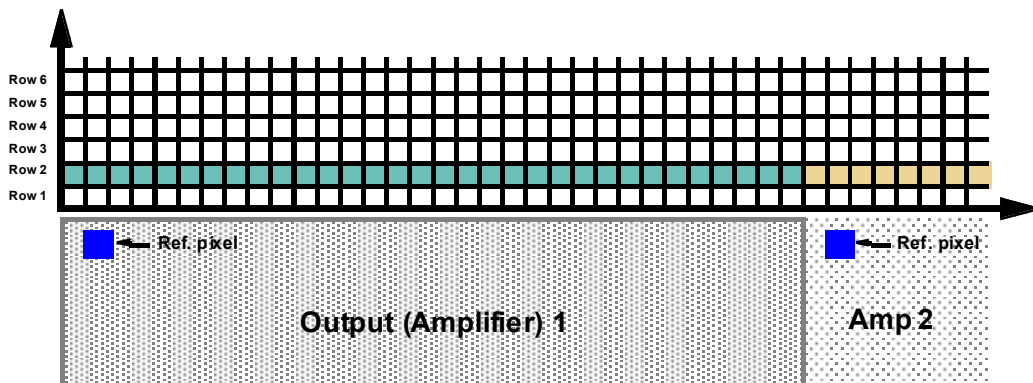


Figure 3-8: Schematic of a portion of the detector array illustrating the parallel readout of the second row of the IR arrays. For each row in the array, the first amplifier reads its reference pixel (fictitious locations shown in blue), followed by the first 32 pixels of the row; the second amplifier simultaneously reads its reference pixel, followed by the next 32 pixels in the row, and so on. The process is repeated for each row of the array. The values of the array reference pixels for the 64 amplifiers are stored in columns 2049:2112 of the raw image.

Table 3-7: Raw Data and Reference Pixel Regions

Raster Dimensions	Image	Detector	Photo-Active Data Section	Amp Reference Pixel Section
2112 × 2048	1	SN019	[1:2048, 2:2047]	[2049:2112, 1:2048]
	2	SN022	[1:2048, 2:2047]	[2049:2112, 1:2048]
	3	SN013	[2:2047, 1:2048]	[2049:2112, 1:2048]
	4	SN011	[2:2047, 1:2048]	[2049:2112, 1:2048]

Calibrated Data

The Archive contains data products that are produced with the NEWFIRM calibration pipeline. The specific calibrated science data products are given in Table 3-5 on page 3-8 and are described in more detail below. Each image has an associated *data quality mask (DQM)*, which is described at the end of this subsection.

InstCal. These images have been processed to remove instrumental signature and have been astrometrically and photometrically calibrated (see “Calibration” on page 3-15), although there are some cases where the calibration can fail (see “Sources of Error” on page 3-22). The pixel values have been normalized to unit exposure time (i.e., $ADU\ s^{-1}$). The data are organized in the FITS file almost identically to that for the raw science data, except for the following:

- The reference pixel regions have been trimmed from the image arrays.
- The resulting images in each extension are all 2046×2046 pixels containing most of the photo-active regions of the detectors.

Resampled. These images are the result of geometrically rectifying InstCal images, where each array has been re-projected to a common tangent-point on the sky, with pixels aligned to a common grid with uniform scale. The Resampled image is stored in the primary header-data unit within the file. Using a common tangent-point (which is selected from a grid with roughly 1° steps in RA, and exactly 1° in Dec) facilitates stacking overlapping images within an observing sequence. The *reduced, re-projected* images are approximately 4092×4092 pixels; the actual size depends on the *WCS* tangent-point selected for a particular image. Both the single-frame and the re-projected images are accompanied by DQMs.

Stacked. When two or more observations of a given target are obtained on the same night using the same filter and have a sufficient degree of spatial overlap (which is usually the case), these images are combined using an average with outlier rejection to remove detector blemishes, gaps between the detectors, and artifacts such as image persistence and cosmic rays. The result is a union of the spatial footprints of the stack, which is stored in a simple FITS image (i.e., not in image extensions), with nearly the same pixel scale as the raw images. In general, these images will be larger—sometimes very much larger—than 4092×4092 pixels because the area of the sky that is mapped can be significantly larger than the instrument FoV.



The exposure duration for Stacked images, as recorded in the `EXPTIME` keyword, refers to the sum of all exposure durations of all images used to create the stack. The exposure depth and noise properties of a stack, particularly from a *Map* sequence, are a discontinuous and possibly complicated function of position in the image because of the gaps between the sensors in the FPA. Use the **exposure map** to track the detailed exposure depth at the pixel level.

Master Calibration. Reference files are created during the course of pipeline processing: namely, darks and flat-fields. These files are used in pipeline processing to remove instrumental signatures from the science data. The Linearity Correction file is created by NOAO scientists from engineering data. See “Calibration Reference Files” on page 3-20. These reference files are 32-bit floating-point images, stored as MEF files with four extensions, matching the raw images.

Concomitant Data. All reduced images are accompanied by DQMs; Stacked images are in addition accompanied by exposure maps. The DQMs and exposure maps are images, with one per extension in the science image. The pixel values in the DQMs are nonzero when affected by detector pathologies and image artifacts such as bad rows or columns, saturation, and regions of passivated pixels; the values are zero otherwise. Table 3-8 below lists mask values that are applicable to *non-stacked* images.

Table 3-8: Data Quality Mask Values

Value	Meaning
0	No problem
1	Bad/invalid pixel identified in the master data quality mask; generally indicates known detector blemishes
2	Bad linearity correction
3	Saturated
4	[Not used]
5	Bad/missing background subtraction
6	Affected by detector persistence
7	[Not used]
8	Transient artifact

Most Stacked images are created from dithered frames, so that most of the pathologies affecting single frames will be obviated. DQMs for Stacked images have the following values: “1” for areas of the re-projected image with no data, “2” for areas with no data *after rejection*, and zero otherwise.

The exposure maps are images whose values are the cumulative exposure duration at each pixel, in seconds, which can be a complicated function of position for *Map* sequences (see “Observing Sequences” on page 3-7). The value of the EXPTIME keyword in a Stacked image is the sum of the exposure durations for all images that contributed to the stack.

3.2.2 Header Keywords

A wide variety of metadata are recorded in the headers of the science frames. Users should browse these headers (and the extension headers) to familiarize themselves with the content. The more critical metadata are described in this subsection. Table 3-9 below lists metadata by the FITS keyword name, the header unit in which the keyword will be found (Primary or Extension), the point in the data processing where the keyword is introduced (or where the value is updated), and the meaning of the keyword (or group of keywords, if they are related). Some of the keywords are indexed by image axis, meaning they come in pairs, as indicated by the suffixes *i* and *j*.



The NEWFIRM processing pipeline was evolving shortly after the instrument began science operations, and not all intended keywords were implemented prior to the start of data archiving in June 2009. Some keywords may be populated in these early data, but the values may not have been correctly updated by the pipeline.

Table 3-9: Important Science Image Keywords

Keyword Name	HDU	Origin	Meaning
Telescope			
AIRMASS	P	R	Atmospheric pathlength for target at observation start
TELESCOP	P	R	Telescope used to obtain these data
TELDEC	P	R	Declination for the telescope position on the sky in degrees
TELRA	P	R	Right ascension for the telescope position on the sky in hh:mm:ss.s
Instrument/Detector Configuration			
DETECTOR	E	R	Identifier of Orion detector in focal plane
FILTER	P	R	Filter name/designation
GAIN	E	R	Detector effective gain, in e^-/ADU
INSTRUME	P	R	Instrument name
NOCFSMPL	P	R	Number of Fowler samples
NOCDGAVG	P	R	Number of digital averages per pixel during readout
NOCCOADD	P	R	Number of on-board co-adds performed for this image
Image Sequences			
NOCDHS	P	R	Name of the image sequence script
NOCDITER	P	R	Dither iteration count
NOCDPAT	P	R	Name of dither pattern
NOCDPOS	P	R	Dither position
NOCDREP	P	R	Dither pattern repetition count
NOCDROF	P	R	Dither offset in RA in arcsec
NOCDDOF	P	R	Dither offset in Dec in arcsec
NOCMITER	P	R	Map pattern iteration count
NOCMPAT	P	R	Map pattern
NOCMPOS	P	R	Map position
NOCMREP	P	R	Map repetition count
NOCMROF	P	R	Map offset in RA in arcmin
NOCMDOF	P	R	Map offset in Dec in arcmin
NOCNO	P	R	Observation number in this sequence
NOCSKY	P	R	Sky offset modulus
NOCTOT	P	R	Total number of exposures in sequence
Time			
DATE-OBS	P	R	Date and time of observation start
EXPCOADD	P	R	Duration of a single exposure in a co-add sequence, in seconds
EXPTIME	P	R	Effective exposure duration, in seconds. For Stacked images the effective exposure duration can be a complicated function of position in the image.
MJD-OBS	P	R	Time of observation start in MJD
TIME-OBS	P	R	Time of observation start
TIMESYS	P	R	The principal time system for all time-related keywords. Always UTC.

Keyword Name	HDU	Origin	Meaning
World Coordinates			
CD <i>i_j</i>	E	R, U	Transformation matrix from pixel to intermediate world coordinates; CD <i>i</i> is the pixel scale for axis <i>i</i>
CRPIX <i>i</i>	E	R, U	Location of the reference point along axis <i>i</i> in units of pixels
CRVAL <i>i</i>	E	R, U	Value of the world coordinate at the reference point for axis <i>i</i> in degrees
CTYPE <i>i</i>	E	R	Name of the coordinate represented in axis <i>i</i>
DEC	P	R, U	Declination for the center of the FoV in degrees
EQUINOX	E	R	Equinox in years for the celestial coordinate system in which the positions are expressed
NAXIS <i>i</i>	E	R	Number of pixels along axis <i>i</i>
PIXSCAL <i>i</i>	E	R	Pixel scale along axis <i>i</i> in arcsec/pixel
RA	P	R, U	Right ascension for the center of the FoV in hh:mm:ss.s
RADESYS	E	R, U	Name of the reference system in which the world coordinates are expressed
WAT <i>i_nnn</i>	E	R, U	IRAF-specific description of the nonlinear portion of the transformation from detector to world coordinates for axis <i>i</i> . This character string contains coefficients for a polynomial; the length of the string is such that it must continue for <i>nnn</i> FITS header records.
Calibration			
BUNIT	E	L2, U	Brightness units of image (adu adu/s electron/s)
DARKINFO	P	L2	Extent to which Dark MasterCal file matches the EXPTIME and the array sampling parameters of this science image
MAGZERO	E	L2	Magnitude corresponding to one count in the image
OBSTYPE	R	R	Type of target observed (object dark dome flat)
PIPELINE	P	L2	Pipeline name
PLVER	P	L2	Pipeline version identifier
PROCTYPE	P	L2, U	Product type (see Table 3-5 on page 3-8)
PRODTYPE	P	L2, U	Product data description (image mask expmap)
PHOTCLAM	P	L2	Central wavelength of bandpass (Å)
PHOTBW	P	L2	RMS width of bandpass (Å)
PHOTDPHT	P	L2	Photometric depth of the exposure. (See “Photometric Calibration” on page 3-19)
PHOTFWHM	P	L2	FWHM of bandpass (Å), i.e., width measured at 50% of peak transmission
SEEING	P	L2	Average FWHM of point sources, in arcseconds
SKYBG	P	L2	Brightness level of sky background averaged over all arrays, in BUNIT
SKYBG1	E	L2	Brightness level of sky background in single array, in BUNIT
SKYNOISE	P	L2	RMS noise in the background level, in ADU

3.2.3 Environmental Data

At present no environmental data are accessible from the Archive, although data from all-sky cameras, seeing monitors, and weather conditions at KPNO are available online.⁴⁰

3.3 Calibration

The current generation of pipeline processing produces Level-2 products, or images where the instrumental signature has been removed and geometric and photometric calibrations have been applied; and Level-3 products, where spatially overlapping images in the same filter (and that have been obtained within the same observing run) have been stacked. The pipeline uses calibration exposures, such as darks and dome flats taken during an observing run, to construct the calibration reference files that are used as input to the processing. For simplicity, the subsections below will first describe the processing of the science images once the calibration reference files are available; then the processes for constructing the calibration reference files will be described with the overall flow as context. The actual sequence of processing in the pipeline software differs somewhat in detail, in part, to optimize the performance of the parallel processing environment.



The calibration pipeline for NEWFIRM reductions is tuned to maximize the use of exposures within the observing run in which they were obtained. As such, the quality of the data depends to a large degree on the quality of the calibration exposures that were obtained by the observer. However, if the quality of the master calibrations is poor (as judged by the pipeline operator), the pipeline will attempt to use calibration data from the nearest prior or subsequent observing runs.

3.3.1 Processing Steps

The flow of the science data through the pipeline is shown in Figure 3-9. Each step of the processing, indicated by the boxes in the center of the figure, is described in detail in the following subsections. Inputs to the processing include the raw science frames, calibration reference files (see “Calibration Reference Files” on page 3-20), and photometric and astrometric catalogs. Outputs include the various reduced science images, plus their associated mask files (see “Image Formats” on page 3-9). Intermediate products that are produced during the course of pipeline processing, but are not archived, are not shown. The processing is segregated by observing run⁴¹, filter, and further by spatially overlapping observing sequences when deriving Stacked images.

⁴⁰ http://www-kpno.kpno.noao.edu/Info/Mtn_Weather/allsky/kpasca.html.

⁴¹ Processing may be further divided into *blocks* of sequential nights for long observing runs to limit the number of exposures that are simultaneously presented to the pipeline.

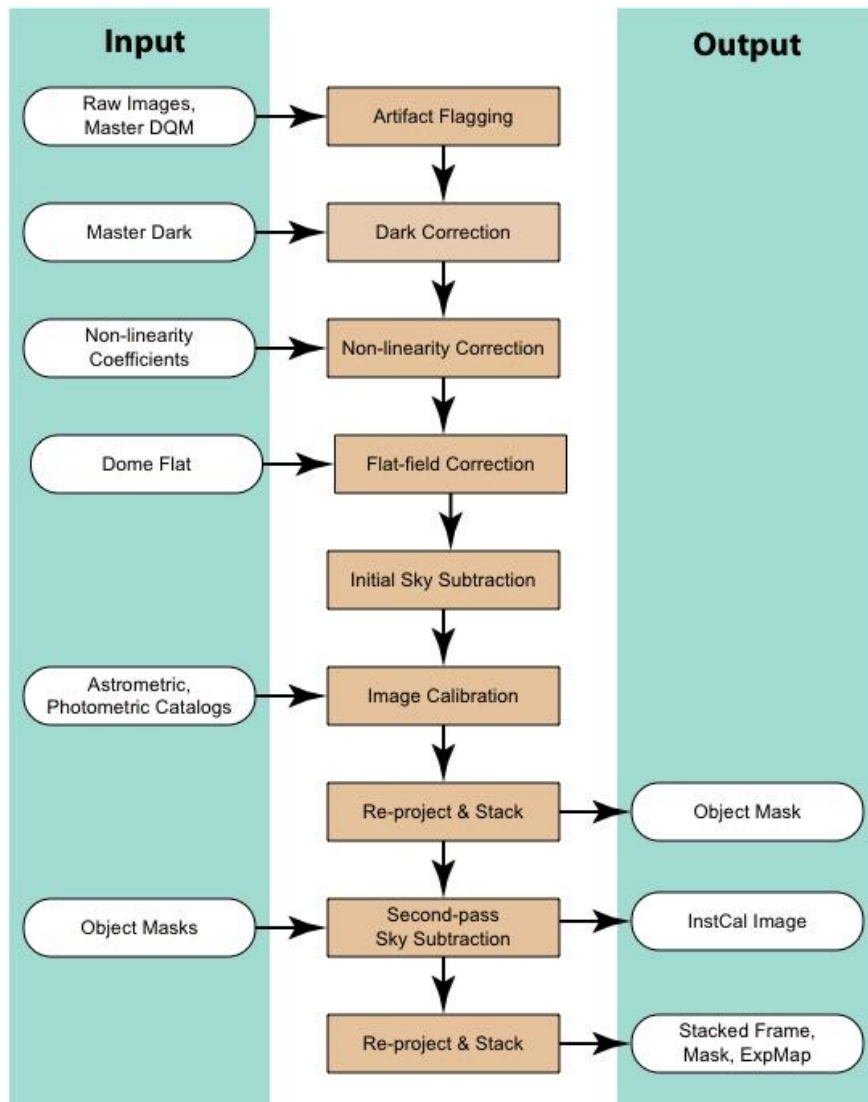


Figure 3-9: Flow of NEWFIRM data through pipeline processing and calibration to produce Level-2 and Level-3 data products. External catalogs, and data products defined in Table 3-5 on page 3-8, are shown as inputs or outputs of the processing. Intermediate products are not shown.

Artifact Flagging

Various image artifacts, including detector blemishes as described in the “Focal Plane” section on page 3-3, are marked in the DQM of each science image. In addition, pixels with values above 8000 ADU (times the product of the number of Fowler samples and Co-adds; see Table 3-3 on page 3-6) are marked as likely to cause persistence on the next five images in an observing sequence. Further artifact flagging occurs later in the processing, including *saturation*, which is detected during linearity correction, and *transients* (e.g., moving objects and cosmic rays), which are detected during the final image stack. The DQM for each InstCal image indicates all detected artifacts noted above. All flagged pixels are excluded from contributing to the final Stacked image; if this process results in areas with no data, such pixels are so flagged (see Table 3-8 on page 3-12 for details).



Note that all pixels in calibrated science frames (InstCal, Resampled, and Stacked) that are flagged in the DQM with a value other than zero are replaced by a linear interpolation using adjacent pixels. The one-dimensional linear interpolation is performed along the shortest dimension of the region over which to interpolate. This process is intended to avoid introducing “ringing” artifacts during the down-stream resampling of the images, as well as to mitigate scaling problems when using image display software.

Dark Correction

The dark current, i.e., the signal introduced by thermal electrons in the detector without external illumination, is very low in the Orion arrays and is typically $0.3\text{ e}^-/\text{s}/\text{pixel}$. However, the amplitude and structure of the dark frames is dominated by electronic bias effects, which can be a strong function of the number of on-chip co-additions, digital averages, and Fowler samples (see “Array Operation” on page 3-5), as well as the exposure time if the integrations are very short. Thus, the dark correction is applied to science frames using the Master Dark image that matches all of these parameters as closely as possible. A keyword, DARKINFO, is inserted into each science header to indicate the extent to which the Master Dark file matches the exposure duration and sampling type of the science exposure.

Linearity Correction

The response of the Orion infrared detectors is not perfectly linear to incident radiation, but generally can be well characterized and corrected (see Dickinson 2009). A schematic of the detector nonlinearity is shown in Figure 3-5 on page 3-7. The linearity correction for NEWFIRM is complicated by the fact that the images as recorded by the instrument do not include all the counts that accumulated in each pixel. This effect is most severe at high incident count rates and results from the method used to record the data, as described in “Array Operation” on page 3-5. In essence, counts that accumulate between the pixel reset and the first (nondestructive) read (t_r) are not reflected in the final difference image (i.e., what is recorded), but they must be accounted for when assessing where the accumulated counts fall on the linearity curve and for evaluating detector saturation. Thus, the magnitude of the linearity correction for a given pixel is dependent on a number of factors, including the number of co-adds, the incident count rate, the exposure duration, and location on the array. The linearity function is of the form $\Lambda(n) = 1 + s \cdot r_0 t$, where r_0 is the true incident count rate over total time t (which is the sum of the integration time and t_r), and s is negative. The final pixel value is the product of the measured counts and a correction factor (with a value >1.0) that takes into account the effects noted above.

Dickinson (2009) points out that the correlated double-sample (CDS) readout technique used for the NEWFIRM detectors means that detector saturation cannot be defined simply in terms of a fixed threshold of measured counts. The counts in a CDS readout will saturate at different apparent levels, depending on the intrinsic count rate, the exposure duration, t_r (see Figure 3-5 on page 3-7), and the number of co-adds and Fowler samples. It is possible to define a threshold in the context of the linearity correction, but this approach will fail at the highest incident count rates. In this regime, the affected pixels may be near saturation by the time the first readout occurs, so that the difference between the saturated second read and the initial read (i.e., the measured counts) actually declines with increasing count rate.



At very high count-rates, identifying a saturation condition over broad areas of the detector (as opposed to within the cores of bright stars) is difficult to do correctly within the pipeline.

Flat-field Correction

The flat-field correction removes the variations in the pixel-to-pixel response of the detector, and scales to a common gain across the focal plane. In the current version of the pipeline, the flat-field is derived for each filter solely from dome-flats (i.e., images of the illuminated dome flat-field screen). The flat-field correction is performed by dividing each science frame by the flat-field calibration reference frame for the corresponding filter. The pixel values are then normalized to unit exposure time. The brightness units, as expressed in the value of the BUNIT keyword, are ADU s⁻¹ for calibrated images.

Sky Subtraction

In ground-based IR imaging, flux from the background dominates the detected signal in broadband filters from most astrophysical sources and can exceed the flux from the faintest stars and galaxies by a few orders of magnitude. The sources of the background flux include the night sky (from OH⁻ emission, moonlight, and a thermal component at *K*-band), heat sources in the telescope dome, the telescope optics, and dark current. The molecular emission in the night sky can vary significantly on few-minute timescales and can vary spatially across the large NEWFIRM FoV. Thus, highly accurate sky subtraction is essential to good photometry, and this is facilitated by relatively short exposure durations (except for narrowband filters) and spatial dithering between exposures.



This *sky-subtraction* stage of the pipeline is where the corrections to single images generally depend upon properties derived from multiple science exposures within an observing sequence.

Determination of the sky background for individual images is a two-pass process. In the **first pass** the sky value for each pixel in the output image is determined by computing a running median with a window of up to 9 exposures in the observing sequence, excluding masked pixels in the input images and rejecting outliers to minimize the influence of transients and astrophysical sources in the field. Note that the input images have only an approximate WCS solution in this step: the implicit assumption is that the images are dithered, with offsets that are larger than the point-source size. For sequences of three or fewer images, initial sky subtraction is performed by subtracting the image closest in time (i.e., pair-wise sky subtraction). For single images (not in a sequence) a smooth, low-order polynomial is used to characterize the background, with rejection of pixel values that are well above the background (i.e., from sources). Finally, if *offset sky exposures* (i.e., exposures of relatively blank sky some distance from an extended target) were obtained as a part of the observing sequence, these will be combined with masking and outlier rejection and used for sky subtraction of the science target. Naturally, offset sky exposures that are dithered will result in improved sky subtraction. The sky is then subtracted from each of the science images, which are then re-projected to a common geometric frame and combined using a median with outlier rejection. The purpose of this Stacked image is to create a mask for all the astrophysical sources in the field. The type of sky subtraction that was performed by the pipeline is recorded in the SSUBINFO header keyword.

In the **second pass**, the source mask is projected back to the geometry of each original (raw) image frame. The sky is re-determined using the above prescription, except that detected astrophysical sources are in addition masked from the input images. Any remaining residuals are removed by fitting and subtracting a low-order fit to the background. The average value of the sky in units of ADUs is written to the extension headers (SKYBG1), and the average over the four arrays is written to the Primary header (SKYBG), for each calibrated science image, including the final stack if any.

Astrometric Calibration

The astrometric, or WCS calibration for science images is described by a two-dimensional polynomial (the function type and coefficients are found in the header) of a tangent-plane projection of stellar coordinates to the image pixel grid. The lower-order terms relate to the location of the reference pixel on the sky, the plate scale, and the rotation of the image, while the higher-order terms relate to nonlinear effects of the optical system such as image distortion. The form and order of the function varies with the filter and to a small degree with the airmass of the observation. The initial values for all but the zero-point terms are taken from prior, full WCS solutions of calibration images where the density of catalog stars in the field is high; the initial value for the pointing is taken from the TELRA and TELDEC header keywords, which are supplied by the telescope control system.

A WCS solution for low-order terms is determined for each array by associating centroids of stars in the science images with objects in the **2MASS** reference catalog. Since the number of suitable stars in any given image (and their distribution within the image) can vary considerably, depending upon such details as the exposure time, ambient seeing, and clouds, the input list to the WCS solution includes roughly 100 additional pseudo-stars, which are merely computed points from the trial WCS solution. Thus, if the number of genuine stars in the image is small compared to the pseudo-stars, the high-order terms in the WCS solution will be dominated by the trial solution. If instead the number of genuine stars is large, they will dominate the WCS solution. In all cases, only the genuine stars contribute to determining the zero-point.

Photometric Calibration

An estimate is made of the magnitude zero-point of each science image by comparing the instrumental aperture magnitude of each field star to their published magnitudes in overlapping passbands in a reference catalog. Currently, the 2MASS reference photometric catalog is used (Skrutskie 2006). Note that the result of the photometric calibration is to populate the science header with keywords—the pixel values remain unchanged, and have units of ADU s^{-1} .

One quantity of use, the photometric depth of the exposure, is defined as:

$$-\frac{2.5}{2.3026} \log\left(\frac{3.988 \cdot Q \cdot \sigma}{\sqrt{A}}\right) + m_{\text{zero}}$$

In physical terms, the photometric depth is the faintest point-source that can result in a 5σ detection above the sky background, in units of magnitudes. In the equation above, Q is the delivered image quality (the average FWHM of point-sources in the image, stored in the image header keyword SEEING) in units of arcseconds, σ is the noise in the background in ADU, A is the area of a pixel in arcsec^2 , and m_{zero} is the

magnitude zero-point. This quantity is stored in the header of the calibrated images as the value of the PHOTDPTH keyword.



Note the importance of the exposure time and the mean sky values that were determined during pipeline processing. These values, plus the detector gain, are stored in FITS header keywords and must be used to reconstruct the original source counts and background (in units of detected photons) when computing the statistical errors on measurements such as source magnitudes.

The quality of the photometric calibration is not well documented, but is believed to be good for well-exposed, broadband images containing a substantial number of catalog stars. For the other filters, the value in the MAGZERO keyword should be reasonably good, and in any case is useful as a measure of sky transparency over an image sequence. See “Sources of Error” on page 3-22 for details.



The J, H, K_s filters used in NEWFIRM match those of the 2MASS catalog very well, and often yield zero-points accurate to ~ 0.05 mag, limited in part by the lack of an aperture correction for the instrumental magnitudes. The mapping from narrowband filters used with the NEWFIRM camera to 2MASS passbands introduces additional uncertainty.

Image Re-projection and Stacking

A Stacked NEWFIRM image is constructed by resampling, using a *sinc* interpolation, the component science images to a common geometric grid. Note that image blemishes and other artifacts are interpolated over in this step, so as not to cause “ringing” in the Resampled images. This form of the science data product is simple to use for image stacking and transient detection, without the need to handle the distortion mapping. The astrometric system is a tangent-plane projection with a uniform sampling of 0.4 arcsec pixel⁻¹, oriented with north “up” (i.e., Declination increases along Axis 2) and east “to the left” (i.e., Right Ascension decreases along Axis 1). The **tangent-point** is selected from a grid on the sky with roughly 1° steps in RA, and exactly 1° in Dec. This selection makes it easy to stack images that are part of a sequence of small spatial dithers.

When stacking, the pipeline scales the input images to a common magnitude zero-point and sky transparency. The input images are weighted by the seeing and sky brightness. Data with a zero-point that is 1 mag below the best zero-point in the observing sequence is rejected from the stack. The final Stacked image is a weighted average of the input images, after masking and outlier rejection.

3.3.2 Calibration Reference Files

The calibration reference files that are used in the pipeline processing are constructed for each observing run where a sufficient number of appropriate exposures exist. For the master flat-field reference file, the exposures that are used for calibration are affected by multiple instrumental signatures. It is important to distinguish between the additive backgrounds and the multiplicative linearity and sensitivity variations in order to avoid biasing the photometric accuracy of the processed science frames.

Static Data Quality Mask

Master data quality masks are used to generate a DQM for each science frame that marks the locations of artifacts (e.g., inoperable rows/columns, PED dead spots, and high-valued pixels that indicate possible saturation or persistence in subsequent images; see Figure 3-3 on page 3-4). When the final Stacked calibration frames are created for each filter, these artifacts are masked from the averages.

Dark

The master dark file is constructed very simply by averaging the frames after rejecting the minimum and maximum values (at least five dark images are required to create the reference file). Once constructed, the dark correction will be applied to all images, matching as closely as possible the exposure time, number of co-adds, and sampling type. A keyword, DARKINFO, inserted into each science header indicates the extent to which the master dark file matches the science exposure.



Since the response of the detector depends upon the rate and method of sampling the array, it is important that the master dark calibration frame correspond to the observations in exposure duration, number of co-additions, and sampling type. Significant deviations in any of these parameters will compromise the accuracy of the dark correction.

Linearity Coefficients

The linearity coefficients are derived from engineering observations that consist of a series of dome-flat exposures that were taken with a range of exposure durations such that the full dynamic range of the detectors is sampled. The intensity of the dome flat-field lamp is monitored during this sequence, and a pixel-by-pixel mapping of the measured counts as a function of illumination level may be derived. Note, however, that at the brighter illumination levels it is necessary to correct for the counts that accumulate during the “reset-to-first read” interval, as discussed in “Array Operation” on page 3-5. In the end, the pixel-to-pixel linearity curves are characterized with simple polynomial coefficients and stored in the master linearity calibration reference file. The coefficients are believed to be temporally stable and are provided to the pipeline processing system by NOAO Science staff (see Dickinson 2009).

Flat-field

Dome flats, or exposures of an illuminated screen affixed to the interior of the telescope enclosure, are used to construct the flat-field reference file. The process for constructing the master dome flat, illustrated in Figure 3-10, begins with flagging artifacts, followed by the dark and linearity corrections on each frame. The images for each filter are then combined (with rejection of outliers and artifact rejection), separately for the illuminated and also for un-illuminated frames. These “lights-on” and “lights-off” frames are then subtracted from one another to eliminate the contribution from thermal emission even when the flat-field lights are off.⁴² The result is then normalized to an average of 1.0 over all four detectors, i.e., the variation of the average sensitivity between detectors is preserved in the Master Flat-field, and hence is removed when applied to the science images.

⁴² The effect is most pronounced for *K*-band exposures.

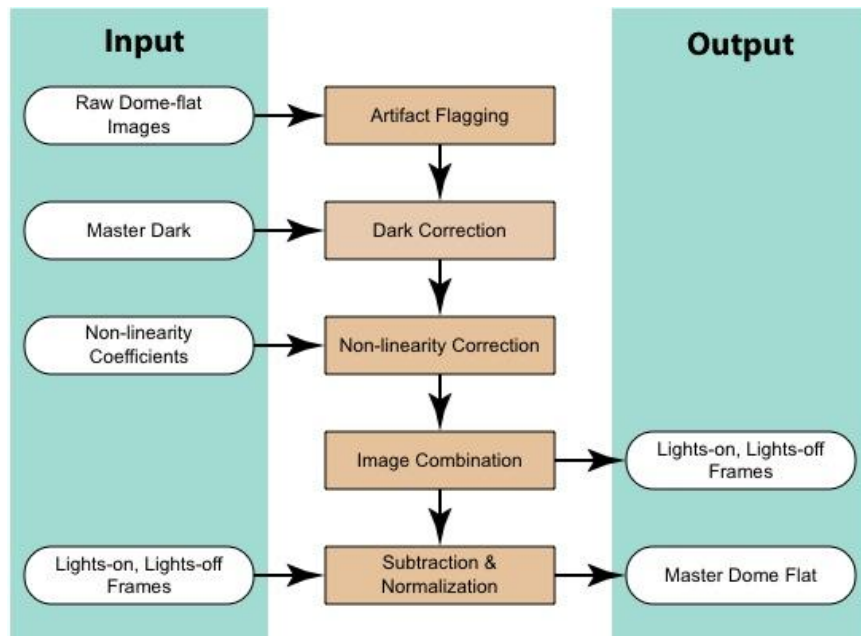


Figure 3-10: Process for deriving the NEWFIRM Master Flat-field for each filter. Input dome-flat frames are uncalibrated and consist of alternating sequences with and without flat-field lamp illumination; these are combined separately and subtracted from one another.

Note that twilight- and sky-flats are neither generated nor used in the calibration pipeline.

3.4 Sources of Error

This section describes the accuracy that can be expected for the major data products, the major sources of error, instrument foibles, and other noteworthy problems and issues with NEWFIRM data.

3.4.1 Astrometry

The astrometric accuracy for the image coordinate system is fundamentally limited by the science image exposure depth and the accuracy of the astrometric catalog used to determine the WCS solution, which is presently that of the 2MASS catalog. This all-sky catalog has a limiting magnitude that provides a good overlap in the brightness range covered by most NEWFIRM exposures. Typical accuracies obtained for the WCS solution (0.2" or 0.5 pix measured in RMS deviations from the fit) are comparable to the accuracy of the catalog (Skrutskie et al. 2006). The accuracy might be improved somewhat if the coordinates of the catalog stars were adjusted for proper motions. The geometric stability of the NEWFIRM camera is very good: <0.1" (Whitaker, et al. 2011).

3.4.2 Photometry

The photometric stability of the NEWFIRM camera has not been rigorously examined, but with care and good flat-fielding, it should be possible to achieve photometric accuracies of ~ 0.02 mag (Whitaker, et al. 2011). At present the photometric calibration achieved by the pipeline processing yields typical accuracies of 0.05 mag for the J , H , and K_s broadband filters, but is less well determined for the narrowband filters. Within a sequence of observations covering the same region of the sky, the photometric zero-points provide a useful diagnostic of the photometric stability of the sky.

The photometric performance for any given image depends mostly on a number of external factors, especially the variable sky emission and the delivered seeing. In Stacked images, the photometric depth varies discontinuously across the image because of the gaps between the sensors in the FPA and depends upon the dither patterns that are used in the observing sequences. Thus, photometric measurements of targets that span these discontinuities may suffer some additional uncertainty.

Spatial structure in the sky background is tracked implicitly by the pixel-by-pixel robust median clipping algorithm used during the two-pass sky subtraction step. However, if the actual spatial structure of the sky background is not well characterized with this technique (for instance, if the field contains objects that span a fair fraction of the FoV for a sensor), then photometry of extended sources may not be accurate.

3.4.3 Anomalies

Metadata

Critical metadata in raw science data files may sometimes be missing or have incorrect values. However, certain of the metadata in the headers of calibrated data, notably the WCS information and the filter name, are corrected during the course of pipeline processing (unless the processing fails). Metadata *added* by the pipeline during processing are not in question.

Dome Lamp State

The status of the dome flat-field lamps as recorded in the header keyword NOCLAMP is unreliable, and at present is correct only by accident. The pipeline uses a heuristic algorithm to distinguish between images that have been illuminated by the lamp versus those that are not. The difference is obvious except in the K_s -band.

Saturated Pixels

Pixel saturation (where the accumulated charge exceeds the full-well, e.g., in the cores of over-exposed stars) is not easy to characterize in extended regions illuminated at a high count-rate (see Figure 3-5 on page 3-7). Saturated regions in flat-field exposures, for example, may not always be flagged accurately in the DQM file.

Image Ghosts

Bright stars can produce three different pupil ghosts, the effects of which may be difficult to remove. Their characteristics in the J -band filter are the following:

- A roughly 300-pixel-diameter ghost, about 17 mag/arcsec^2 fainter than the integrated magnitude of the source star. The ghost is offset radially by hundreds of pixels with respect to the field center; the size of the offset depends upon the distance of the source from the field center.
- A roughly 100-pixel-diameter ghost, about 14 mag/arcsec^2 fainter than the integrated magnitude of the source star, and nearly centered on it. This ghost could give rise to the appearance of false nebulosity around bright stars in Stacked images.
- A compact, star-like ghost of 4 pixels in diameter, which is 8.5 mag fainter than the source star and offset radially from it by hundreds of pixels, in a field-dependent manner. This ghost might appear in Stacked images as bogus point sources near bright stars. But since the radial position of this ghost is field-dependent, it may be rejected from the stack if the dither pattern is sufficiently large.

Background for Narrowband Filters

Images of astrophysical targets obtained with the ultra-narrow filters ($1.056 \mu\text{m}$ and $1.063 \mu\text{m}$) contain ring-like features in the background, as shown in Figure 3-11. These ultra-narrowband filters are designed to capture the designated emission line feature with high transmission over the entire field of view at zero redshift. Owing to the convergent beam of the optical system, the filter bandpass shifts in wavelength with radial position in the FoV: at field center, the designated line falls near the blue edge of the high transmission window; at field corner, near the red edge. The “ring” features are due to the presence of OH emission lines in the night sky background near the passband of the narrowband filter. The passband shifts slightly as a function of position (distance from the field center, in particular), and thus different amounts of the OH emission pass through the filter as a function of radius from the field center, leading to the rings.

The ring features are an additive background that varies in time. It is easily characterized and, depending on the distribution of sources in the exposure, can be removed by the pipeline.

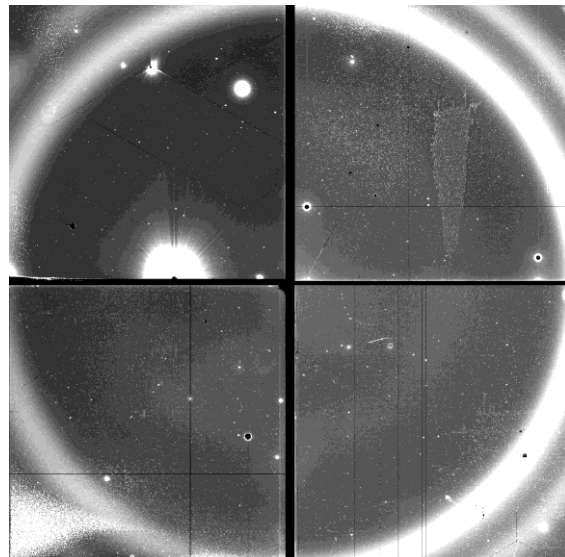


Figure 3-11: Image of the night sky with the $1.056 \mu\text{m}$ ultra-narrowband filter showing the “ring” feature in the background, which results from night-sky OH emission at the edge of the filter passband.

3.5 References & Further Information

Contributing Authors

Several people have contributed to the technical knowledge of the NEWFIRM camera. Extensive material was contributed by Ron Probst (NEWFIRM Project Scientist) and Mike Merrill (Telescope Scientist and detector expert); by the pipeline development team of Rob Swaters, Frank Valdes, Mark Dickinson, and Tracy Huard; and by Dick Shaw. Documentation on the reduction of NEWFIRM data with the IRAF `newfirm` package is also fairly extensive, much of which was authored by Frank Valdes.

References

- Dickinson, M., Huard, T., Swaters, R., & Valdes, F. G. 2010, *NEWFIRM Quick Reduce Pipeline and Data Analysis Tools* (Tucson: NOAO), available online:
<http://www.noao.edu/staff/med/newfirm/QRP/>
- Dickinson, M. 2008, *NEWFIRM Linearity Calibration and Correction*, [NOAO-DPP Doc. PL016](#) (Tucson: NOAO)
- Fowler, A. M., & Gatley, I. 1990, [ApJ, 353, L33](#)
- Merrill, K. M. 2008, *Orion SCA Laboratory Test Results Summary* (Tucson: NOAO), available online:
http://www.noao.edu/ets/newfirm/documents/ORION_SCA_lab_tests_final.pdf
- Probst, R. 2008, *NEWFIRM Quick Guide for Proposal Preparation* (Tucson: NOAO), available online:
http://www.noao.edu/ets/newfirm/documents/Quick_Guide_for_Proposal_Preparation.pdf
- Probst, R. G., George, J. R., Daly, P. N., Don, K., & Ellis, M. 2008, *First Light with NEWFIRM*, [SPIE, 7014, 93](#)
- Skrutskie, M. F., et al. 2006, *The Two Micron All-Sky Survey (2MASS)*, [AJ, 131, 1163](#)
- Whitaker, K. E., Labbe, I., van Dokkum, P. G., et al. 2011, *The NEWFIRM Medium-Band Survey: Photometric Catalogs, Redshifts, and the Bimodal Color Distribution of Galaxies out to $z \sim 3$* , [AJ, 735, 86](#)

For Further Reading

A document repository⁴³ for NEWFIRM is available, where many of the above-referenced papers may be found. The JHK_s filter passbands follow the Mauna Kea Observatory prescription:

Tokunaga, A. T., Simons, D. A., & Vacca, W. D. 2002, [PASP, 114, 180](#)

The following is a discussion of large-format InSb detectors, such as those used in NEWFIRM:

Hoffman, A. W., Corrales, E., Love, P. J., Rosbeck, J., Merrill, M., Fowler, A., & McMurtry, C. 2004, *2K x 2K InSb for Astronomy*, [SPIE, 5499, 59](#)

⁴³ Available at <http://www.noao.edu/ets/newfirm/>.

The reduction of NEWFIRM data outside the automated pipeline, including a general discussion of IRAF data reduction techniques for IR mosaics, may be found in:

Dickinson, M., & Valdes, F. G. 2009, *A Guide to NEWFIRM Data Reduction with IRAF*, [NOAO-SDM Doc. PL017](#) (Tucson: NOAO)

Additional papers on the NOAO pipeline processing system generally and the NEWFIRM pipeline in particular have appeared in the proceedings of the ADASS conference series.

Scott, D., Pierfederici, F., Swaters, R. A., Thomas, B., & Valdes, F. G. 2007, *The NOAO High-Performance Pipeline System: Architecture Overview*, in [ASP Conf. Ser. 376](#), ed. R. A. Shaw, F. Hill, & D. J. Bell (San Francisco: ASP), 265

Swaters, R. A., Valdes, F., & Dickinson, M. E. 2009, *The NOAO NEWFIRM Pipeline*, in [ASP Conf. Ser. 411](#), ed. D. Bohlender, P. Dowler, & D. Durand (San Francisco: ASP), 506

Papers describing the science results from NOAO Surveys conducted with NEWFIRM offer useful insights into NEWFIRM data reduction and calibration:

Van Dokkum, P. G., Labbe, I., Marchesini, D., et al. 2009, *The NEWFIRM Medium-Band Survey: Filter Definitions and First Results*, [PASP, 121, 2](#)

Ly, C. Lee, J. C., Daniel, D. A., et al. 2011, *The H α Luminosity Function and Star Formation Rate Volume Density at z=0.8 from the NEWFIRM H α Survey*, [ApJ, 726, 109](#)

Chapter 4

Dark Energy Camera

Version 1.2, May 2015

In This Chapter...
Instrument Overview4-1
Data Products4-7
Calibration ...4-13
DECam Sources of Error ...4-27
References & Further Information ...4-33

The Dark Energy Camera (DECam) began operation on the Blanco 4-m telescope at CTIO in late 2012. It was built by the Dark Energy Survey Collaboration to carry out the Dark Energy Survey⁴⁴ (**DES**). The survey began in September 2013 and will occupy about 30% of the observing time over five years (mostly in the August–February observing semester). DECam is also available for community use, and calibrated data products are produced with a pipeline that is similar to that used for the DES.

The material for this chapter has been drawn from a large number of sources, including DECam technical documents, the DES website,⁴⁵ data file headers, software design documents, and input from experts.

Interested users should consult the references at the end of this chapter for details of the instrument description and pipeline operation. Additional resources are cited throughout this chapter and are listed along with other background material in the last section.

4.1 Instrument Overview

DECam is a prime focus optical imager that is mounted on the Blanco 4-m telescope. It features a 3 deg^2 field of view (**FoV**) and a large focal plane array (**FPA**) consisting of sixty-two $2\text{K}\times 4\text{K}$ **CCDs**, with a total of 520 million pixels. A schematic of the instrument and its deployment on the telescope is shown in Figure 4-1.

⁴⁴ See the DES homepage at: <https://www.darkenergysurvey.org/index.shtml>.

⁴⁵ See the DECam instrument website at <http://www.ctio.noao.edu/noao/content/Dark-Energy-Camera-DECam>.

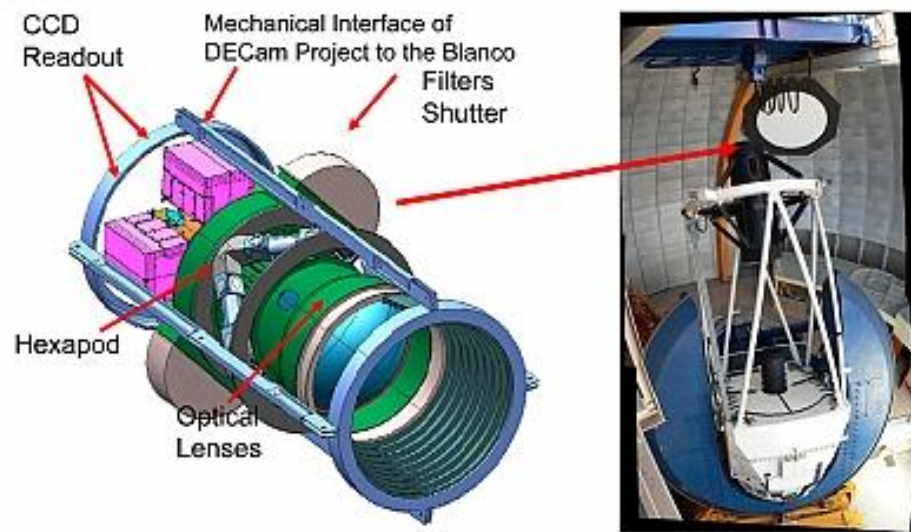


Figure 4-1: Dark Energy Camera (DECam) shown in schematic (left) and as mounted at the prime focal station on the Blanco 4-m telescope (right).

The major components are an optical corrector, 4 filter slides each holding 2 filters, a shutter, and a cryostat (“imager vessel”) holding the focal plane of 62 science CCDs, 8 wave-front sensing CCDs, 4 guide CCDs, and pre-amplifiers. Four electronics crates are mounted behind the imager. The CCD vessel, shutter, filters, and corrector are supported as a single unit by a hexapod that provides accurate adjustability in three dimensions: focus, lateral translations, tip, and tilt. This provides a real-time focus and alignment system to maintain high image quality.

4.1.1 Instrument Capabilities & Design

Optical Corrector

The corrector for the camera is a five-element, all fused silica design (see Figure 4-2), where the final element (C5) is the cryostat window. The large and steeply curved front element (C1) is not coated; the remaining elements have multi-layer anti-reflection coatings. These coatings contribute to the short-wavelength cutoff of the system throughput at around 340 nm.



The DECam corrector does not include atmospheric dispersion correction optics. Thus, images obtained in the bluer filters (*u*, *g*) at moderate to high airmass will show significant PSF distortions in the direction of the parallactic angle.

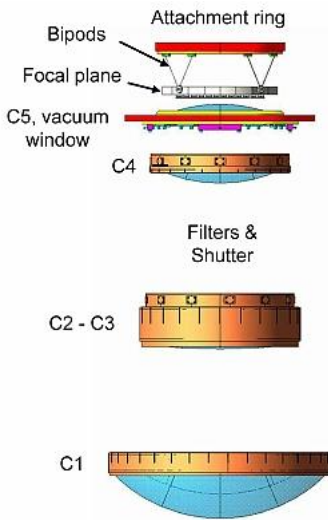


Figure 4-2: Exploded cross-section view of the 5-element DECam optical corrector, relative to the focal plane (near the top). The orientation corresponds to the telescope pointing at the zenith.

Camera

The details of the camera characteristics are given in Table 4-1. The camera is mounted at the prime focal station of the Blanco 4-m telescope. The pixel scale samples the delivered point spread function (**PSF**) well, which is seeing-limited at all wavelengths. The image quality at the 4-m telescopes is good, with little (<5%) focus gradient or PSF variation across the field of view. Charge diffusion in the CCDs and the performance of the optics are major contributors (~0.45 arcsec) to the PSF width (Roodman 2013). The pixel scale gradually increases from the center to the edge of the FoV due to pincushion distortion. There is very little vignetting.

Table 4-1: DECam Camera Characteristics

Field of view	2° diameter circular field, 3 deg ² coverage
Focal ratio	f2.7
Pixel scale of FPA, center/edge	0.2637 / 0.2626 arcsec/pixel
Plate scale	17.57 arcsec/mm
Inter-CCD gaps	
Rows:	3.0 mm (201 pix)
Columns:	2.3 mm (153 pix)
Delivered image quality	~0.8 arcsec in excellent seeing conditions
Filter set	<i>u, g, r, i, z, Y, VR</i>

Focal Plane

The CCDs are mounted on an aluminum plate in a hexagon pattern (see Figure 4-3) and are coplanar to approximately 15 μm (RMS). Note that the center of the field falls inside a gap between the S4 and N4 CCDs. Four pairs of focus and alignment sensors are positioned near the edge of the FoV, with the CCDs in each pair mounted 1.5 mm above and below the focal plane, respectively.

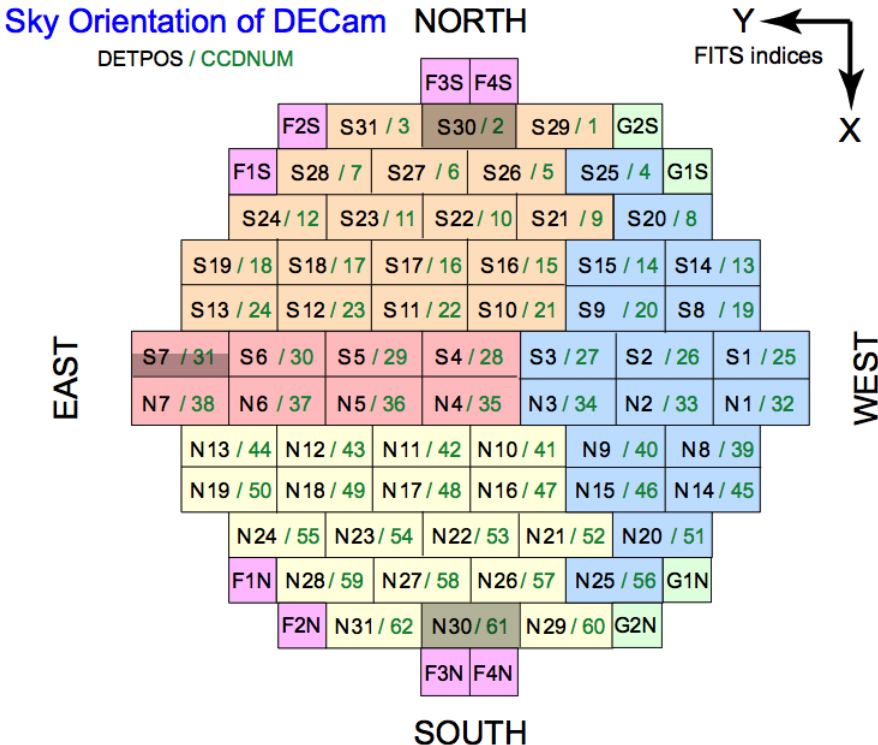


Figure 4-3: The arrangement of the DECam FPA on the sky⁴⁶, which includes twelve 2Kx2K CCDs for guiding (green) and focus (magenta) control. Science CCDs are controlled with one of four sets of read-out electronics (orange, pink, blue, yellow). Two of the CCDs do not function properly, and the gain for one amp on a third CCD is unstable (grey). Note that the raw image amplifier coordinates are remapped to detector coordinates. The images are transposed such that in the sky orientation shown above, north is up (Declination decreases along the x-axis) and east is to the left (Right Ascension increases along the y-axis).

The delivered image quality, measured from the PSF of well-exposed stars under excellent observing conditions, is sampled very well by the detectors; image quality is seeing-limited at all wavelengths. The image quality at the Blanco is good with little focus gradient or PSF variation across the FoV. The pixel scale is slightly variable (0.3% per radial degree) from the center to the edge of the FoV due to pincushion distortion.

Sensors

The CCD detectors are 250 μm thick, fully-depleted devices. This is about 10 times thicker than conventional thinned CCDs. The thickness was chosen to improve the quantum efficiency in the near infrared (Estrada et al. 2010). A substrate voltage maintains the field through the depleted region so that photoelectrons are efficiently collected. However, charge diffusion is a significant contributor to the image quality budget. There are other effects specific to this type of CCD, such as “tree-rings” due to small spatial variations in the substrate doping, and electrostatic effects such as “brighter-fatter” (Antilogus, et al. 2014) that cause the PSF width to increase with source intensity. There is also some nonlinearity in response for

⁴⁶ Adapted from the DES Science Verification Wiki at: <https://cdcvn.fnal.gov/redmine/projects/des-sci-verification/wiki/Ccdmap>.

all CCDs at high count levels, and for some CCDs at low counts. The detectors reach peak quantum efficiency (QE) above 85% at $\sim 6500 \text{ \AA}$, but have useful sensitivity from the atmospheric cut-off near 3200 \AA to $\sim 1 \mu\text{m}$. Each of the science CCD detectors has two amplifiers with which to read the pixel arrays; pixel binning is not supported. The typical detector properties are given in Table 4-2.

Table 4-2: Sensor Characteristics

Sensor type	LBNL thick, fully depleted CCDs
Array dimensions	2048×4096 pixels
Pixel dimensions	$15 \times 15 \mu\text{m}$, $250 \mu\text{m}$ thick
ADC dynamic range	16 bit
Gain	$4 e^-/\text{ADU}$
Read noise	$6 e^-$
Dark current	$0.17 e^-/\text{s}$
Well capacity	$\sim 180 \text{ Ke}^-$ (ranges from 130 to 210 Ke^-)
CTE	>0.999995
Linearity	Within 1% below 160,000 ADU
Read time	20 s

The adopted gain means that the CCDs reach full-well on bright sources before the analog-to-digital converters saturate at 65K *ADU*. Saturated stars bleed along columns, but not excessively. However, extremely saturated stars cause bleeding and overflow in the serial register. Charge transfer for all the CCDs was excellent when tested in the laboratory. Linearity is good in general, but there is some nonlinearity. Finally, the QE is stable and, except at the very ends of the wavelength range, is very similar from device to device. Nevertheless, photometric transformations from instrumental magnitudes to standard systems should be calculated per detector.

Shutter

Exposures are controlled with a *Bonn shutter*,⁴⁷ where two blades sweep across the focal plane in very accurate synchronization; the elapsed time between the passing of the two blades over a position in the focal plane defines the exposure time. The blade-pair sweeps in alternate directions each exposure. The shutter timing parameters substantially exceeded specifications. The timing accuracy is better than 1 ms at any position across its 600-mm-diameter circular apertures (Reif 2010). The shutter exposure time repeatability is better than 5 ms, and the shutter allows a continuous range of exposures from 100 ms or greater. The absolute timing of an exposure is measured to a precision of 10 ms, and the accuracy of the shutter timing is <50 ms.

Filters

The camera includes seven large-format filters that are similar to those for the SDSS (*u, g, r, i, z*) with the addition of a near-IR *Y* filter and a very broad (500–760 nm) *VR* filter. The system throughputs for this set are shown in Figure 4-4. The filters all feature multi-layer interference coatings on both sides of a 62-cm-

⁴⁷ See <http://www.bonn-shutter.de>.

diameter fused silica substrate. All filters were supplied by Asahi Spectra Co. and exhibit steep transmission edges and flat tops, and no significant out-of-band response.

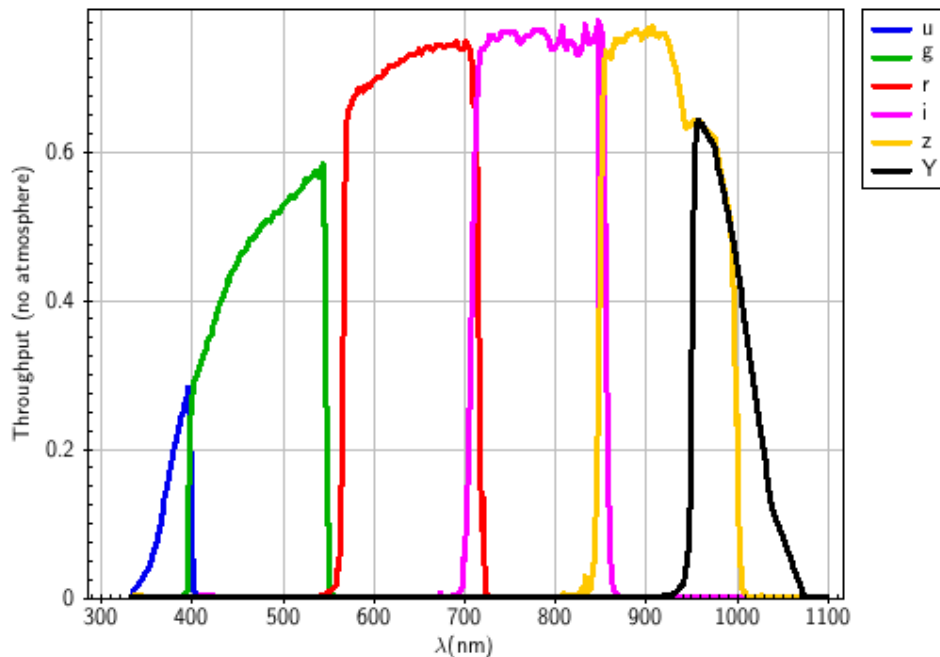


Figure 4-4: Total system throughput for each filter as a function of wavelength, including QE and throughput, but excluding atmospheric transmission.

There are small differences in transmission and wavelength of the transmission edges as a function of radial distance from the center of the filter. DECam has an auxiliary system (called *DECAL*) that illuminates a dome-mounted flat-field screen with near monochromatic light, and can scan the system response (telescope primary, optical corrector, filters, CCDs) through each filter as a function of position on the focal plane—in principle, for every pixel.

4.1.2 Operations

Most observers obtain multiple exposures of their fields using the same filter in order to reject cosmic rays; often this is combined with a sequence of small spatial *dithers* in order to observe in the gaps between the CCDs in the FPA and to enable the construction of continuous regions of sky that are free of gaps and detector artifacts. The DES Survey and some community observing programs construct sequences of (slightly) overlapping images to *map* larger regions of sky from the component tiles. Finally, most (but not all) observing programs obtain calibration frames, such as bias (zero) frames and dome flats, in order to facilitate calibration. See “Calibration” on page 4-13 for a detailed discussion of how the calibration frames are used in the data reduction process.

4.2 Data Products

This section describes the content and format of the various data products that are produced by the Community Pipeline (CP) for the Dark Energy Camera. Most of the products are generated during the course of calibration processing, the details of which are discussed in the next subsection. The data products from the CP can be distinguished by the combination of the PROCTYPE, PRODTYPE, and OBSTYPE keywords in the FITS primary header; the possible values are summarized in Table 4-3. The processing level (see “Table 1-2: Levels of Data Processing” on page 1-4) at which the product is generated is given in the *Proc. Level* column.

Table 4-3: DECam Data Product Types and Contents

PROCTYPE	PRODTYPE	OBSTYPE	Proc. Level ⁴⁸	Description
Raw	image	object	1	Raw data as obtained at the telescope, with some additional metadata included in the header
InstCal	image	object	2	Calibrated, sky-subtracted, single-frame image
InstCal	mask	object	2	Data quality mask for InstCal
InstCal	wtmap	object	2	Inverse variance array for InstCal
Resampled	image	object	2	Calibrated, sky-subtracted, re-projected image
Resampled	mask	object	2	Data quality mask for Resampled image
Resampled	wtmap	object	2	Inverse variance array for Resampled
Stack	image	object	3	Stack of multiple, overlapping, calibrated frames with sky subtracted
Stack	mask	object	3	Data quality mask for calibrated, Stacked image
Stack	wtmap	object	3	Inverse variance array for Stacked image
Stack	expmap	object	3	Exposure map for calibrated, Stacked image
MasterCal	image	BPM	Ext	Static Bad Pixel Map
MasterCal	table	cross-talk	Ext	Cross-talk coefficients
MasterCal	table	linearity	Ext	Linearity look-up table
MasterCal	image	zero	2	Master Bias Residual calibration image
MasterCal	image	dome flat	2	Master Dome Flat-field calibration image
MasterCal	image	star flat	Ext	Star-flat photometric correction image
MasterCal	image	fringe frame	Ext	Master Fringe pattern

4.2.1 Image Formats

The science image data from DECam is stored in FITS multi-extension files (MEFs, the general structure of which was described in Chapter 1). The detailed arrangement of the image portions among the exten-

⁴⁸ “Ext” means the MasterCal is produced externally to the pipeline.

sions differs, depending upon whether the data are raw (unprocessed) or reduced. The files may be stored in a compressed format. The internal structure and data type for the various data products is summarized in Table 4-4 below, including the number and type of FITS extension(s). When retrieved from the Archive, the data files have all been compressed with FITS tile-compression. This applies to images with both integer and floating-point native representations; floating-point compression is applied using the Rice compression technique, which should not significantly degrade the dynamic range of the data.

Table 4-4: Product Organization and Data Types

PROCTYPE	PRODTYPE	Ext Type	N. Ext	Data Type
Raw	image	IMAGE	70	16-bit int
InstCal	image	IMAGE	61	32-bit float
	dqmask	IMAGE	61	32-bit int
	wtmap	IMAGE	61	32-bit float
Resampled	image	[primary]	61	32-bit float
	dqmask	IMAGE	61	32-bit int
	wtmap	IMAGE	61	32-bit float
Stack	image	[primary]	N tiles	32-bit float
	dqmask	IMAGE	N tiles	32-bit int
	expmap	IMAGE	N tiles	32-bit int
	wtmap	IMAGE	N tiles	32-bit float
MasterCal	image	IMAGE	61/8	32-bit float

Raw Data

Raw data from DECam are integers and include virtual overscan along each row at the beginning and end of the CCD readouts, which is stored with the image pixels as shown in Figure 4-5. Note that the coordinate origin for all detectors is in the lower-left corner of the read-out section (for the convenience of image display), rather than at the location of the read-out amplifier. The output from each amplifier (including the overscan regions) is stored in a separate image extension in the FITS MEF file (see Chapter 1); there are as many image extensions in the raw science file as detectors in the focal plane (with the non-functioning S30 detector excluded). The size and location of the photo-active regions and the overscan are given in Table 4-5.

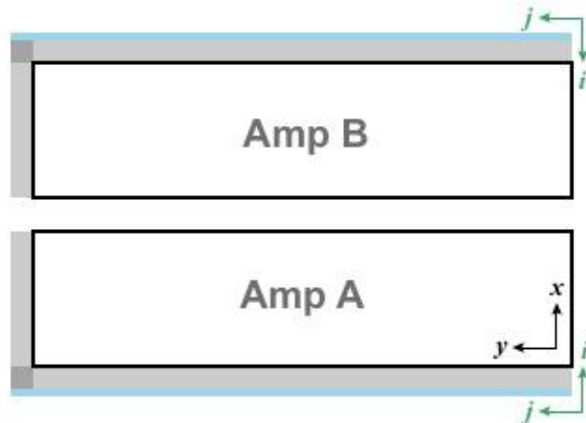


Figure 4-5: Schematic of the DECam sensor N1/32 just after read-out. Virtual overscan regions are indicated as shaded boxes (blue: pre-scan; grey: over-scan), but are expanded for clarity. Amplifier locations are near the origin of the green amplifier coordinate axes (*i*,*j*), prior to transformation to detector coordinates (black coordinate axes).

Table 4-5: Science Array and Overscan Regions

Detectors	Amp	Photo-Active Data Section	Prescan	Y Overscan	X Overscan
1N–31N	A	[57:1080, 1:4096]	[1:6, 1:4146]	[1:1080, 4097:4146]	[7:56, 1:4146]
	B	[1081:2104, 1:4096]	[2155:2160, 1:4146]	[1081:2160, 4097:4146]	[2105:2154, 1:4146]
1S–31S	A	[1081:2104, 1:4096]	[2155:2160, 1:4146]	[1081:2160, 4097:4146]	[2105:2154, 1:4146]
	B	[57:1080, 1:4096]	[1:6, 1:4146]	[1:1080, 4097:4146]	[7:56, 1:4146]

Calibrated Data

The NOAO Science Archive contains calibrated products that are produced with the DECam Community Pipeline. The specific calibrated science data products are listed in Table 4-3 on page 4-7 and described in more detail below. Each image has an associated data quality mask (DQM) and weight array. The science images are compressed using FITS tile compression (Pence et al. 2010), which provides an acceptable level of lossy compression.

InstCal. These images have been processed to remove instrumental signature and have been astrometrically and photometrically calibrated (see “Calibration” on page 4-13), although there are some cases where the calibration can fail (see “DECam Sources of Error” on page 4-27). The pixel brightness unit is ADU, though variations in gain among CCDs in the FPA have been removed by the flat-field. The data are organized in the FITS file almost identically to that for the raw science data, except for the following:

- The overscan regions have been trimmed from the science image arrays.
- The resulting images in each extension are all 2046×4094 pixels containing most of the photo-active regions of the detectors.

Resampled. These images are the result of geometrically rectifying InstCal images, where each array has been re-projected to a common *tangent-point* on the sky, with pixels aligned to a common grid, and a uniform 0.27 arcsec/pixel scale. The Resampled image is stored in the primary header-data unit within the file. Using a common tangent-point (which is selected from a grid with roughly 1° steps in RA, and exactly 1° in Dec) facilitates stacking overlapping images within an observing sequence. The *reduced, re-projected* images are approximately 2046×4094 pixels; the actual dimensions depend on the **WCS** tangent-point selected for a particular image. Both the single-frame and the re-projected images are accompanied by DQMs and Weight Maps.

Stacked. When two or more observations of a given target are obtained on the same night using the same filter, have similar exposure times, and have a sufficient degree of spatial overlap (which is generally the case), these images are combined using an average with outlier rejection to remove detector blemishes, gaps between the detectors, and artifacts such as image persistence and cosmic rays. The result is a union of the spatial footprints of the stack, which is stored in FITS MEF images, with nearly the same pixel scale as the raw images. In general, these images will be composed of tiles, one per extension, where each tile is no larger than 16K×16K pixels.



The exposure duration for Stacked images, as recorded in the **EXPTIME** keyword, refers to the sum of all exposure durations of all images used to create the stack. The exposure depth and noise properties of a stack of dithered images are a discontinuous and possibly complicated function of position in the image. Use the exposure map to track the detailed exposure depth at the pixel level.

Master Calibration. Reference files are created during the course of pipeline processing, such as residual bias structure, dome flat-fields, etc., for each night. In addition, some calibrations are determined externally: generally, those that require analysis of specialized exposures sometimes obtained over time spans longer than a typical observing run. All of the calibration files are used in pipeline processing to remove instrumental signatures from the science data.

Concomitant Data. All processed images are accompanied by DQMs and Weight Maps; Stacked images are also accompanied by Exposure Maps. The DQMs, Weight Maps, and Exposure Maps are images, though they are stored in compressed form, with as many extensions as in the corresponding science image. Some utilities (such as SAOimage DS9) can display and work with compressed files directly, but other utilities may require that the files be uncompressed FITS images before they can be used. The pixel values in the DQMs are non-zero when affected by detector pathologies and image artifacts such as bleed trails, saturation, and cosmic rays; the values are zero otherwise. Table 4-6 lists mask values that are applicable to *non-stacked* images.



The DQ mask encodings and meanings for non-stacked DECam data, as produced by v3.5.0+ of the CP, that were archived after late October 2014, have been changed. Data processed prior to this date have the original encoding scheme and associated meanings, which were in accord at the time with images provided by the DES. This may affect down-stream analysis software that may be used, e.g., to perform photometric measurements of sources. The table below lists the old and new conventions in the CP.

Table 4-6: Data Quality Mask Values

Convention prior to late October 2014			Convention after late October 2014	
Value	Bit	Meaning	Value	Meaning
0	–	No problem	0	
1	0	Bad/invalid pixel identified in the master data quality mask; generally indicates known detector blemishes	1	Bad/invalid pixel
2	1	Saturated	2	Null value (for Resampled and Stacked images)
4	2	Interpolated	3	Saturated
8	3	[Not used]	4	Bleed trail
16	4	Single exposure cosmic ray	5	Cosmic ray
32	5	[Not used]	6	Low weight
64	6	Charge bleed trail	7	Difference detection (derived from multiple exposures)
128	7	Multi-exposure transient	8	Long streak (e.g., satellite trail)

Most Stacked images are created from dithered frames, so that most of the pathologies affecting single frames will be mitigated. DQMs for Stacked images have the following values: “1” for areas of the re-projected image with no data, “2” for areas with no data *after rejection*, and zero otherwise.

The exposure maps are images whose values are the cumulative exposure duration at each pixel, in seconds, which can be a complicated function of position for dither sequences. The value of the EXPTIME keyword in a Stacked image is the sum of the exposure durations for all images that contributed to the stack.

4.2.2 Header Keywords

A wide variety of metadata are recorded in the headers of the science frames. Users should browse these headers (and the extension headers) to familiarize themselves with the content. The more critical metadata are described in this subsection. Table 4-7 lists metadata by the FITS **keyword** name, the header unit in which the keyword will be found (Primary or Extension), the point in the data processing where the key-

word is introduced (or where the value is updated), and the meaning of the keyword (or group of keywords, if they are related). Some of the keywords are indexed by image axis, meaning they come in pairs, as indicated by the suffixes *i* and *j*, or by amplifier *k*.

Table 4-7: Important Science Image Keywords

Keyword Name	HDU	Origin	Meaning
Telescope			
AIRMASS	P	R	Atmospheric pathlength for target at observation start
GUIDER	P	R	Status of guider control (value other than 1 indicates no active guiding)
OBJECT	P	R	Field observed (named by observer)
TELESCOP	P	R	Telescope used to obtain these data
TELDEC	P	R	Declination for the telescope position on the sky (deg)
TELRA	P	R	Right ascension for the telescope position on the sky in hh:mm:ss.s
Instrument/Detector Configuration			
DETECTOR	E	R	Identifier of detector in FPA
DETPOS	E	R	Detector position in FPA (see Figure 4-3 on page 4-4)
FILTER	P	R, U	Filter name/designation
GAIN <i>k</i>	E	R	Detector effective gain for amp <i>k</i> (e^-/ADU)
INSTRUME	P	R	Instrument name
RDNOISE <i>k</i>	E	R	Read noise for amp <i>k</i> (e^-)
SATURAT <i>k</i>	E	R	Detector saturation for amp <i>k</i> (ADU)
Time			
DATE-OBS	P	R	Date and time of observation start (ISO 8601 format)
DARKTIME	P	R	Time interval over which dark current accumulated (s)
EXPCOADD	P	R	Duration of a single exposure in a co-add sequence (s)
EXPTIME	P	R	Effective exposure duration (s). For Stacked images the effective exposure duration can be a complicated function of position in the image.
MJD-OBS	P	R	Time of observation start (MJD)
OPENSHUT	P	R	Time when shutter opened (ISO 8601 format)
TIME-OBS	P	R	Time when observation was initiated (hh:mm:ss.sss)
TIMESYS	P	R	The principal time system for all time-related keywords. Always UTC.
World Coordinates			
CD <i>i_j</i>	E	R, U	Transformation matrix from pixel to intermediate world coordinates; CD <i>i_i</i> is the pixel scale for axis <i>i</i>
CRPIX <i>i</i>	E	R, U	Location of the reference point along axis <i>i</i> in units of pixels
CRVAL <i>i</i>	E	R, U	Value of the world coordinate at the reference point for axis <i>i</i> in degrees
CTYPE <i>i</i>	E	R	Name of the coordinate represented in axis <i>i</i>
DEC	P	R, U	Declination for the center of the FoV (deg)
EQUINOX	E	R	Equinox in years for the celestial coordinate system in which the positions are expressed
LTM <i>n_m</i>	E	R	Detector to image transformation matrix term

Keyword Name	HDU	Origin	Meaning
LTV n	E	R	Detector to image transformation constant term
NAXIS i	E	R	Number of pixels along axis i
PIXSCAL i	E	R	Pixel scale along axis i (arcsec/pixel)
PVi_m	E	L2	Image distortion coefficient for axis i
RA	P	R, U	Right ascension for the center of the FoV (hh:mm:ss.s)
RADESYS	E	R, U	Name of the reference system in which the world coordinates are expressed
WCSCAL	P	L2	“Successful” if a valid WCS solution was found.
Calibration			
BUNIT	P,E	L2, U	Brightness units of image (usually adu)
FWHM	P	L2	Median FWHM of sources, in arcseconds
MAGZERO	E	L2	Magnitude corresponding to one count in the image
OBSTYPE	R	R	Type of target observed (object dark dome flat)
PLDNAME	P	L2	Pipeline name
PLVER	P	L2	Pipeline version identifier
PROCTYPE	P	L2, U	Product type (see Table 4-3 on page 4-7)
PRODTYPE	P	L2, U	Product data description (image mask expmap)
REDAMPT1	P	L2	Interpolation method used for image remapping (default: Lanczos)

4.2.3 Environmental Data

At present no environmental data are accessible from the Archive, although data from all-sky cameras, seeing monitors, and weather conditions at KPNO are available on the Web.⁴⁹

4.3 Calibration

The pipeline processing system for DECam, the “Community Pipeline,” is based on the algorithms and work-flow of the image processing stages of the pipeline developed for the DES. The CP produces Level-2 products (images where the instrumental signature has been removed and astrometric and photometric calibrations have been applied) and Level-3 products where spatially overlapping images in the same filter (and that have been obtained within the same observing run) have been stacked. The pipeline uses calibration exposures, such as darks and dome flats taken during an observing run, to construct some of the calibration reference files that are used as input to the processing. For simplicity, the subsections below will first describe the processing of the science images once the calibration reference files are available, then the processes for constructing the calibration reference files will be described with the overall flow as context. The actual sequence of processing in the pipeline software differs somewhat in detail, in part, to optimize the performance of the parallel processing environment.

⁴⁹ http://www-kpno.kpno.noao.edu/Info/Mtn_Weather/allsky/kpasca.html.



The community pipeline for DECam is tuned to maximize the use of exposures within the observing run in which they were obtained. As such, the quality of the data depends to a large degree on the quality of the calibration exposures that were obtained by the observer. However, under most circumstances, the pipeline will attempt to use Master Calibration files from prior observing runs if good quality, contemporaneous calibration data are not available.



Single calibrated images (and eventually co-adds) as produced by the DESDM processing pipeline are being included in the NSA holdings. These images will have superior astrometric and photometric calibrations.

4.3.1 Single-Frame Processing

The flow of the science data through the single-image portion of the pipeline is shown in Figure 4-6. Each step of the processing, indicated by the boxes in the center of the figure, is described in detail in the following subsections. Inputs to the processing include the raw science frames, calibration reference files (see “Calibration Reference Files” on page 4-24), and photometric and astrometric catalogs. Outputs include the various reduced science images, plus their associated mask and weight files (see “Image Formats” on page 4-7). Intermediate products that are produced during the course of pipeline processing, but not archived, are not shown. The processing is segregated by *observing block, filter*, and further by spatially overlapping observing sequences when deriving Stacked images.

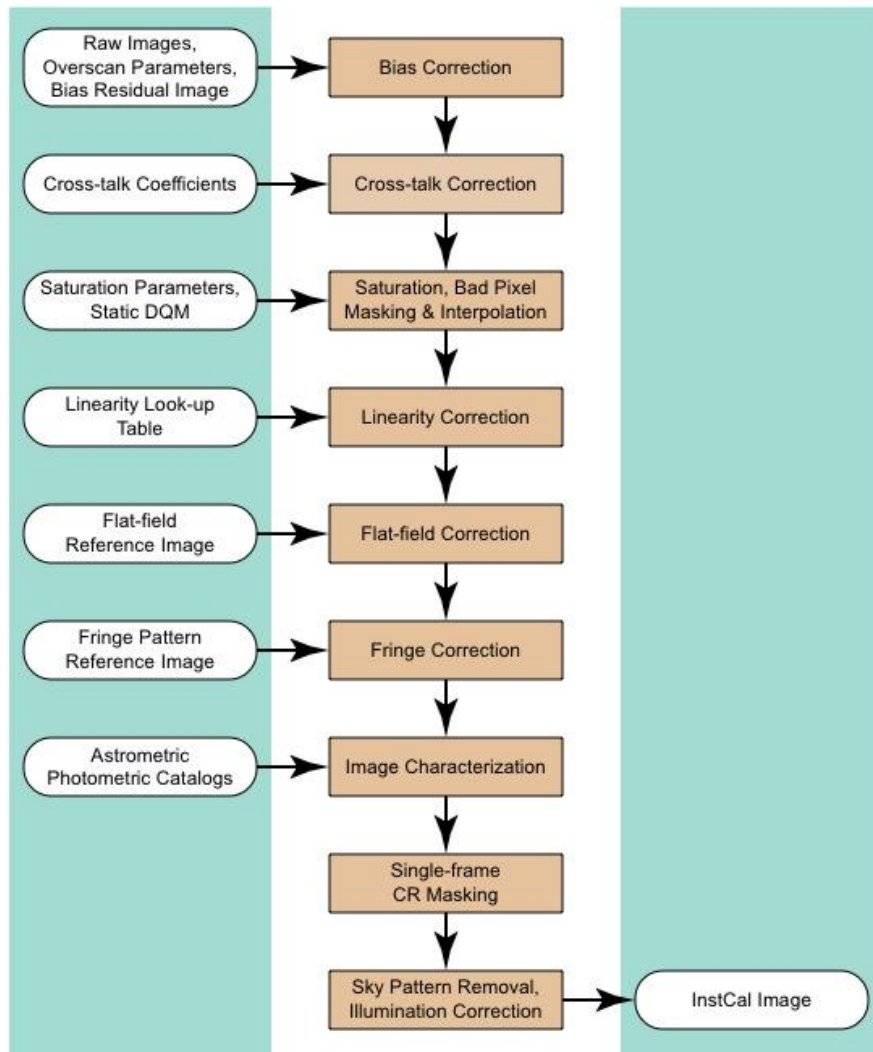


Figure 4-6: Flow of data taken with a common filter through the Community Pipeline processing and calibration, to produce Level-2 data products. External catalogs, and data products defined in Table 2-3 on page 2-7, are shown as inputs or outputs of the processing. Intermediate products that are not archived are not shown. Processing flow in the actual CP differs slightly, for computational efficiency.

Bias Correction

The bias correction is applied to remove the (additive) electronic bias that is present in the signal chain. The bias is, for the most part, composed of a constant pedestal, but it has structure that is related to the electronic stability of the bias during read-out of the detector. The processing pipeline removes the bias contribution in a two-step process. The first step, generally known as “*overscan subtraction*,” is made using values from the overscan regions of the raw image. Each of two amplifiers on each science CCD reads out half of the image independently, and each contains an overscan region (see Figure 4-5 and Table 4-5 on page 4-9). A single bias value is determined along the serial direction from the combination of overscan pixels (along axis i in the figure), excluding a small number of pixels near the ends. Each line is

treated independently (i.e., there is no smoothing of overscan values in the parallel direction) because of the potential for bias-level jumps during readout (caused by the simultaneous readout of the smaller ancillary CCDs in the focal plane). A statistical rejection of outlier overscan values eliminates possible transient and cosmic ray effects. This correction is parameterized: by default the pre-scan region is not used, nor are the last 5 overscan pixels; the average of the remaining values is subtracted from the science pixels. The virtual overscan regions (i.e., the pre-scan and the post-scan: see Figure 4-5 on page 4-9) are then removed from the image.

In the second step, the Master Bias residual image is subtracted from each science image to remove higher-order structure. Master Biases are created by the pipeline by combining many individual bias exposures (usually) taken during the night, or by selecting one from the Calibration Library that is near in time to the epoch of the science exposures.

Crosstalk Correction

A small but significant amount of *cross-talk* occurs between the video channels of the CCDs in the FPA (Paech 2013). The effect is to add (or subtract) a small fraction of the signal from one amplifier of a CCD into the signal chain of the other, or between adjacent CCDs, such that “ghosts” of bright objects appear in the paired CCD. This is a noticeable additive effect of ~0.01% for channels from the same CCD (i.e., between amplifier outputs), but is typically smaller between adjacent CCDs. The proportionality coefficients differ from one video channel to another, but are thought to be relatively stable over time.

The CP computes a correction for every pixel in an amplifier caused by every other amplifier, using pre-computed coefficients. The corrections are determined off-line and captured in a Master Cross-talk Coefficients file. The correction is linear up to a given threshold and nonlinear up to the limit of the digital converter.⁵⁰ The crosstalk correction to be subtracted from a pixel in a particular amplifier is computed by summing the pixel readout at the same time in all other amplifiers. This applies to all values even though noticeable effects only occur for very bright signal levels.

Artifact Masking

Various image artifacts, including detector blemishes as described in the “Focal Plane” section on page 4-3, are marked in the DQM of each science image. Further artifact flagging occurs later in the processing, including **saturation**, which is detected during nonlinearity correction, and cosmic rays, which are detected on single exposures and again if an image stack is created. The single exposure identification is based on finding pixels that are significantly brighter than nearest neighbor pixels; i.e., have “sharp” edges. This algorithm has been tuned to avoid flagging the cores of unresolved sources, and exposures with very good image quality ($\text{FWHM} < 3.3$ pixels) are not searched.

The DQM for each InstCal image indicates all detected artifacts noted above. All flagged pixels are excluded from contributing to the final Stacked image; if this process results in areas with no data, such pixels are so flagged (see “Concomitant Data” on page 1-9 for details).

⁵⁰ See the DES/SV Wiki: https://cdcs.fgov/redmine/projects/des-sci-verification/wiki/Nonlinear_Crosstalk.



Note that all pixels in calibrated science frames (InstCal, Resampled, and Stacked) that are flagged in the DQM with a value other than zero are replaced by a linear interpolation using adjacent pixels. The one-dimensional linear interpolation is performed along the shortest dimension of the region over which to interpolate. This process is intended to avoid introducing “ringing” artifacts during the down-stream resampling of the images, as well as to mitigate scaling problems when using image display software.

[Dark Correction]

The dark current in the DECam sensors is extremely low, and no dark correction is performed in the pipeline. Raw dark exposures, if obtained by an observer, are ignored in the CP.

Nonlinearity Correction

The DECam CCDs exhibit varying amounts of nonlinear response to reference fluxes at both low and high count levels, as illustrated in Figure 4-7. The effect is also apparent in science data, but the effect at low count levels affects only a subset of the CCDs in the FPA (Lin 2013). Look-up tables (LUTs, determined externally to the pipeline) capture the derived correction for each amplifier of each CCD. The LUTs contain fields for raw ADUs and a correction in ADU for each amplifier. The correction for a given (fractional) ADU value is a linear interpolation between bounding ADU entries in the table.

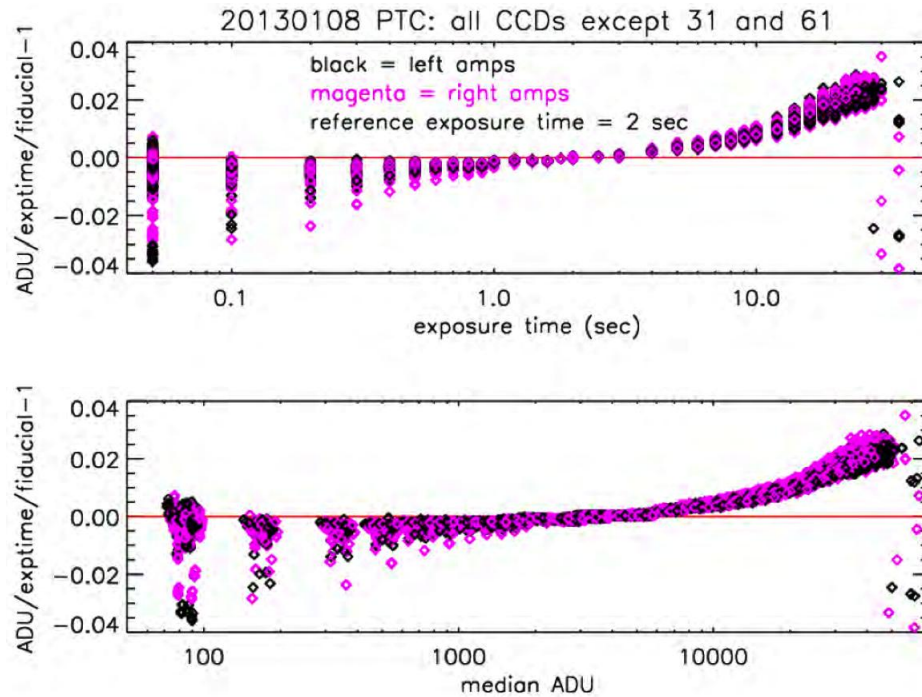


Figure 4-7: Deviations from response linearity (*upper*) and photon-transfer measurements (*lower*) for CCDs in the FPA, illustrating the magnitude of the needed correction at high and, in many cases, low count levels.

[Brighter-Fatter Correction]

A correction for the *brighter-fatter* effect (Antilogus, et al. 2014) is under development. See Section 4.4.3.

Flat-field Correction

The principal, pixel level, gain normalization consists of dividing by a Master Dome-flat (see Figure 4-12). Master Dome-flats are created by the pipeline from dome flat exposures (usually) taken during the same night. The normalized flats correct for variations in gain across all CCDs, but they do not adjust the mean gain to unity; thus, flat-fielded data have brightness units of ADU rather than e^- . The Master Dome-flats are, themselves, corrected for large-scale effects: namely, camera reflections and differences in response between the dome lamp illumination and a typical dark sky. The corrections are derived from stellar photometry of a calibration field obtained during special calibration programs. These calibrations are called star-flat fields or *Star-flats*.

The star-flats account for the additive contribution of the camera reflection in the dome flat-fields (see Figure 4-8), which otherwise would bias the photometry. This does not remove the effect of camera reflections from the on-sky exposures; that is handled later as part of removing background patterns. The Master Star-flats also do not account for differences in illumination response from the time and conditions of the star-flat observations nor the coarseness of the photometric sampling. This is also treated later as part of a sky illumination calibration.

Fringe Pattern Correction

The reddest filters (z and Y) show an interference pattern, or *fringe pattern*, shown in Figure 4-8. The pattern occurs because of interference between the incident, nearly monochromatic light from night sky emission lines (from both air glow and reflected city lights) and light that is reflected internally between layers of the CCD substrate. The details of the fringe pattern depend mostly upon the spatial variation in thickness of the top layer in the substrate, but also depend upon a number of other factors including the wavelengths of the incident emission lines, the composition of the substrate, the temperature of the CCD, and the focal ratio of the incident beam. This pattern is temporally stable and is removed by subtracting a scaled fringe pattern template. This calibration image has a mean value of zero and is produced externally to the CP from special calibration programs. The calibration pattern is scaled by the median of the exposure (i.e., an approximation to the sky value) and then subtracted from the science image.



The fringe pattern scales with the strength of narrow night sky emission lines, but does not scale perfectly with the broadband background level. Until the scaling algorithm is improved, some residual fringe pattern will likely remain in z - and Y -band science images.

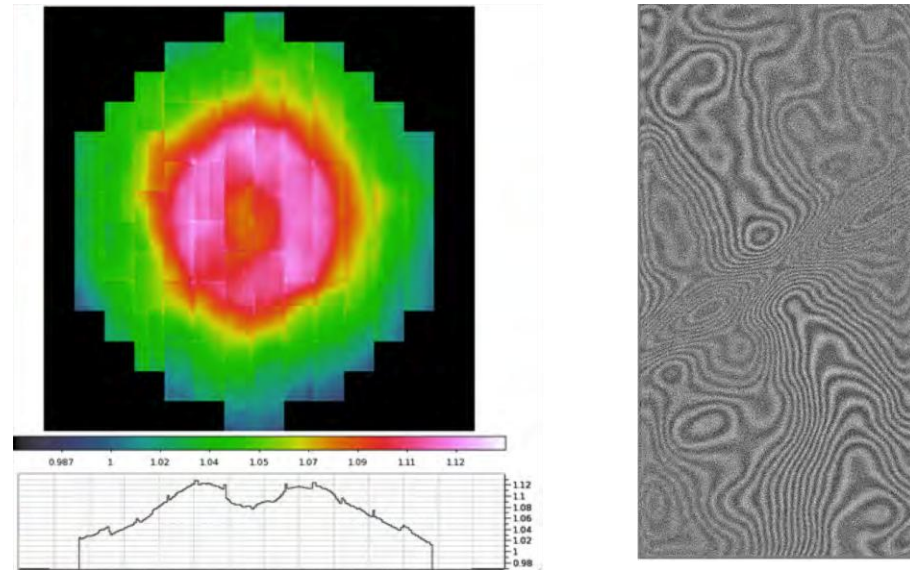


Figure 4-8: Pupil ghost pattern in a g-band dome-flat over the full FPA (*left*) from Bernstein (2013), and Y-band fringe-pattern for a central CCD (*right*). The fringe correction is only applied for z- and Y-band exposures.

Astrometric Calibration

The astrometric, or WCS calibration for Raw and InstCal images is described by a two-dimensional polynomial (the function type and coefficients are found in the header) of a tangent-plane (TPV) projection of stellar coordinates to the image pixel grid. The lower-order terms relate to the location of the reference pixel on the sky, the plate scale, and the rotation of the image, while the higher-order terms relate to non-linear effects of the optical system such as pincushion distortion. The form and order of the function varies with the filter and to a small degree with the *airmass* of the observation. The initial values for all but the zero-point terms are taken from prior WCS solutions of images where the astrometry of the stars in the field is known with very high accuracy; the initial value for the pointing is taken from the TELRA and TELDEC header keywords, which are supplied by the telescope control system. A WCS solution is determined for each array by associating centroids of stars in the science images with objects in the reference (**2MASS**) catalog. Note that the Resampled and Stacked image WCS is re-mapped to a simple, tangent-plane coordinate system.



There are plans to make use of the Pan-STARRS astrometric catalog in the CP for exposures that overlap that survey. The RMS of relative astrometric solutions on a single CCD is expected to approach 10 mas within the area of the survey.

Photometric Calibration

An estimate is made of the magnitude zero-point of each science image by comparing the instrumental magnitude of field stars to their published magnitudes in overlapping passbands in a reference catalog. Currently, the USNO-B1 reference photometric catalog is used. Note that the result of the photometric

calibration is to populate the science header with keywords—the pixel values remain unchanged, and have brightness units of ADU, with a gain averaged over the FoV.

One quantity of use, the photometric depth of the exposure, is defined as:

$$-\frac{2.5}{2.3026} \log\left(\frac{3.988 \cdot Q \cdot \sigma}{\sqrt{A}}\right) + m_{\text{zero}}$$

In physical terms, the photometric depth is the faintest point-source that can result in a 5σ detection above the sky background, in units of magnitudes. In the equation above, Q is the half-light width of point-sources (expressed as the value of the header keyword FWHM in the image header) in units of arcseconds, σ is the noise in the background (SKYSIGMA) in ADU, A is the area of a pixel in arcsec², and m_{zero} is the magnitude zero-point.

At present the photometric calibration is only approximate (i.e., not adequate to support science). For the other filters, the MAGZERO keyword may be useful as a rough estimate of exposure depth as a measure of sky transparency over an image sequence. See “DECam Sources of Error” on page 4-27 for details. The photometric zero-points for DES survey data can be calibrated to a very high accuracy, and the response function has been shown to be stable to within a few mmag over many-month timescales (Bernstein 2013).



While the magnitudes for the USNO-B1 catalog are of high quality, the mapping from filters used with DECam to USNO-B1 bandpasses introduces significant (but uncharacterized) additional uncertainties. The resulting magnitude zero-point and photometric depth written to the headers of DECam science data by the CP are uncertain by an unknown amount that could approach 0.5 mag or more. Images produced by DES should have considerably better accuracy.

Sky Pattern Removal

Sky pattern removal attempts to make the non-astrophysical background across an exposure uniform on large spatial scales. This applies to the non-remapped exposures from which remapped images and stacks are subsequently produced. The most prominent background pattern is a color-dependent camera reflection that appears as a large image of the pupil, i.e., a “pupil ghost.” This is an additive effect (which accounts for ~10% of the photons in dome-flats: Bernstein 2013). The second pattern is a gradient across the field that may include contributions from strong moonlight or differential atmospheric transmission. Some of these are actually response variations rather than additive background, but in the CP v3.5.x, all sources of low spatial frequency variation are treated as additive background.

The patterns are extracted from a special, low-resolution, full-field sky image. The sky in each CCD is carefully measured from histograms of rectangular blocks of pixels. Each block becomes a single pixel in a low-resolution image. The values for all CCDs are put together into a simple full-field image that preserves the geometry of the focal plane and includes masks where there are no data.

The pupil pattern is modeled by fitting in polar coordinates about the center of the pattern over a range of radii. Outside of these radii the pattern is assumed to be absent. A polynomial is fit across each radius bin.

The inner and outer rings define a background where the contribution of the pattern is assumed to be zero. The order of the polynomial for the background rings is high enough to track background gradients, and the background at each point within the ring is a linear interpolation between the inner and outer fit values at a given azimuth. For the azimuthal fits of the background-subtracted rings in the pattern, a constant is currently used. The constant values at each radius are then fit by a polynomial. These choices produce a ring fit with no azimuthal structure. This pattern is subtracted from the low-resolution sky image and the actual exposure data.

After removal of a pupil pattern the focal plane sky image is median filtered with a window that is larger than a single CCD. This filtering is able to remove sky patterns such as those produced by moonlight through the dome slit, while not being unduly influenced by remaining amplifier gain variations. The background is adjusted to a zero mean and then subtracted from the full exposure data. This results in an image with a count level matching the exposure, but with the reflection and background structure removed, i.e., a nearly uniform background.

Illumination Correction

This correction makes the ensemble response to flux from the night sky, after removing patterns due to camera reflections and illumination gradients, uniform across the field of view. This is done by combining all exposures of 60 s or more, in the same filter and over a small sequence of nights (usually an observing run), using source masks and medians to eliminate source light. This dark-sky illumination calibration is divided into each individual exposure.

The pipeline operator reviews the calibrations to ensure there were enough exposures with good dithering and minimal impact of sources. If the operator accepts the calibration, it is applied to the exposures. If the calibration is rejected, then a MasterCal near the epoch of the exposures is selected from the Calibration Library.

[Pixel Area Correction]

Pincushion distortion in the camera optics introduces a smooth radial change in the plate scale, as shown in Figure 4-9. Thus, the sky area subtended by a pixel in un-remapped individual exposures (i.e., the InstCal images) will change with distance from the camera optical axis. This is a small effect in DECam (<1% at the extreme edge) but, depending on how one performs photometry, this may introduce a significant systematic effect in flux measurements. The remapping and subsequent co-added stacks explicitly make the pixel areas the same (apart from the very small tangent plane projection), and so fixed aperture photometry would be as accurate as the gain calibration allows.

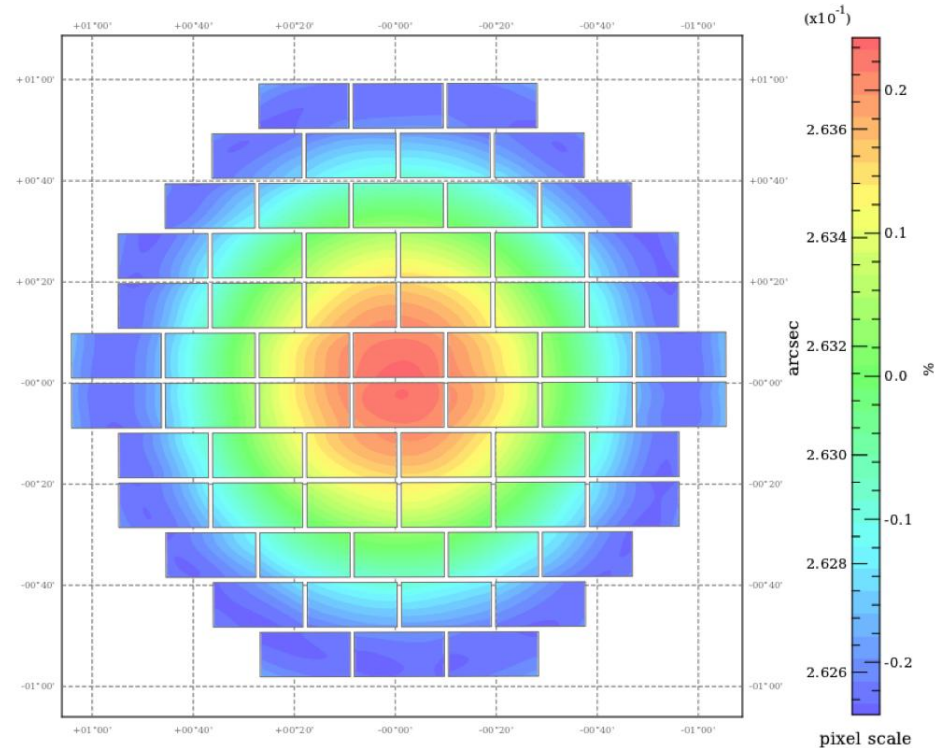


Figure 4-9: Map of pixel scale over the DECam FPA. The small radial gradient is due to pincushion distortion in the camera optics.

4.3.2 Image Co-addition

The processing flow for image co-addition is illustrated in Figure 4-10, and results in image stacks that generally have a greater spatial extent than single exposures. Stacked images are composed of overlapping Resampled images in an observing block using a common filter, and have brightness units of ADU.

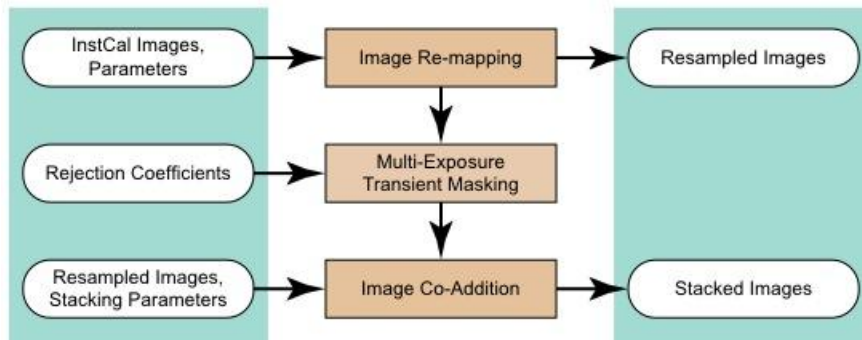


Figure 4-10: Community pipeline processing flow for co-addition of spatially overlapping images obtained with a common filter.

Remapping

The astrometric calibration allows remapping the data to any desired projection and sampling. Note that if the astrometric calibration failed (see the keyword WCSCAL in the header) then full remapping is not performed, though a data product will still be produced sans accurate astrometric calibration. The two reasons for remapping are (1) to provide data where instrument distortions have been removed, particularly pixel size variations on the sky that can affect photometry programs, and (2) to register images for stacking. The CP resamples (i.e., interpolates) each exposure to a standard tangent plane projection with north up (increasing along the y-axis), east to the left (increasing along the x-axis), and a uniform scale of 0.27 arcsec/pixel.

The ***tangent-point*** is selected from a ***healpix***⁵¹ grid on the sky and consideration is given to assigning overlapping exposures to the same tangent point. With this approach, exposures with the same CP standard tangent plane project can be combined without further interpolation. The algorithm that assigns exposures that have different nearest grid point, but are adjusted to the same grid point because they overlap significantly, requires a significant overlap (roughly 30% or more). Programs that shift exposures by nearly a full DECam FoV will produce separate tangent point groupings (and hence co-add Stacks).

The remapping is one where right ascension decreases with image column and declination increases with image line. In other words, when an image is displayed in the usual way with pixel (1,1) at the lower left north is up and east is left. Note that in a tangent plane projection these criteria are only exact at the tangent point, which is not necessarily at the center of the field. This means that the celestial axes will depart from alignment with the image rows and columns and the pixel sizes will vary. The former alignment effect is most noticeable at declinations near the equatorial pole and the latter pixel size variation is negligibly small for the DECam FoV. The interpolation method is reflected in the image headers (keyword REDAMPT1), and is a Lanczos interpolator in pipeline Version 3 and earlier.

Multi-Exposure Transient Masking

The pipeline detects and masks transients in overlapping exposures. Transients include cosmic rays, satellite trails, and asteroids, i.e., any detection on a single image that deviates significantly from the median in brightness of all images in the Stack. However, the algorithm is designed to be insensitive to differences within galaxies and the cores of stars. It also becomes statistically insensitive when there are very few exposures in regions of overlap.

The algorithm works by first creating a stack from a median of the remapped exposures, after removing the high spatial-frequency component. The median is then subtracted from the constituent exposure, and the spatial footprint of all detections that are above background are marked. These footprints include a small amount of boundary growth. The footprints are marked in the data quality maps, and the corresponding regions in the weight maps are set to zero. Finally the constituent exposures are averaged, excluding masked pixels.

There is one detail to note: this algorithm does not include any PSF matching. This means that small changes in the seeing can produce residuals at the cores of bright stars or galaxy cores. To avoid inappropriate masking of these features, the instrumental flux of detected residual sources is compared to the flux in the median image using the same footprint. The residual source flux is required to be greater than 70%

⁵¹ A hierarchical, equal-area, isolatitude pixelization of a sphere: see <http://healpix.jpl.nasa.gov>.

of the median flux. So for blank sky, all statistically meaningful transients are detected; but in regions of stars and galaxies, only significant sources are found.

Image Stacking

The CP combines exposures that overlap significantly (exposures are considered overlapping when they have the same tangent-point after remapping). Exposure patterns that map fields larger in radius than a DECam FoV will generally produce separate co-adds rather than one very large one. The overlapping exposures are separated into multiple stacks by exposure time: very short ($t < 10\text{s}$), short ($10\text{s} \leq t < 60\text{s}$), medium ($60\text{s} \leq t < 300\text{s}$), and long ($t > 300\text{s}$). If a group has more than 50 exposures it is divided in the smallest number of subgroups which all have less than 50 exposures (not for scientific reasons, but rather to make the data handling manageable). Of the exposures that are identified for a stack, some are excluded if they have the potential to degrade the image quality of the stack. The following metrics are examined to detect and remove such outliers:

- Relative flux scaling (e.g., low magnitude zero-points due to clouds)
- Seeing
- Sky brightness

Note that fewer than half of the full-FPA exposures are allowed to be rejected; otherwise all exposures are used.

When stacking, the pipeline scales the input images to a common magnitude zero-point and sky transparency. The co-adds are the weighted sum of the contributing exposures, excluding pixels marked in the data quality mask. There are two stacks produced for each set of exposures that satisfy the criteria above. One has no background adjustments beyond those applied to the non-remapped data as described previously. The other subtracts an additional background from each CCD. This is a higher spatial frequency filtering, which can produce a better matching of overlapping CCDs but can also subtract light from sources subtending 10% or more of a CCD. Because it is difficult for the pipeline to decide which is appropriate for a data set, the two versions are produced from which the investigator can choose.

4.3.3 Calibration Reference Files

Many of the master calibration reference files used in the pipeline processing are constructed for each observing run when a sufficient number of appropriate exposures exist. Others are constructed externally, from specialized observations and analyses. All of the MasterCal files are placed in a Calibration Library, and are available for use for any subsequent processing run should contemporaneous calibration data be unavailable or of insufficient quality.

For all but the bias structure file, the exposures that are used for calibration are affected by multiple instrumental signatures. It is important to distinguish between the additive backgrounds and the multiplicative sensitivity variations in order to avoid biasing the photometric accuracy of the processed science frames. Thus, the path to creating the reference files is an iterative one, and involves isolating the various effects, storing a characterization of the effect in a template image or a table, and using these characterizations to construct down-stream reference files.

The non-astrophysical background includes two artificial sources: a pupil ghost and a fringe pattern. The nature of these effects and that of the flat-field was explained above; key properties of these effects on *science images* are summarized in Table 4-8. Each effect differs somewhat in its spatial scale, amplitude, color dependence, and stability. Note that the background effects may not be apparent at all in some science images.

Table 4-8: Background Characteristics

Effect	Contribution	Spatial Scale (pix)	Amplitude	Color Dependence	Notes
Pupil Ghost	Additive	4000	Up to 10%	Moderate	Spatially stable per filter; amplitude depends on field brightness.
Fringe Pattern	Additive	10 to 100	~1% of sky	z- & Y-bands only	Spatially stable per filter; amplitude variable in minutes to hours.
Tree Rings	Multiplicative	100	10%	Minor	Strongest feature in dome-flat exposures.
Flat-field	Multiplicative	2 to 100	<1% ⁵²	Moderate	Exclusive of tree-ring features. Stable spatially & temporally, apart from shadows of dust particles.



Master Calibration files that are generated externally to the CP have not yet been archived. Until this is corrected, the files may be obtained from the CTIO website: <http://www.ctio.noao.edu/noao/content/DECam-Calibration-Files>

Static Bad-Pixel Mask

A Master Bad-Pixel mask is used as the initial DQM for each science frame, which marks the locations of static detector blemishes. The Master Static BPMs are created externally to pipeline processing (Marriner 2013), in part from engineering measurements of the saturation level for each amplifier. Masked regions are very stable in time.

Cross-Talk Coefficients

The crosstalk coefficient file contains coefficients for the nonlinear crosstalk correction. The coefficients are indexed by pairs of affected and source CCD amplifiers. This file is derived externally (see Paech 2013), and may be updated periodically as needed.

Linearity LUTs

The nonlinearity corrections are derived externally from engineering observations that consist of a series of dome-flat exposures that were taken with a range of exposure durations, such that the full dynamic range of the detectors is sampled. The intensity of the dome flat-field lamp is monitored during this sequence, and a pixel-by-pixel mapping of the measured counts as a function of illumination level is cap-

⁵² Localized variations of >10% are common near detector blemishes or dust particles.

tured in the linearity corrections for each pixel of each CCD (see Lin 2013). The nonlinearity correction has proven to be temporally stable, but the cause of low-level (<100 ADU) nonlinearity is not understood.

Bias Residual Image

All bias exposures from a night, independent of proposal, are processed into a single Master Bias Residual calibration. The first steps are the same as previously described for science exposures; namely, electronic bias, crosstalk, saturation masking, and bad pixel masking and interpolation. After these calibrations the exposures are combined, in CCD pixel space, by averaging the pixel values with lowest and highest values excluded. A weight map is also produced for error propagation. Master Bias Residual calibrations are verified for quality before being applied in the CP; low quality calibrations will be rejected in favor of one from an earlier observing run.

WCS Coefficients

The Master WCS Coefficients file contains the keyword-value pairs required for the TPV world coordinate system. In addition to the structural keywords, the file also provides the initial, high-order WCS coefficients for each CCD. These keywords and coefficients override values in the raw exposure headers.

Flat-fields

Dome Flats. Dome flats, or exposures of an illuminated screen affixed to the interior of the telescope enclosure, are used to construct the flat-field reference files, one per filter. The process for constructing the Master Dome-flat, illustrated in Figure 4-11, begins with flagging artifacts, followed by the dark and nonlinearity corrections on each frame. The flats are then scaled per CCD by the average of the central section ([500:1500,1500:2500]) with bad pixels excluded using the instrument bad pixel map. The pixels are then combined, in CCD pixel space, by averaging the pixel values, with lowest and highest values excluded. A Weight Map for error propagation is also produced.

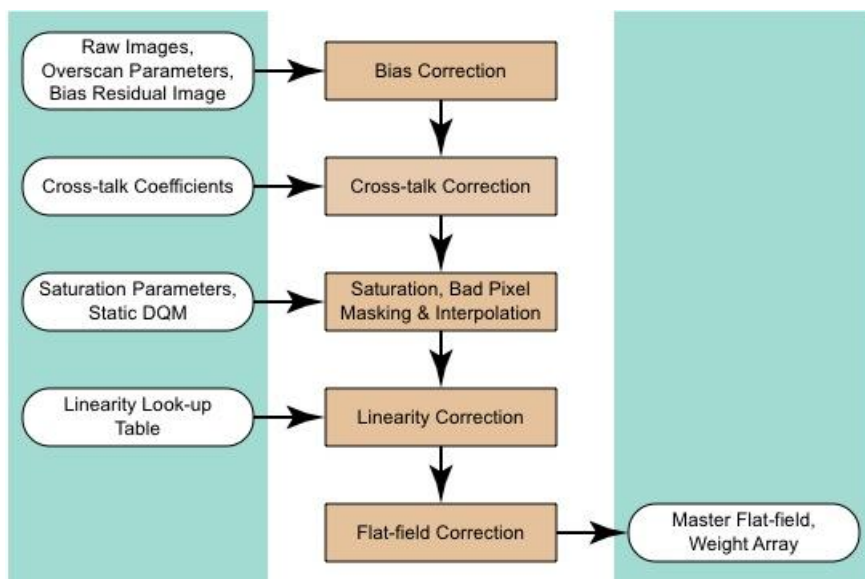


Figure 4-11: Community pipeline processing flow to create Master Flat-fields with a common filter from raw dome-flat exposures.

Star Flats. The Master Star-flat calibrations, one per filter, are created outside of the CP. They are produced from many dithered exposures of a moderately dense stellar field taken as part of a separate calibration program. These exposures are processed through the normalized dome flat calibration. The logic is that the dithering produces many instances of the same star over the detector. Spatial variations from the average instrumental magnitude for that star provide a measure of the relative response differences between those sampled points. By combining measurements of a large number of stars, a flat-field map is produced that makes the instrumental magnitudes, and hence the response of the camera, uniform across the field of view.

Fringe Template

The fringe patterns in the z and Y filters are derived periodically, externally to the CP, but are quite stable in time. They are derived from many on-sky exposures of sparse fields. The exposures are combined with outlier rejection to exclude sources. The stack is filtered to extract the fringe pattern with a mean of zero. During processing the template is scaled and subtracted from the science exposures.

Illumination Correction

Illumination calibrations, grouped by filter, are derived from numerous images that are dithered and sufficiently unaffected by large sources. This provides a gain correction to the more static star-flat calibration. The calibration consists of images for each CCD with flat-field pixel values. The values are spatially smoothed.

4.4 DECam Sources of Error

This section describes the accuracy that can be expected for the major data products, the major sources of error, instrument foibles, and other noteworthy problems and issues with DECam data. For a summary of known issues, see <http://www.ctio.noao.edu/noao/content/DECam-Known-Problems>.

4.4.1 Astrometry

The absolute astrometric accuracy for the image coordinate system is fundamentally limited by the science image exposure depth and the accuracy of the astrometric catalog used to determine the WCS solution, which is presently that of the 2MASS catalog. This catalog has the advantage of full-sky coverage and a limiting magnitude that provides sufficient overlap in the brightness range covered by most DECam exposures. Typical absolute accuracies obtained for the WCS solution are ~ 200 mas, but accuracies (i.e., RMS deviations from an astrometric model) of 100 mas have been routinely achieved for the DES survey. *Relative* astrometry of ~ 10 mas was achieved during Science Verification, but this is only possible after removing the geometric distortions known as tree rings (see Section 4.4.3). Too, the astrometric scale changes considerably within ~ 100 pixels of the edge of the detectors, by up to 30 mas.

4.4.2 Photometry

Photometric stability. The photometric response of DECam, based upon the repeatability of zero-points on calibrator star fields, appears to be temporally very stable. Accuracies of <0.02 mag were achieved for point-sources during the DES Science Verification.

Point-Source Photometry. Most of the pixel-to-pixel variation in flat-field images originates with size variation of pixels, as discussed in Section 4.4.3. Thus, flat-field corrections using dome flats actually *degrade* the accuracy of photometric measurements and artificially suppress the inferred uncertainties.

Photometric calibration. At present, the photometric calibration provided by the CP processing (using the USNO-B1 catalog as a photometric reference) is not adequate for science. Rather, it is intended mainly to provide an estimate of exposure depth to support queries to the Archive. While the systematic uncertainty may be large, within a sequence of observations covering the same region of the sky, the relative uncertainties are significantly smaller and provide a useful diagnostic of the photometric stability of the sky. Nevertheless, it is possible within the DES survey data to calibrate the photometric response across the FPA with an uncertainty of <2 mmag for a single night's data.

The photometric performance for any single image depends mostly on a number of external factors, especially the variable sky absorption and the delivered seeing. In Stacked images, the photometric depth varies discontinuously across the image, so that photometric measurements of targets that span these discontinuities may suffer some additional uncertainty. However, the DES team has demonstrated that it is possible to calibrate the photometric response across the FPA < 2 mmag for a single night's data.

Sky Subtraction. The sky pattern removal is known to be problematic and subject to significant systematic errors. Photometry of very extended sources should be done with care, particularly on images with complex sky backgrounds or significant image ghosts. Photometry of faint sources with low (<100 ADU) background should be checked with care, as many of the amplifiers show nonlinear response to such weak signals. While an empirical correction for low light-level nonlinearity is applied, the cause of this effect is not understood.

4.4.3 Anomalies

Detector Performance

Device Failures. Some of the CCDs in the FPA (see Figure 4-3 on page 4-4) exhibit inferior performance: N30 showed a very low full-well and poor charge transfer efficiency, prior to failing altogether in November 2012. From 30 November 2013, CCD S30 ceased functioning, and data from that CCD are no longer included in the image MEF files. The B amplifier of S7 has very poor linearity and an unstable gain ($\sim 10\%$) at count levels below ~ 600 ADU, which compromises the photometric accuracy in that portion of the image.

Nonlinearity. All CCDs exhibit nonlinear response at high count levels, consistent with a quadratic component to the response function; this is easily corrected in the pipeline. Some CCDs also exhibit low-level nonlinearity below ~ 100 ADU. This effect is not currently understood, but is corrected empirically in the pipeline. Users of data with background rates near or below this level should check their photometry carefully.

Tree Rings. Among the most striking features of a flat-field image is a pattern of concentric arcs, termed *tree rings*, as shown for one CCD in Figure 4-12. This feature is believed to result from imperfections in the substrate from the manufacture of the CCDs. The tree ring feature is actually a geometric effect: a systematic variation in pixel sizes, rather than a QE variation. A correction for the pixel size variation for all CCDs in the FPA is in development, but Plazas et al. (2014) showed that this effect inflates the astrometric residuals by up to 0.1 pix (26 mas). In addition, the flat-field correction improperly removes the variation in intensity, rather than treating the root cause. Thus, photometric residuals are inflated by about 0.5%.



Figure 4-12: Dome flat-field for a single sensor, showing various features including glowing edges, tape “bumps” along the edges and corners, and “tree rings.” Most of the visible structure is due to variations in physical pixel size.

Tape Bumps. Multiple, small features are evident in flat-fields, shown in Figure 4-13. These features are the result of small squares of double-sided tape, approximately 1.5 mm square and 100 microns thick, that were placed in each corner of the CCDs to maintain their relative position during the FPA assembly (see Nerylo, Diehl, & Estrada 2006). The depth of the features is a few percent, they are apparent in all passbands, and they are stable over few-week time spans provided the CCDs are maintained at a constant temperature. The effect on sensitivity can be removed with the flat-field, but the physical effect of the tape introduces small, local geometric distortions that are not removed with the flats.⁵³

⁵³ For details, see the DES Science Verification Wiki: https://cdcvn.fnal.gov/redmine/projects/des-sci-verification/wiki/Flat-field_structure.

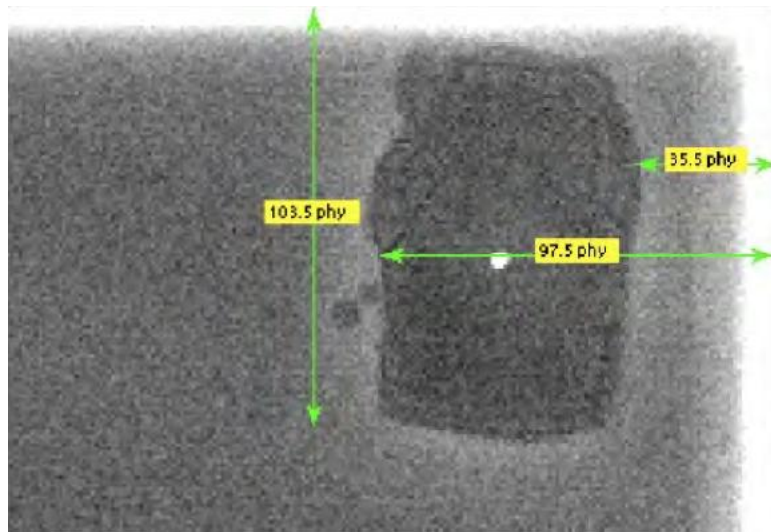


Figure 4-13: Small portion of flat-field image in the area of a “tape bump” artifact that was introduced during FPA assembly.

Brighter-Fatter Effect

The thick CCDs used in DECam are susceptible to electrostatic effects as charge accumulates during an exposure. Known as the *brighter-fatter* (B-F) effect, the physical model is of charge-induced shifts of pixel borders (Antilogus et al. 2014). The most obvious manifestation is a correlation between exposure levels of point-sources and their width, although it also results in correlated noise in flat-fields. Work by Gruen et al. (2015) showed that a star with a peak brightness of 25,000 ADU has a ~0.5% wider half-light radius than one with a peak of 5000 ADU. Stars with peak counts near saturation lose ~2% of the expected signal in the central pixel. The B-F effect is nearly independent of wavelength, although the amplitude varies between CCDs and appears to be temporally stable. It results in sub-optimal point-source photometry on faint sources (since the PSF shape is defined for bright targets) and biased shape measurements of angularly small sources. A correction is in development that could reduce the effect by a factor of 10.

Saturated Pixels

Pixel saturation (where the accumulated charge exceeds the full-well, e.g., in the cores of over-exposed stars) can result in charge trails and other effects. Saturation will overflow the serial register for very bright stars in the field, as illustrated in Figure 4-14. No correction is available for this effect, but it is largely limited to a single Amp on the image, apart from low-level leakage of the bleed trail through cross-talk.

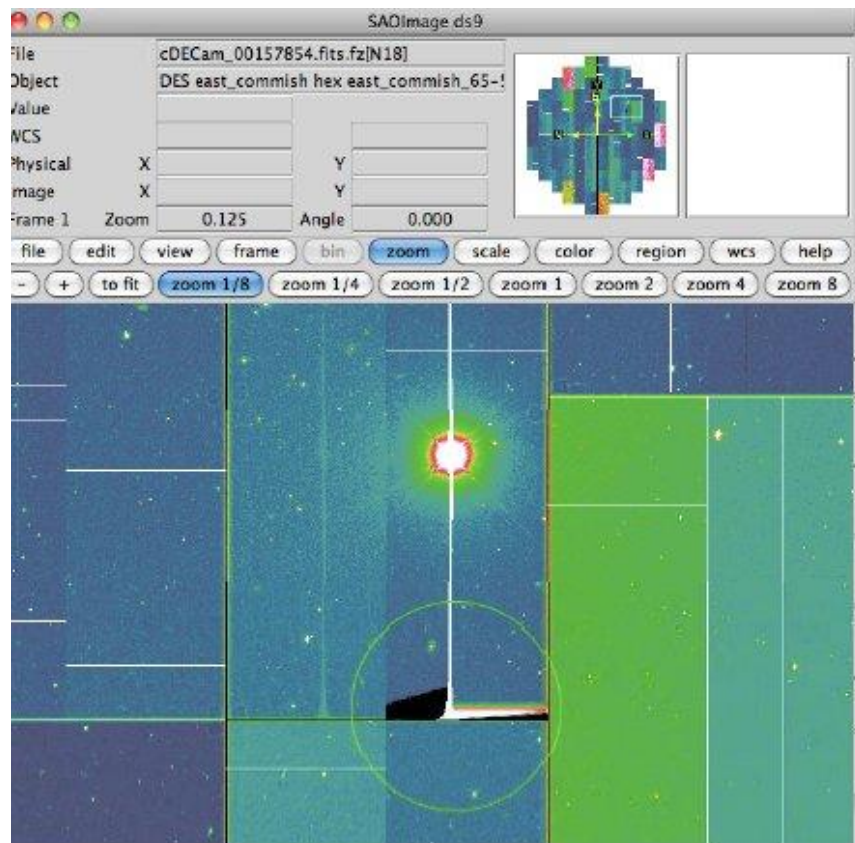


Figure 4-14: A portion of the DECam FPA as displayed in DS9, showing the effects of signal from a very bright star bleeding along columns and subsequently overflowing the serial register. Note that the prominent bleed trail is visible as cross-talk in the paired amplifier of the affected CCD.

Image Ghosts

In addition to the primary pupil ghost described in Figure 4-8 on page 4-19, bright stars can produce other ghosts in DECam images, owing to scattered light along a variety of paths. The effects of the ghosts are difficult to remove, but it is usually feasible to mark the affected regions in the image DQM for downstream analysis. The ghost characteristics take on different forms, depending on the source of the scattering. Figure 4-15 (Kent 2013) shows ghosts created from a double reflection inside the C5 corrector element, and a reflection between the focal plane and the front surface of C4. There are many other kinds of reflections that result in detectable ghosts.

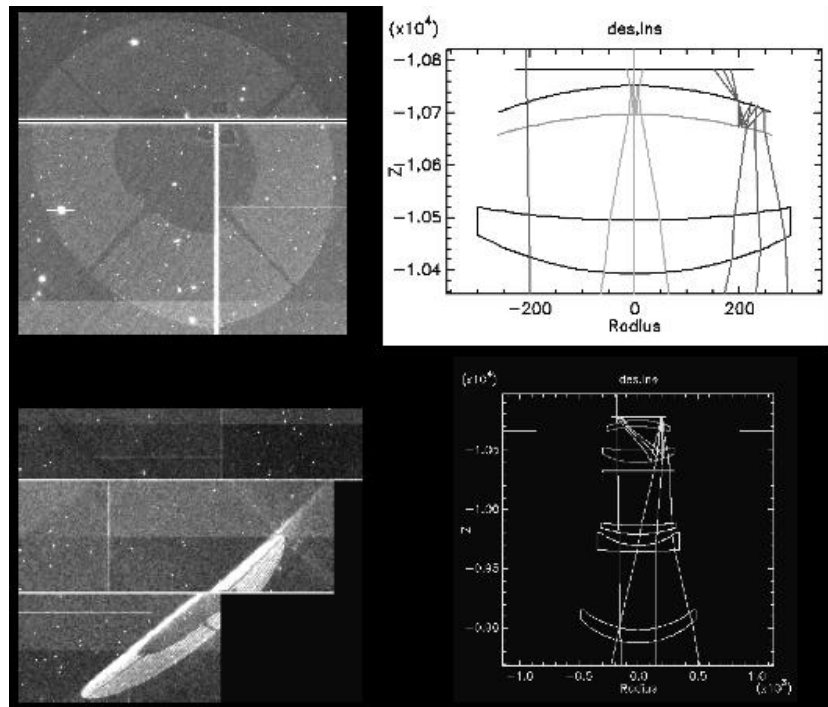


Figure 4-15: Portions of the DECam FPA showing the effects of low-level ghosts from bright stars where light scatters within the C5 corrector element (*upper*), and between the focal plane and the front surface of C4 (*lower*).

Ghosts from very bright stars that lie just outside the field of view were traced to reflections off the edge of the filters and their housing. In March 2014, the filter edges were masked and the interior surfaces of the filter housing were painted, essentially eliminating this ghost as shown in Figure 4-16.

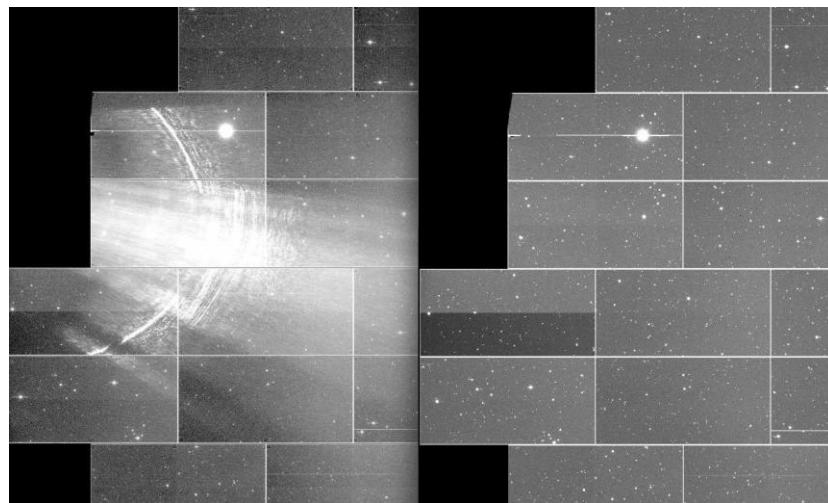


Figure 4-16: Eastern portion of DECam exposures showing the effects of a strong ghost from a bright star just outside the FoV, before (*left*) and after (*right*) the filter edges were masked.

Image Quality

The image quality is limited by a variety of factors, including, to a large degree, the atmospheric conditions (seeing) that prevail at the time of the observations. Prior to DECam commissioning, and continuing to the present, various improvements have been made to the Blanco 4-m telescope systems, including guiding and active optics. An update to the wavefront sensing system that is expected to improve the FWHM of point-sources by 0.07 arcsec was installed in October 2014. Other improvements to the primary mirror active optics in early January 2015 have reduced significantly the astigmatism at large hour angles. While further improvements in the image quality are possible, the floor of 0.47 arcsec is set by the telescope and camera optics, differential atmospheric refraction, and charge diffusion in the CCDs.

4.5 References & Further Information

Contributing Authors

Several members of the DES Collaboration and technical staff at Fermi National Accelerator Laboratory, as well NOAO staff members Alastair Walker, Tim Abbott, and Dara Norman, have contributed to the technical description of DECam and its calibration. Frank Valdes authored the description of DECam data processing with the Community Pipeline.

Acknowledgement to DES

Users should include an acknowledgement to the Dark Energy Survey collaboration (see Section **Error! Reference source not found.** for the applicable text) in the acknowledgement section of any paper using DECam data. The primary reference for the DECam instrument description is Flaugher, et al. (2015).

References

- Antilogus, P., Astier, P., Doherty, P., Guyonnet, A., & Regnault, N. 2014, *The Brighter-Fatter Effect and Pixel Correlations in CCD Sensors*, *J. Inst.*, **9**, C3048
- Bernstein, G. 2013, *On-Sky Performance of the Dark Energy Camera*, DES Document 7610-v1, available online: <http://des-docdb.fnal.gov:8080/cgi-bin>ShowDocument?docid=7610>
- Depoy, D. L., et al. 2008, *The Dark Energy Camera (DECam)*, *SPIE 7014*, 13
- Derylo, G., Diehl, T., & Estrada, J. 2006, *0.25 mm-Thick CCD Packaging for the Dark Energy Survey Camera Array*, *SPIE, 6276-08*
- Flaugher, B., Diehl, H. T., Honscheid, K., et al. 2015, *The Dark Energy Camera*, AJ, submitted; available online: <http://arxiv.org/abs/1504.02900>
- Estrada, J., Alvarez, R., Abbott, T., et al. 2010, *Focal plane detectors for Dark Energy Camera (DECam)*, *SPIE, 7735-1R*, 1

- Gruen, D., Bernstein, G. M., Jarvis, M., Rowe, B., Vikram, V., Plazas, A. A., & Seitz, Stella 2015, *Characterization and Correction of Charge-Induced Pixel Shifts in DECam*, in Proc. PACCD 2014, in press. Available online: <http://xxx.lanl.gov/pdf/1501.02802.pdf>
- Kent, S. 2013, *Ghosting Analyses*, DES/SV Wiki: https://cdcvn.fnal.gov/redmine/projects/des-sci-verification/wiki/Ghosting_Analyses
- Lin, H. 2013, *CCD Nonlinearities*, DES Document 7292-v1, available online: <http://des-docdb.fnal.gov:8080/cgi-bin>ShowDocument?docid=7292>
- Marriner, J. *Bad Pixel Mask*, DES Document 7302-v1, available online: <http://des-docdb.fnal.gov:8080/cgi-bin>ShowDocument?docid=7302>
- Paech, K. 2013, *DECam Crosstalk – Performance of Non-Linear Corrections*, DES Document 7303-v2, available online: <http://des-docdb.fnal.gov:8080/cgi-bin>ShowDocument?docid=7303>
- Pence, W. D., White, R. L., & Seaman, R. 2010, *Optimal Compression of Floating-point Astronomical Images Without Significant Loss of Information*, *PASP*, 122, 1065
- Plazas, A. A., Bernstein, G. M., & Sheldon, E. S. 2014, *On-sky Measurements of the Transverse Electric Fields’ Effects in the Dark Energy Camera CCDs*, *PASP*, 126, 750
- Reif, K. 2010, *A Bonn Shutter for the Dark Energy Survey Camera*, DES Document 4398-v1, available online: <http://des-docdb.fnal.gov:8080/cgi-bin>ShowDocument?docid=4398>
- Roodman, A. 2013, *Image Quality & Pointing*, DES Document 7408-v1, available online: <http://des-docdb.fnal.gov:8080/cgi-bin>ShowDocument?docid=7408>

For Further Reading

A document repository⁵⁴ for DECam is available on the Web, where many of the above-referenced papers may be found.

The following paper is an illuminating discussion of the “brighter-fatter” effect on bright point-sources imaged with deep-depleted CCDs:

Honscheid, K., & Bernstein, G. 2013, *DES Science Verification Report*, [DES-doc-6985](#)

Holland., S. E., Bebek, C. J., Lolbe, W. F., & Lee, J. S. 2014, *Physics of Fully Depleted CCDs*, *J. Instrumentation*, 9, 3057

Stubbs, C. W. 2013, *Precision Astronomy with Imperfect Fully-Depleted CCDs—An Introduction and a Suggested Lexicon*, available online: <http://lanl.arxiv.org/abs/1312.2313>

An additional paper on the NOAO pipeline processing system in general, and the DECam pipeline in particular, was written by the pipeline authors.

⁵⁴ Available at <http://www.noao.edu/ets/newfirm/>.

Valdes, F., Gruendl, R., and the DES Project 2014, *The DECam Community Pipeline*, in ASP Conf. Ser. 485, eds. N. Manset, & P. Forshay (San Francisco: ASP), 379

The DESDM pipeline is described in a presentation at the DECam Community Science Workshop:

Gruendl, R. 2015, *DECam Pipeline and Products*, presented at the DECam Community Science Workshop, available online: <http://www.noao.edu/meetings/decam2015/abstract/Gruendl-Robert>

Chapter 5

C/KOSMOS

Version 1.0, April 2015

In This Chapter...

Instrument Overview5-1

Data Products.....5-9

Data Reduction...5-11

References & Further Information...5-13

The Kitt Peak Ohio State Multi-Object Spectrograph (KOSMOS) began operation on the Mayall 4-m telescope in the fall of 2013, and the nearly identical COSMOS began operation on the Blanco 4-m telescope at CTIO in mid 2014. The spectrographs (hereafter referred to together as C/KOSMOS) were adapted from the successful MDM instrument, OSMOS, built by Paul Martini and the instrumentation group at The Ohio State University. Key features of the original design are described in the OSMOS User's Manual.⁵⁵ This chapter will describe the instrument design and operation and the raw data formats as well as outline the data reduction process. There is no pipeline for these instruments to generate calibrated data products.

The material for this chapter has been drawn from a variety of sources, including C/KOSMOS technical documents, the *C/KOSMOS Instrument Manual* (Points et al. 2014), data file headers, the KOSMOS web pages,⁵⁶ and input from experts. Interested users should consult the references at the end of this chapter for details of the instrument description and operation. Additional resources are cited throughout this chapter, and are listed along with other background material in the last section.

5.1 *Instrument Overview*

The C/KOSMOS instruments are optical imaging and multi-object spectrographs, mounted at the Cassegrain focal station of each telescope; Figure 5-1 shows KOSMOS mounted on the Mayall telescope. These two spectrographs are nearly identical in their design. The optical design enables imaging, long-slit and multi-slit spectroscopy over a 100 arcmin² field, rapid reconfiguration of observing modes, and the capacity to have a wide range of slits, *filters*, and dispersers mounted simultaneously. The current detectors are efficient 2K×4K back-illuminated **CCDs** from e2v Technologies, although an additional Dewar with LBNL red-sensitive devices is planned for each spectrograph. The dispersers are high-efficiency

⁵⁵ See the OSMOS User's Guide at: <http://www.astronomy.ohio-state.edu/MDM/OSMOS/>.

⁵⁶ See the NOAO System Technology Center website: <http://www.noao.edu/nstc/kosmos/>.

grisms with $R \sim 2100$, with useful throughput from 3600–10,000 Å. There are two 6-position filter wheels containing various order-blocking filters, the **SDSS** g , r , i filters, and a few available slots to accommodate 4-inch filters from the observatory library.



Figure 5-1: KOSMOS mounted at the Cassegrain focus of the Kitt Peak 4-m telescope.

5.1.1 Optical Design

C/KOSMOS has an all-refractive design, as illustrated in Figure 5-2 and as described by Martini et al. (2014), consisting of a 5-element, f/7.9 collimator and a 9-element, f/2.7 camera with a 26° field of view to provide broad wavelength coverage in spectroscopic mode. The coatings on the lenses reduce their reflectivity to <1%. The shutter at the front of the camera is a twin-blade design and permits exposure times as small as 0.01 s, although photometric accuracy better than 1% requires exposures longer than 0.5 s. A 6-position slit wheel is positioned behind the shutter and normally contains one open position for imaging and target acquisition, with the remaining slots available for facility long-slits or custom multi-object slits.

Between the collimator and the camera are three 6-position wheels: one for the dispersers and two others that hold imaging and dedicated order-blocking filters. One slot on each wheel remains empty to enable rapid switching between imaging and spectroscopic modes. The two 6-position filter wheels are tilted by 8° from the optical axis to minimize ghost reflections. The dispersers are two high-efficiency grisms with $R \sim 2100$, one optimized for the blue spectral region and one for the red. The camera properties are summarized in Table 5-1.

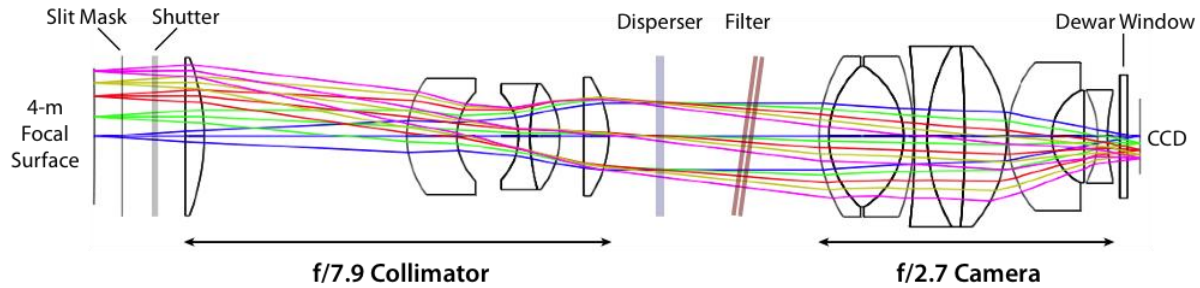


Figure 5-2: Schematic of the C/KOSMOS optics. Light from the telescope focal surface (*left*) passes through the slit mask and the collimator, the disperser (in spectroscopic mode), and filter (if deployed) before entering the camera and being detected by the CCD (*right*).

Table 5-1: C/KOSMOS Camera Characteristics

	KOSMOS	COSMOS
Imaging field of view	11.6' circular	11.6' circular
Telescope focal ratio	f3	f3
ADC ⁵⁷ usage	N/A	Recommended
Pixel scale	0.292 arcsec/pix	0.292 arcsec/pix
Rotator range	0–180°	0–360°, excl. 87–93°
Available filters ⁵⁸	Wheel 1: GG395, GG455, GG495, OG530, OG570 Wheel 2: SDSS <i>g, r, i</i> ; user-selected 4-in filters	



The ADC is *not* used with KOSMOS on the Kitt Peak 4-m telescope because the corrected FoV is too small. Observers are advised to mitigate atmospheric dispersion by keeping the slits aligned with the parallactic angle during exposures at moderate to high airmass, but they are not obligated to do so.

Detectors

The detector properties are listed in Table 5-2 for the e2v CCDs, which are optimized for blue sensitivity. They are cosmetically excellent, have very high CTE, low dark current and read noise, which is typical of this generation of CCD; the devices provide good sampling in imaging and spectroscopic modes. The read-out time is fairly short, but smaller regions of interest (ROI) are even quicker. This is particularly important for acquiring targets with slit-masks.

⁵⁷ Atmospheric Dispersion Corrector.

⁵⁸ Both filter wheels include a clear (open) position. Note that the 8° tilt of the filter wheel shifts the transmission of interference filters somewhat to the blue; the effect is significant for narrowband filters.

Table 5-2: Typical Sensor Characteristics

Sensor Type	e2v back-illuminated CCD model 44-82 (LBNL CCD in development)
Array Dimensions	2048×4096 pix
Pixel dimensions	15×15 μm
ADC dynamic range	16 bit
Gain	0.6 e^-/ADU
Read noise	5 e^-
Dark current	~0.01 $e^-/\text{pix/hr}$
Well capacity	~2000 Ke^-
CTE	>0.999995
Read Time	full array: 46 s 2048×2048 ROI: 26 s
Binning (xxy)	1×1, 1×2, 2×2 pix

The quantum efficiency (QE) of the e2v sensors is very high and optimized for excellent performance in the blue spectral region. Red-optimized LBNL CCDs are expected to become available in the future. The typical QE for these devices is shown in Figure 5-3.

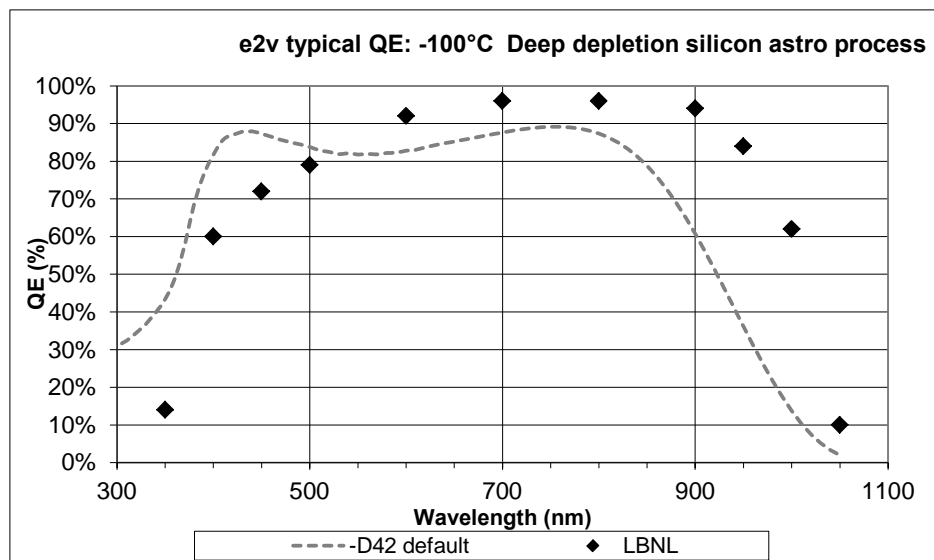


Figure 5-3: QE for typical e2v devices (dashed curve) is very high in the blue, but less so in the far red. The planned LBNL CCDs have much higher QE in the red (diamonds).

Dispersers

Two dispersers are currently offered on each instrument, although there is room in the disperser wheel for up to three others. Each is a high-efficiency, volume-phase holographic (**VPH**) grating bonded between a pair of prisms (hence, **grism**) that maintains a zero-deviation optical path in spectroscopic mode. The full spectral range cannot be obtained in a single exposure, so one grism is optimized for the blue spectral region and the other for red. The spectral coverage using the facility long slits is given in Table 5-3.

Table 5-3: C/KOSMOS Spectrograph Characteristics

	Blue Grism	Red Grism
Fringe frequency	1172 lines/mm	842 lines/mm
Resolution	2000–2600	2000–2600
Spectral scale	0.53–0.75 Å/pix	0.84–1.06 Å/pix
Coating optimization	350–700 nm	500–1000 nm
Spectral Coverage		
Blue Slit:	3500–6200 Å	5000–9000 Å
Center Slit:	3800–6600 Å	5800–9400 Å
Red Slit	4300–7000 Å	6100–10,000 Å
Facility long-slit widths (10' length)	0.6", 0.9", 1.2", 1.5", 3.0"	

5.1.2 Imaging and Field Acquisition

Images from C/KOSMOS can be obtained through a filter or in white light. The 11.6-arcmin field of view, as projected onto the detector is illustrated in Figure 5-4 (adapted from Martini et al. 2014). The spatial extent (and the maximum length of a long slit) is limited by the detector format to $\sim 10 \times 10$ arcmin when the $2K \times 2K$ imaging region of interest (ROI) is used for read-out. Multi-object spectroscopy requires obtaining an exposure with a custom slit mask inserted, but with no disperser (see Figure 5-2 on page 5-3), to ensure that light from all targets in the field passes through the intended custom slits. Subsequent MOS exposures through the disperser place the spectra from the various slits onto the detector format.

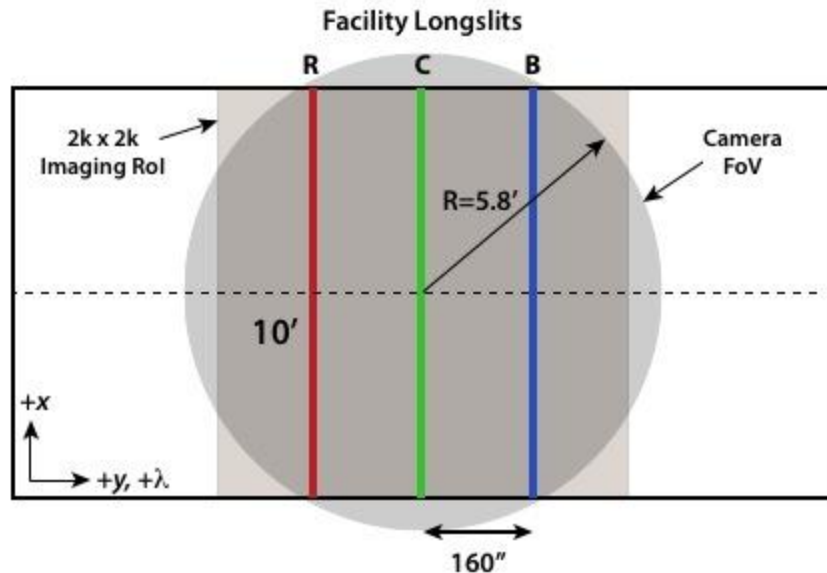


Figure 5-4: Schematic of the 11.6-arcmin (diameter) corrected field of view of the camera (grey circular region) as projected onto the detector geometry (clear rectangular region), the 2Kx2K imaging region of interest (light brown square), and the boundary separating the two amplifier regions (dashed line). The detector intercepts the dispersed spectra, where wavelength increases left to right along the image y -axis. The facility long-slit mask (with 3 slits: **R**, **C**, **B**), subtends 10 arcmin spatially, the slits are offset 160 arcsec from one another. Image orientation in celestial coordinates depends upon the instrument rotator angle.

5.1.3 Spectroscopy

Spectra may be obtained with either of two dispersers, using either long slits or custom slit masks designed by the observer. Facility long slits are available for spectroscopy of isolated point-sources and extended objects; these slits cover the full spatial extent of the field. Three of them (named 3pxR, 3px, and 3pxB) are approximately 0.9 arcsec (3 pixels) wide. They are displaced relative to one another along the dispersion axis to extend the spectral coverage (see Figure 5-4). Other slit widths are available (see Table 5-3). Some observers make use of a smaller ROI along the spatial dimension to minimize CCD read-out time.

The throughput is shown in Figure 5-5 and is heavily modulated by the grating efficiency function; the effect of displacing the slit along the dispersion axis is to move the peak of the throughput curve to the location of the slit.

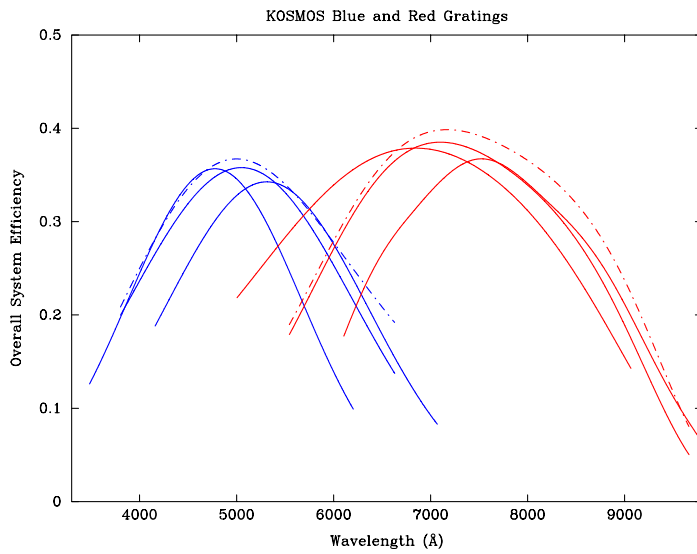


Figure 5-5: Total spectroscopic efficiency of KOSMOS (including the instrument, telescope, for airmass = 1.0) with the blue and red VPH grisms. The three solid lines for each grism correspond to the blue, center, and red long-slit options.

5.1.4 Operations

C/KOSMOS spectroscopic observing consists of the sequence of exposures given below to acquire a field and obtain spectra; acquisition may have required some iteration for custom slit masks of fields with multiple targets:

1. Image the intended field (possibly through a filter)
2. Image the field through the slit mask
3. Compute an offset to center the targets in the slits
4. Re-image the field through the slit mask to verify acquisition (repeat steps 3–4 if necessary)
5. Insert the disperser and blocking filter, and take one or more spectroscopic exposures
6. Obtain a comparison arc exposure if needed

Only the data from steps 1, 4, and 5 are of interest for data reduction. Unfortunately, it is not easy to infer the types of exposures from the results of an Archive search. Table 5-4 shows the header keywords to use in distinguishing direct images of the full field from images of the slit mask, and from spectra, along with example values for the keywords.

Table 5-4: Header Keywords and Values to Identify Exposure Types

Exposure Type				
Keyword	Field	Slit	Spectrum	Meaning
OBSMODE	imaging	acq	sos_slit	Observation mode
KSDPOS	Open	Open	r2k	Dispersing element
KSFILCMD	SDSS-r	SDSS-r	OG530	Filter designation
KSSPOS	Open	Ori-1	Ori-1	Slit mask designation

An example of a target field and subsequent acquisition and spectral exposures is shown in Figure 5-6 for a custom multi-object slit mask. The spectroscopic targets are numbered as they appear in the slit mask definition file (*.kms, see Section 5.2.2), which the PI of the program created during the process of designing the slit mask⁵⁹ that was manufactured for their program.

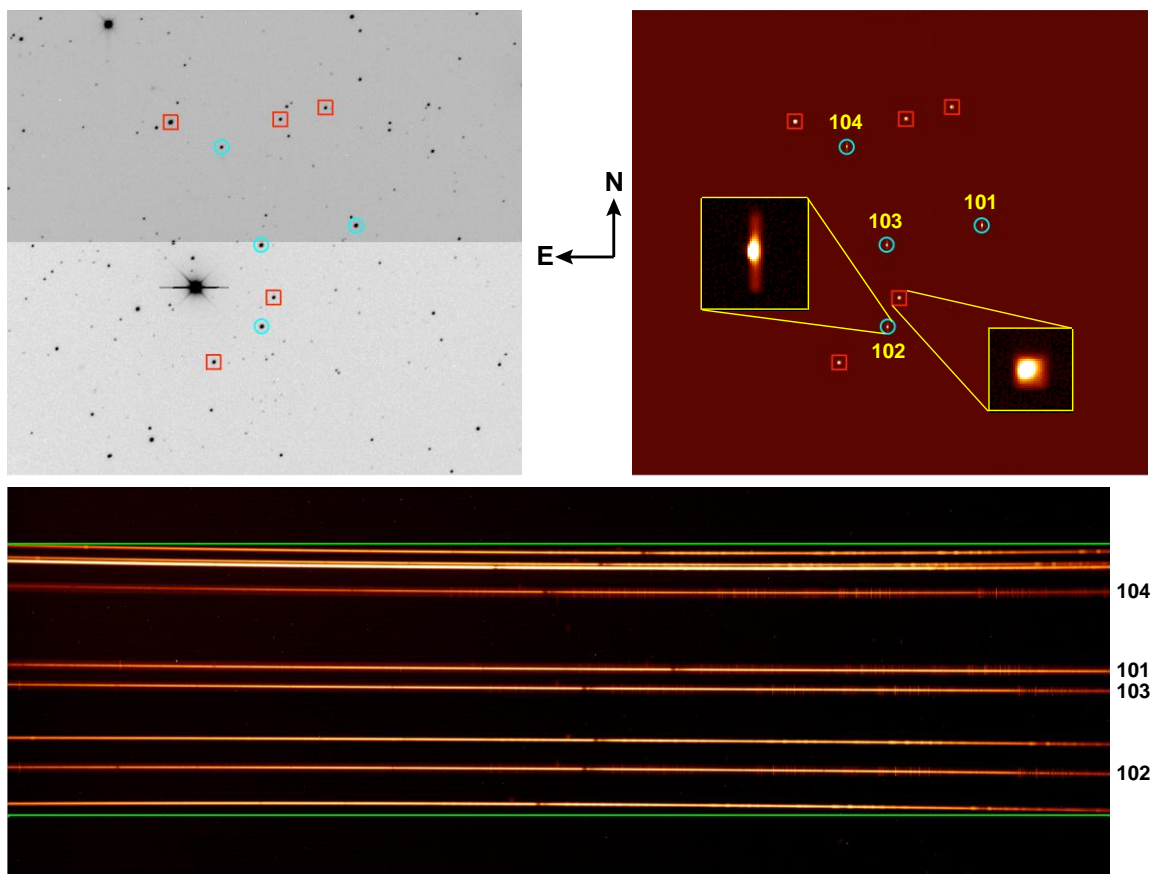


Figure 5-6: An example acquisition and spectroscopic sequence: an image of the field (*upper left*) where the spectroscopic targets (*blue circles*) and guide stars (*red squares*) have been highlighted; an image of the field through the slit mask (*upper right*), showing expanded views of one target and one guide star, and where the spectroscopic targets have been numbered; and the dispersed spectrum (*lower*), where the targets are again numbered. Note the small curvature of the spectrogram on the detector, in contrast to the superimposed horizontal lines (*green*).

⁵⁹ The process of designing a slit mask is described at http://www.ctio.noao.edu/~points/CKOSMOS/ckosmos_mos.html.

5.2 Data Products

5.2.1 Raw Data

No processing pipeline has been implemented at NOAO to calibrate spectra obtained with C/KOSMOS, so only raw data products are available from the Archive as they were obtained in the observing environment. Raw data from C/KOSMOS are 32-bit integers and include virtual *overscan* along each row at the beginning and end of the CCD readouts, which is stored with the image pixels as shown in Figure 5-7. Note that the coordinate origin is in the lower-left corner of the read-out section (for the convenience of image display), rather than at the location of the read-out *amplifiers*. The output from each amplifier (including the overscan regions) is stored in a separate image extension in the FITS *MEF* file (see Chapter 1). The size and location of the photo-active regions and the overscan are given in Table 5-5.

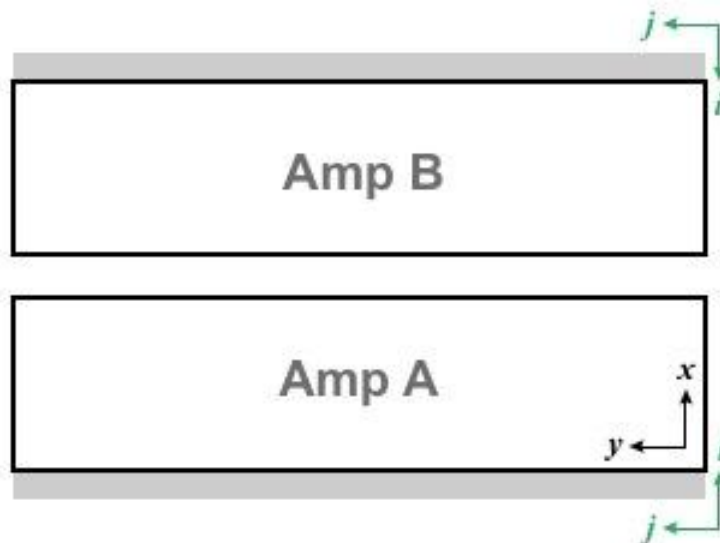


Figure 5-7: Schematic of the C/KOSMOS sensor just after read-out. Virtual overscan regions are indicated as shaded boxes (grey), but are expanded for clarity. Amplifier locations are near the origin of the green amplifier coordinate axes (i,j), prior to transformation to detector coordinates (black coordinate axes).

Table 5-5: Science Array and Overscan Regions

Amp	Photo-Active Data Section	X Overscan
A	[1:1024, 1:4096]	[1025:1074, 1:4046]
B	[1025:2048, 1:4096]	[2049:2098, 1:4146]

5.2.2 KMS Files

Observations obtained in multi-object spectroscopic mode are associated with the custom slit masks that were manufactured for the observing program. The specifications for the various slits (see Figure 5-6) are contained in KMS files (i.e., ASCII files with a .kms extension), and include the coordinates of the center of the field and the coordinates, shape, and location of each slit in the mask. No such files are generated for the facility long-slits.



Custom slit masks for C/KOSMOS are designed by the PI of each science program. The KMS files are **not** currently archived, nor is the information about the slit specification stored in the image headers. Some users may find the KMS files critical to associating MOS spectrograms with specific targets. Contact the Help Desk if you need these files.

5.2.3 Header Keywords

The keywords listed in Table 5-6 are especially important for reducing the raw data; keywords listed under “Instrument Configuration” are essential for identifying the semantic content of the images. The keywords listed under *World Coordinates* are of marginal value as no world coordinate system (WCS) solution has been pre-computed; the WCS refers to the linear pixel coordinates and their transformation from amplifier coordinates. However, the CD1_1 value gives the approximate image scale in arcsec/pix, and the CD2_2 value gives the approximate dispersion in Å/pix when a grism is in place.

Table 5-6: Header Keywords

Keyword Name	HDU	Meaning
Telescope		
AIRMASS	P	Atmospheric pathlength for target at observation start
OBSERVAT	P	Observatory that operates this telescope
TELESCOP	P	Telescope used to obtain these data
TELDEC	P	Declination for the telescope position on the sky (deg)
TELRA	P	Right ascension for the telescope position on the sky in hh:mm:ss.s
Instrument/Detector Configuration		
AMPNAME	E	Identifier of the amplifier in CCD
CCDNAME	E	Identifier of detector in FPA
CCDSUM	E	Binning factor on CCD in x,y
GAIN	E	Detector approximate gain for amp <i>k</i> (e^-/ADU)
RDNOISE	E	Detector approximate read noise for amp <i>k</i> (e^-)
SATURAT	E	Detector saturation for amp <i>k</i> (ADU)
Instrument/Detector Configuration		
DISPERSR	P	Disperser in use

Keyword Name	HDU	Meaning
FILTER	P	Filter name/designation
GCCROTAT	P	Instrument rotator angle (deg E of N)
INSTRUME	P	Instrument name
KSDPOS	P	Identifier for slit mask in use
KSFILCMD	P	Name of filter in use
KSSPOS	P	Identifier of disperser in use
OBSMODE	R	Observing mode (acq imaging sos_slit mos_slit)
OBSTYPE	P	Type of target observed (object comp dark focus flat zero)
SLITWHL	P	Slit mask in use; not present in imaging mode
Time		
DATE-OBS	P	Date and time of observation start (ISO 8601 format)
DARKTIME	P	Time interval over which dark current accumulated (s)
EXPCOADD	P	Duration of a single exposure in a co-add sequence (s)
EXPTIME	P	Effective exposure duration (s). For Stacked images the effective exposure duration can be a complicated function of position in the image.
MJD-OBS	P	Time of observation start (MJD)
TIME-OBS	P	Time when observation was initiated (hh:mm:ss.sss)
TIMESYS	P	The principal time system for all time-related keywords. Always UTC.
World Coordinates		
CD <i>i</i> _j	E	Transformation matrix from pixel to intermediate world coordinates; CD <i>i</i> _ <i>j</i> is the pixel scale for axis <i>i</i>
CRPIX <i>i</i>	E	Location of the reference point along axis <i>i</i> in units of pixels
CRVAL <i>i</i>	E	Value of the world coordinate at the reference point for axis <i>i</i> in degrees
CTYPE <i>i</i>	E	Name of the coordinate represented in axis <i>i</i>
DEC	P	Declination for the center of the FoV (deg)
LTMn_m	E	Detector to image transformation
LTVn	E	Detector to image transformation
NAXIS <i>i</i>	E	Number of pixels along axis <i>i</i>
RA	P	Right ascension for the center of the FoV (hh:mm:ss.s)
RADECSYS	E	Name of the reference system in which the world coordinates are expressed

5.3 Data Reduction

Since no calibration pipeline is available (or planned) for C/KOSMOS data, users will have to perform the reductions themselves. Data reduction will require obtaining all calibration frames for the observing run(s) that contain the data of interest. The types of exposures are listed in Table 5-7. Note that the specific target for some types of exposures may be ambiguous (e.g., telescope vs. spectrograph focus); clues to the type of target may be found in the OBJECT and OBSMODE fields in the image header.

Table 5-7: Types of C/KOSMOS Exposures

OBSTYPE	OBSMODE	Meaning
object	acq	Target acquisition through slit mask
comp	sos_slit	Spectrogram of a comparison arc lamp
dark	imaging	Finite duration exposure with shutter closed (not used)
flat	imaging	Image of the illuminated dome screen or the twilight sky
	sos_slit	Spectrogram of the illuminated dome screen or the twilight sky
	imaging	Image of a field to focus the telescope
focus	sos_slit	Non-dispersed image of the illuminated dome spot through the slit mask to focus the camera
object	imaging	Image of a target field
	sos_slit	Spectrogram of a target field
zero	acq	Zero-second bias exposure

Data reduction for C/KOSMOS is straightforward and similar to that for many MOS spectrographs. The following is an outline of the process.

- 1) Combine calibration frames
 - a) Apply overscan correction to bias frames, trim, and combine to make Master Bias Residual
 - b) Apply overscan and bias corrections to imaging flat-field frames, trim, and combine to make Master Imaging Flats (one per filter)
 - c) Apply overscan and bias corrections to imaging flat-field frames, trim, and combine to make Master Spectral Flats (one per spectral configuration)
- 2) Process images
 - a) Apply overscan, trim, apply Master Residual Bias
 - b) Apply Master Flat-field correction (per filter)
 - c) Solve for WCS⁶⁰
- 3) Process spectral images
 - a) Apply overscan, trim, apply Master Residual Bias
 - b) Combine spectral exposures if needed
 - c) Identify targets in 2-D spectrograms, and record extraction parameters
- 4) Trace and extract spectra
 - a) Extract targets
 - b) Extract comparison arcs and spectral flats
- 5) Identify Arc spectral lines and apply dispersion solution
- 6) Perform flux calibration (if needed for your program)
 - a) Prepare sensitivity correction per extraction window
 - b) Apply sensitivity correction to science targets

⁶⁰ An image of the field can be retrieved from the ESO Online Digitized Sky Survey (<http://archive.eso.org/dss/dss/>) using the coordinates from the RA and DEC header keywords.

5.4 *References & Further Information*

Contributing Authors

Many people have contributed to the technical knowledge of the C/KOSMOS spectrographs. Extensive material (including figures) was contributed by instrument PI Paul Martini and collaborators at The Ohio State University. Sean Points and Jay Elias lead the commissioning effort for both spectrographs, and they, along with Paul Martini and Tim Beers, authored the *C/KOSMOS Instrument Manual*.

References

Martini, P., et al. 2014, *KOSMOS and COSMOS: New Facility Instruments for the NOAO 4-meter Telescopes*, SPIE, 9147, oZ

Points, S., Elias, J., Martini, P., & Beers, T. 2014, *C/KOSMOS Instrument Manual*, (Version 1.7; Tucson, AZ: NOAO), available online:

<http://www.noao.edu/nstc/kosmos/Documents/KOSMOSManualv1.7.pdf>

For Further Reading

The OSMOS spectrograph, which was built by P. Martini and collaborators at The Ohio State University for the 2.4-m Hiltner Telescope at the MDM Observatory, was described in detail in:

Martini, P., Stoll, R., Derwent, M. A., et al. 2011, *The Ohio State Multi-Object Spectrograph*, PASP, 123, 187

Glossary

Version 2.0, February 2015

The following are definitions of common terms and acronyms found throughout this *Handbook*.

2MASS

Two-micron all-sky survey, consisting of images and catalogs of sources in the *J*, *H*, and *K*-bands. See the project website (<http://www.ipac.caltech.edu/2mass/>) for details.

ADC

An *atmospheric dispersion corrector* generally consists of a pair of prisms that are used in the optical system of a telescope or instrument to compensate for the dispersive effect of Earth's atmosphere.

ADU

For CCD amplifiers, one analog-to-digital unit (*ADU*) is one count, corresponding to a quantity of detected photons given by the detector gain setting.

Airmass

The pathlength of light from an astrophysical source through Earth's atmosphere. It is given approximately by $\sec z$, where z is the angular distance from the zenith (the point directly overhead, where airmass = 1.0) to the source location on the sky.

Amplifier

An electronic component of a *sensor*, which is used to recover the signal during read-out. Often, multiple amplifiers on each sensor enable simultaneous read-out of adjacent regions of each detector.

Background

In an image, the background consists of contributions from the sky (e.g., clouds or scattered moonlight) and from the telescope and camera optics, which must be distinguished from the astrophysical background. The sky and instrumental backgrounds are characterized and removed by the processing software using a low-order spatial function whose coefficients may be recorded in the image metadata.

CCD

A charge-coupled device (*CCD*) is a detector that is sensitive to optical-band light. CCDs are used extensively in astronomy because of their high quantum efficiency, excellent linearity, and high dynamic range.

Co-add image

A synonym for *Stacked image*.

CTIO

Cerro-Tololo Inter-American Observatory, located near La Serena, Chile.

Dark Energy Survey

This wide-area survey of the Southern Hemisphere sky, being carried out on the Blanco 4-m telescope at CTIO by the *Dark Energy Survey* (DES) collaboration, will cover over 5000 deg^2 to depths as faint as $m \sim 24$ in the *g,r,i,z,Y* passbands. See the project website (<http://www.darkenergysurvey.org/index.shtml>) for details.

Dither

A *dither* pattern of exposures in a sequence, with small relative spatial offsets, is intended to provide full coverage of a region of sky in spite of gaps between adjacent detectors in the **FPA**. See **map** pattern.

DQM

The data quality mask (**DQM**) is an array that encodes problems, pathologies, and other information about the quality of an associated science image at the pixel level.

Filter

A *filter* in astronomy is an optical element used to restrict the **passband** of light reaching the focal plane; i.e., it transmits a selected range of wavelengths. Filter elements are often designed to match standard photometric passbands, such as those used in the **SDSS** survey: *u, g, r, i, z*.

FITS

The Flexible Image Transport System (**FITS**) is an international standard in astronomy for storing images, tables, and metadata in disk files. See the [IAU FITS Standard](#) for details.

Flat-field

A *flat-field* generally refers to an image of a source with a spatially uniform distribution of light, which is used to calibrate variations in the detector pixel-to-pixel sensitivity.

Fowler sample

During the read-out of an infrared detector, a *Fowler Sample* refers to multiple, sequential reads of the entire array; this procedure is performed both at the start and at the end of an exposure, and the mean difference is retained.

FPA

A focal-plane array (**FPA**) is the arrangement of multiple **sensors** in the focal plane of a camera.

FoV

The field of view (*FoV*) of a telescope or a camera, expressed in square degrees, usually includes only the area projected onto the **FPA**.

Healpix

A hierarchical, equal-area, isolatitude pixelization of a sphere. This tessellation scheme subdivides the celestial sphere such that each pixel covers the same surface area, and each can be assigned a hierarchical index that facilitates rapid look-ups in databases by coordinates. See <http://healpix.jpl.nasa.gov> for details.

InstCal

An *InstCal* image is a Level-2 NOAO data product, and is the result of pipeline processing an image to remove instrumental signature, provide a characterization of the **WCS**, and an approximate photometric zero-point. InstCal images usually have associated concomitant data, such as a **DQM**.

JD

The Julian Date (*JD*) of any instant is the Julian day number for the preceding noon (*UTC*), plus the fraction of the day elapsed since that instant. The Julian day number is a running sequence of integral days, starting at noon, since the beginning of the Julian Period; JD 0.0 corresponds to noon on 1 January 4713 BCE. Various [Julian Date converters](#) are available on the Web. For example, 18h 00m 00.0s UT on 2014-July-01 corresponds to JD 2,456,840.25.

Keyword

In the astronomy data domain, *keyword* is most closely associated with a named metadatum stored in a FITS header, which is assigned a particular scalar or text value.

KPNO

Kitt Peak National Observatory, located near Tucson, Arizona, USA.

Map

A **map** often refers to a pattern of exposures in a sequence, with large but overlapping spatial offsets, intended to provide full coverage of a region of sky larger than the *FoV* of a camera. Often combined with a *dither* pattern.

Master Calibration

Master Calibrations are inputs to the data calibration pipelines to remove elements of the instrumental signature, such as variations in pixel-to-pixel sensitivity. They are often constructed from co-adds of calibration exposures, but may be characterizations of effects seen in a science image, represented in one or more tables.

MEF

Multi-Extension FITS (*MEF*) file is a file containing multiple data structures (*header-data units*, in the vernacular) such as tables or binary images. See Chapter 1 for details.

Metadata

Metadata, or data that describes one or more data products, are collected from a variety of sources, including the observing environment and processing pipelines. These data are often represented in FITS headers as **key-word=value** pairs.

MJD

The Modified Julian Day (*MJD*) is shorthand for numerically compressed Julian Day: $MJD = JD - 2,400,000.5$, which makes MJD = 0 correspond to UT midnight on 1858-Nov-17. The half-day offset from JD aligns the start of the day with modern civil timekeeping.

Observing Block

An *observing block* is a set of exposures obtained within a period of time that is defined by the maximum number of images that can be dealt with by the processing pipeline, typically 50. Images are divided for processing by the *filter* used, but may be subdivided by intervals of time (blocks) of perhaps one to a few days to stay below the limit of files to process.

Overscan

Refers to the portion of the **amplifier** read-out of either: (a) non photo-active pixels, or (b) additional read-out of the serial register after all science pixels have been accumulated (sometimes called *virtual overscan*). The *overscan* is often appended to the science pixels in the assembled amplifier image as a separate region. This region is useful to science processing software for estimating the stability of the DC offset in the read-out electronics.

Passband

A *passband* refers to the window of wavelength or the energy range admitted by an optical system; specifically the transmission as a function of wavelength or energy. Typically the passband is limited by a **filter**. The width of the passband may be characterized in a variety of ways, including the width of the half-power points of the transmission curve, or by the equivalent width of a filter with 100% transmission within the passband, and zero elsewhere.

Processing Level

The *processing level* is a numeric shorthand for the extent of pipeline processing from *raw data* (Level 1) to single-frame calibrated (*InstCal*) images with instrument signature removed (Level 2), to co-added (*Stacked*) images (Level 3), to *source catalogs* (Level 4) that may be derived from levels 2 or 3. *Master Calibration* data do not fit neatly into this scheme. See Table 1-2 on page 1-4 for details.

PSF

The point-spread function (*PSF*) is the distribution of intensity on an image originating from an unresolved point-source (i.e., a star). Often the PSF is not the same *Airy shape* as would be expected from a finite-aperture optical system, owing primarily to atmospheric effects and imperfections in the optical system and the detector.

Raw Data

Data as obtained from an instrument in the observing environment are *raw data*, and they form the input for data calibration pipelines. Raw data may consist of exposures of astronomical targets or fields, or be one of many calibration exposures that are combined to remove the instrumental signature from science data.

Saturated

A portion of an exposure may be *saturated* if the local brightness exceeds the ability to record the signal in the image. There are two types of saturation: one in which the number of detectable photons exceeds the local full-well (i.e., the supply of electrons) in one or more detector pixels, and the other where the number of photo-electrons exceeds the range of the A-to-D converter.

SDSS

The *Sloan Digital Sky Survey* is a digital survey of roughly $10,000 \text{ deg}^2$ of sky around the north Galactic pole, plus a $\sim 300 \text{ deg}^2$ stripe along the celestial equator. See <http://www.sdss.org> for details.

Seeing

Seeing is an astronomical term for characterizing the stability of the atmosphere, as measured by the width of the point-spread function (*PSF*) on images. The PSF width is also affected by a number of other factors, including the airmass, passband, and the telescope and camera optics.

Stacked image

A synonym for *Co-Add image*, a *Stacked image* is the combination of multiple input images that overlap at least partially. For NOAO images, the inputs are aligned to a common projection and pixel grid, corrected to the same photometric scale and zero-point, with bad pixels and artifacts masked. (Image *PSFs* should ideally be matched prior to co-addition.) Stacked images have had non-astrophysical background removed.

Tangent Point

The Celestial Sphere is projected onto a flat focal plane, so applicable *WCS* geometry involves a *tangent point* where the spherical and Cartesian coordinate systems intersect. The tangent point is often selected as the center of the optical axis, or the center of the *FoV*, but it need not be.

UTC

Coordinated Universal Time (by the French acronym *UTC*) is the most common international time standard in use today. It is a successor to Greenwich Mean Time (GMT). UTC is based on International Atomic Time (TAI) with leap seconds added to compensate for the slowing rate of the Earth's rotation.

WCS

A World Coordinate System (*WCS*) is a mapping from image pixel coordinates to physical coordinates; in the case of images, the mapping is to sky coordinates, generally in an equatorial (RA, Dec) system. The *WCS* is expressed in *FITS* file extensions as a collection of header **keyword**=**value** pairs (basically, the values of parameters for a selected functional representation of the mapping) that are specified in the *FITS Standard*.